Vol. 76, A, Part II (April to June), 2006

ISSN 0369-8211

Proceedings of the National Academy of Sciences, India

Section A - Physical Sciences

Published by

The National Academy of Sciences, India

5, Lajpatrai Road, Allahabad-211002

The National Academy of Sciences, India

(Registered under Act XXI of 1860)
Founded 1930

COUNCIL FOR 2005

Regd. No. R.N. 35621/78

Contents

Chemistry

Mathematics

PROCEEDINGS

OF THE

NATIONAL ACADEMY OF SCIENCES, INDIA

2005

VOL. LXXV SECTION–A PART II

Photochemical degradation of p-chloroaniline by photo-Fenton's reagent

DEEPIKA MOGRA, HARISH SWARNKAR, JITENDRA VARDIA and SURESH C. AMETA

Photochemistry Laboratory, Department of Chemistry, M.L. Sukhadia University, Udaipur - 313 002, India

Received March 31, 2003; Revised May 6, 2004; Accepted September 2, 2004

Abstract

There are number of techniques available for waste water treatment but each has its own limitations. Fenton's reagent is an established reagent, used for hydroxylation. Its use for degradation of organic pollutants has also been suggested, but the reaction stops after complete consumption of Fe^{3+} ions. The Fe^{3+} ions can be regenerated from Fe^{2+} ions under these conditions with an additional requirement of light. This will make the process cyclic in nature and photodegradation will proceed more smoothly. The photochemical degradation of p-chloroaniline on titanium dioxide was carried out in the presence of Fenton's reagent, and progress of the reaction was observed spectrophotometrically. The effect of the variation of various parameters such as pH, concentration of p-chloroaniline, Fe^{2+} ion concentration, amount of photocatalyst, amount of hydrogen peroxide, light intensity etc. on the photodegradation of p-chloroaniline was observed. A tentative mechanism for this degradation has also been proposed.

(**Keywords:** photochemical degradation / photo-Fenton's reagent / p-chloroaniline /titanium dioxide)

Introduction

Fenton's reagent[1] is one of the most powerful inorganic oxidising reagents, used to treat a variety of industrial wastes containing a range of toxic organic compounds. The process may be applied to waste water, sludges or contaminated soils. Sedlak[2] investigated the effect of $FeCl_3$, $K_3[Fe(CN_6)]$ and $Na_2[Fe(CN)_5NO]$ on photochemical reactions of H_2O_2 with benzene. $FeCl_3$ markedly raises the phenol content in the product in the reaction initiated by U.V. radiation, i.e. it catalyses hydroxylation, while the cyano complexes catalyse photodestruction of the benzene ring. Photocatalytic degradation of trinitrotoluene and trinitrobenzene influenced by H_2O_2 was observed by Dillert *et al.*[3] Polszynska *et al.*[4] studied the reactivity of mono substituted benzenes towards reactive species formed in the Fe(II) / H_2O_2 aqueous system. Jacob *et al.*[5] investigated the mechanism of reaction between benzene and H_2O_2 in the presence of dioxygen with added Fe^{3+} or Cu^{2+} ions. Three reaction products phenol, 2-hydroxyl-2-4-hexadiendial and 3-hydroxy-2-4-hexadiendial have been obtained. Nedoloujko and Kiwi[6] reported that transient intermediate species are active during the Fenton's mediated degradation of quinoline in oxidative media by pulsed laser spectroscopy. Ruppert *et al.*[7] describes the photo-Fenton reaction an effective photochemical waste-water treatment process. Prousek *et al.*[8] reported the utilization of Fenton reaction for the degradation of conventionally used dyes and coloured

waste water. Prousek and Duriskova[9] studied the oxidative degradation of poly (ethylene glycol) by the Fenton and photo-Fenton's reactions. Photodegradation of malachite green in the presence of Fe^{3+} / H_2O_2 under visible irradiation has been observed by Wu *et al.*[10] Sanchez *et al.*[11] reported the degradation of 2, 4-dichlorophenoxy acetic acid by *in situ* photogenerated Fenton reagent. New evidences against hydroxyl radicals as reactive intermediates in the thermal and photochemically enhanced Fenton reaction have been given by Bassmann *et al.*[12] Walling[13] studied intermediates in the reaction of Fenton's type reagents. It was observed that organic dyes were effective in degrading some of pesticides whereas iron compounds especially in combination with H_2O_2 as the oxidising agent proved to be more effective for degrading all the target pesticides. Yasmin[14] has reported photochemical degradation of phenoxy derivatives using photo-Fenton's reagent. Recently, Mogra *et al.*[15,16] reported the photochemical degradation of p-dichlorobenzene and chlorobenzene by photo-Fenton's reagent. The present study discusses the photodegradation of p-chloroaniline using photo-Fenton's reagent.

Materials and Method

The photochemical degradation of p-chloroaniline (Merck) was studied in the presence of titanium dioxide, Fenton's reagent and light. Stock solution of p-chloroaniline (1.0 x 10^{-2} M) was prepared in doubly distilled water. The photochemical degradation of p-chloroaniline was observed by taking 2.0x10^{-5} M of solution, 7.0 x 10^{-5} M ferric ions, 0.40 mL hydrogen peroxide and 0.03 g semiconductor (titanium dioxide) was added. It was irradiated with a 200 W tungsten lamp (Philips; light intensity = 60.0 mWcm^{-2}). The intensity of light at various distances from the lamp was measured using solarimeter (SM CEL 201). A water filter was used to cut off thermal radiations. The pH of the solution was measured using digital pH meter (Systronics Model 324). The desired pH of the solution was adjusted using standard sulphuric acid and sodium hydroxide solutions. The necessary condition for the correct measurement of the absorbance is that the solution must be free from the suspended semiconductor particles and other impurities; a centrifuge (Remi 1258) was used to remove these species. The absorbance of the reaction mixture was determined by spectrophotometer (uv-visible spectrophotometer; JASCO 7800). Measuring absorbance at regular time intervals monitored the progress of the reaction.

Results and Discussion

An aliquot of 4.0 mL was taken out from the reaction mixture and the absorbance was measured at λ_{max} = 370 nm. It was observed that the absorbance of the solution decreases with increasing time intervals; which indicates that the concentration of p-chloroaniline decreases with increasing time of exposure. A plot of 1 + log (absorbance) against time was linear and follows pseudo-first order kinetics. The rate constant was measured with the expression :

$$k = 2.303 \times \text{slope} \quad (1)$$

The results are presented graphically in Fig. 1.

Effect of pH The effect of pH on photocatalytic degradation was also investigated. The
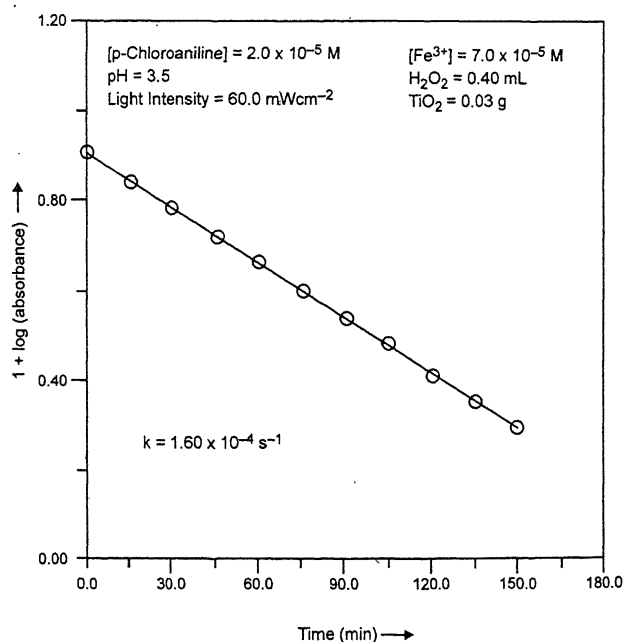
Fig. 1–A Typical run.

results are reported in Table 1. It is evident from data that the rate of photocatalytic degradation of p-chloroaniline increases with increase in pH upto 3.5 and then, the rate of the reaction decreases with increasing pH. At pH > 4.5, some turbidity appeared and measurement of absorbance becomes difficult as well as erroneous and therefore, the effect of pH was studied up to 4.5 only. The photocatalytic degradation depends strongly on the pH of the reaction medium. The hydroxyl radicals are generated in three steps - (i) the reaction between ferrous ions and hydrogen peroxide (equation 3), (ii) photochemical reaction of ferric ions and water (equation 2) and (iii) reaction between holes and water (equation 6). The increase in pH of the medium will favour the step (i) where OH^- ions formed alongwith hydroxyl radicals, whereas protons are generated in step (ii) and (iii). Thus it may be concluded that the step (i) dominates over step (ii) and (iii) in the pH range below 3.0. However, retardation of the reaction above pH 3.5 suggests the dominance of steps (ii) and (iii) over step (i).

Table 1 – Effect of pH.

[p-Chloroaniline] = 2.0×10^{-5} M $[Fe^{3+}] = 7.0 \times 10^{-5}$ M
TiO_2 = 0.03 g H_2O_2 = 0.40 mL
Light intensity = 60.0 $mWcm^{-2}$

pH	$k \times 10^4$ (s^{-1})
1.0	0.09
1.5	0.40
2.0	0.81
2.5	1.02
3.0	1.31
3.5	1.60
4.0	1.49
4.5	1.38

Effect of p-chloroaniline concentration : The effect of p-chloroaniline concentration on the rate of its photocatalytic degradation was observed and the results are summarised in Table 2. The rate of photocatalytic degradation was found to increase with increasing concentration of p-chloroaniline up to 2.00×10^{-5} M. On further increase, a sudden decrease in the rate of degradation was observed. This may be explained on the basis that on increasing the concentration of p-chloroaniline, the reaction rate increases, as more molecules of p-chloroaniline are available for degradation. However, on increasing the concentration above 2.00×10^{-5} M, the movement of p-chloroaniline molecules towards semiconductor surface is hindered because of its larger concentration and as a result, decrease in the rate of degradation was observed.

Table 2 – Effect of p-chloroaniline concentration.

TiO_2 = 0.03 g   pH = 3.5
Light intensity = 60.0 $mWcm^{-2}$ $[Fe^{3+}] = 7.0 \times 10^{-5}$ M
H_2O_2 = 0.40 mL

[p-Chloroaniline] $\times 10^5$ M	$k \times 10^4$ (s^{-1})
0.50	1.10
0.75	1.12
1.00	1.15
1.25	1.20
1.50	1.29
1.75	1.41
2.00	1.60
2.25	1.39
2.50	1.26
2.75	1.01
3.00	0.77

Effect of ferric ion concentration : The effect of concentration of Fe^{3+} ions on the rate of photocatalytic degradation of p-chloroaniline was observed by keeping all other factors identical. The results are summarised in Table 3. It is clear from the data that the rate of photodegradation increases on increasing concentration of Fe^{3+} ions up to 7.0×10^{-5} M, while a reverse trend was observed beyond this limit. This may be explained on the basis that on increasing the Fe^{3+} ions in the reaction mixture, the concentration of Fe^{2+} ions

also increases. This results in an enhanced generation of the active species •OH radicals and as a consequence, the rate of photocatalytic degradation also increases. However, on increasing the concentration of Fe^{3+} ions further, the rate of the reaction was found to decrease. This is because of the fact that the Fe^{3+} ions impart a yellow colour to the solution and at larger concentrations, it may act as a filter to the incident light and the desired light intensity will not reach the surface of the semiconductor and, therefore, a decrease in the rate of reaction was observed.

Table 3 – Effect of Fe^{3+} ion concentration.

[p-Chloroaniline] = 2.0 x 10^{-5} M; H_2O_2 = 0.40 mL
pH = 3.5; TiO_2 = 0.03 g
Light Intensity = 60.0 $mWcm^{-2}$

$[Fe^{3+}]$ x 10^4 M	k x 10^4 (s^{-1})
0.10	0.33
0.20	0.68
0.30	0.97
0.40	1.14
0.50	1.31
0.60	1.45
0.70	1.60
0.80	1.25
0.90	1.00
1.00	0.79
1.10	0.60

Effect of hydrogen peroxide : The effect of amount of hydrogen peroxide on the photocatalytic degradation of p-chloroaniline was also investigated. The results are tabulated in Table 4. It was observed that the rate of the reaction increases as the amount of H_2O_2 was increased and it attained an optimum value at 0.40 mL. Thereafter, the rate of degradation becomes virtually constant. This saturation like behaviour can be explained on the basis that the surface of semiconductor titanium dioxide is completely covered by hydrogen peroxide molecules. Any further amount of hydrogen peroxide will remain in the bulk of the solution and in turn, will not add to the rate of the reaction as observed[16] earlier.

Effect of amount of semiconductor : The effect of amount of semiconductor on the photocatalytic degradation of p-chloroaniline was investigated and the results are tabulated in Table 5. The rate of photodegradation of p-chloroaniline increases with an increase in the amount of semiconductor up to 0.03 g and on further increase, the rate of reaction becomes almost constant. This may be attributed

Table 4 – Effect of hydrogen peroxide.

[p-Chloroaniline] = 2.0 x 10^{-5} M; $[Fe^{3+}]$ = 7.0 x 10^{-5} M
pH = 3.5; TiO_2 = 0.03 g
Light Intensity = 60.0 $mWcm^{-2}$

H_2O_2 (mL)	k x 10^4 (s^{-1})
0.10	0.09
0.20	0.60
0.30	1.21
0.40	1.60
0.50	1.59
0.60	1.61

Table 5 – Effect of amount of semiconductor.

[p-Chloroaniline] = 2.0 x 10^{-5} M; H_2O_2 = 0.40 mL
pH = 3.5; $[Fe^{3+}]$ = 7.0 x 10^{-5} M
Light Intensity = 60.0 $mWcm^{-2}$

Amount of semiconductor (g)	k x 10^4 (s^{-1})
0.010	1.00
0.015	1.21
0.020	1.33
0.025	1.48
0.030	1.60
0.035	1.61
0.040	1.59
0.050	1.60

to the fact that the number of exposed semiconducting particles will increases as the amount of semiconductor powder was increased and as a result, the number of electron-hole pairs will also increase. This will result into a corresponding increase in the rate of the reaction. On further increasing the amount of semiconductor, the numbers of exposed semiconducting particles will not increase as the exposed surface area will limit the number of particles directly exposed to the light source and the reaction rate remains almost constant after this limit.

Effect of light intensity : The effect of light intensity on the photocatalytic degradation of p-chloroaniline was investigated. The results are tabulated in Table 6. A linear behaviour between the rate constant and light intensity was observed, which indicates that an increase in the light intensity will increase the rate of reaction. This may be attributed to the increased number of photons striking TiO_2 particles per unit area per second and as a result, more electron-hole pairs are generated. This, in turn, will increase the number of active species, the hydroxyl radicals. As a consequence, an overall increase in the rate of the reaction has been observed.

Table 6 - Effect of light intensity.

[p-Chloroaniline] = 2.0×10^{-5} M [Fe^{3+}] = 7.0×10^{-5} M
H_2O_2 = 0.40 mL TiO_2 = 0.03 g
pH = 3.5

Light Intensity ($mWcm^{-2}$)	$k \times 10^4$ (s^{-1})
20.0	0.10
30.5	0.50
40.0	0.89
50.0	1.40
60.0	1.60
70.0	2.06
80.0	2.54

Mechanism : On the basis of the experimental observations and corroborating the existing literature, a tentative mechanism has been proposed for the photocatalytic degradation of p-chloroaniline with photo-Fenton's reagent in the presence of semiconducting TiO_2 powder.

$$Fe^{3+} + H_2O \xrightarrow{h\nu} Fe^{2+} + OH^{\bullet} + H^+ \quad ..(2)$$

$$Fe^{2+} + H_2O_2 \longrightarrow Fe^{3+} + OH^- + OH^{\bullet} \quad ..(3)$$

$$TiO_2\,(SC) \xrightarrow{h\nu} h^+_{(VB)} + e^-_{(CB)} \quad ..(4)$$

$$H_2O_2\,(ads.) + 2\,h^+ \longrightarrow O_2 + 2\,H^+ \quad ..(5)$$

$$h^+_{(VB)} + H_2O \longrightarrow OH^{\bullet} + H^+ \quad ..(6)$$

$$ClC_6H_4NH_2 + OH^{\bullet} \longrightarrow \text{Products} \quad ..(7)$$
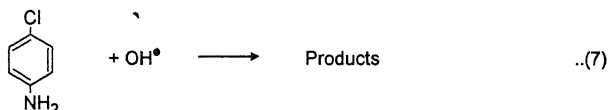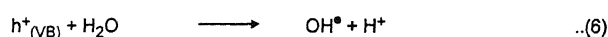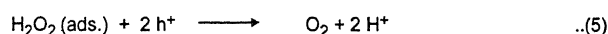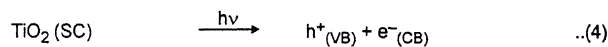
The aqueous solution of ferric ions on exposure to light dissociates a water molecule into a proton and •OH radical and itself reduce to ferrous ions. These ferrous ions will decompose H_2O_2 into hydroxyl ion and hydroxyl radical, while ferrous ions undergo oxidation to ferric ions. TiO_2 on exposure generates an electron-hole pair. This hole may dissociate the H_2O_2 adsorbed on the semiconductor surface into oxygen and proton whereas a hole may decompose water into a proton and a hydroxyl radical. The hydroxyl radical will degrade the p-chloroaniline adsorbed on semiconductor surface into products. The participation of hydroxyl radicals as an active oxidising species was confirmed by using hydroxyl radical scavangers, where the rate of photodegradation was drastically reduced.

Photocatalytic method of treating waste water gets an edge over other methods of treatment because it does not add to pollution any further. The active oxidising species, the hydoxyl radicals, will dimerize to give hydrogen peroxide, which may degrade ultimately to water and oxygen.

References

1. Fenton, H.J. (1894) *J. Chem. Soc.* **65** : 899.
2. Sedlak, P. (1990) *Ph.D. Thesis*, Praha.

3. Dillert, R., Fornefett, I., Siebus, V. & Bahnemann, D. (1996) *J. Photochem. Photobiol.* **94A** : 221.

4. Polszynska, J., Kowalski, J. & Sobkowiak, A. (1998) *Polish J. Chem.* **72** : 2514.

5. Jacob, N., Balakhrishnan, J. & Reddy, M.P. (1977) *J. Phys. Chem.* **81** : 17.

6. Nedoloujko, A. & Kiwi, J. (1997) *J. Photochem. Photobiol.* **110A** : 141.

7. Ruppert, G., Baur, R. & Heisler, G. (1993) *J. Photochem. Photobiol.* **73A** : 75.

8. Prousek, J., Ivanova, E. & Kocmanikova, M. (1997) *Chem. Listy.* **91** : 48.

9. Prousek, J. & Duriskova, I. (1998) *Chem. Listy.* **92** : 218.

10. Wu, K.G., Zhang, T.Y., Zhao, J.C. & Hidaka, H. (1998) *Chem. Lett.* **8** : 857.

11. Sanchez, L., Peral, J. & Domenech, X. (1996) *Electrochim. Acta.* **41** : 1981.

12. Bassmann, S.H., Oilveros, E., Gob, S., Siegwast, S., Dahlen, E.P., Payawan, L., Strub, M., Warner, M. & Braun, A.M. (1998) *J. Phys. Chem.* **102** : 5542.

13. Walling, C. (1998) *Acc. Chem. Res.* **31** : 155.

14. Yasmin, (2001) *Ph.D. Thesis,* Sukhadia University, Udaipur, India.

15. Mogra, D., Mehta, M., Ameta, R. & Ameta, S.C. (2002) *J. Indian. Chem. Soc.* **79** : 593.

16. Mogra, D., Ameta, R., Chhabra, N. & Ameta, S.C. (2003) *Intl. J. Chem. Sci.* **1**(1) : 211.

PROC. NAT. ACAD. SCI. INDIA, 75(A), II, 2005

Equilibrium studies of 3-hydroxy-2-phenylquinazolin-4-one with bivalent transition metal ions in presence of other chelating agents

P.NARENDER, RENU RANI, P. MADHAVA REDDY and B.SATYANARAYANA*

Bio-Inorganic Division, Department of Chemistry, OU College of Engineering, Osmania University, Hyderabad-500 007, India

**Author for Correspondence.*

Received April 29, 2003; Revised March 10, 2004; Accepted June 14, 2004

Abstract

A quantitative study of binary and ternary metal-ligand equilibria involving Co(II), Ni(II), Cu(II) and Zn(II) with 3-hydroxy-2-phenylquinazolin-4-one(HPQ) in presence of glycine(gly), alanine(ala), proline(pro) and ethylenediamine(en) has been studied at 30^0 C, in10% (v/v) aq. ethanol medium and at 0.1 M (KNO_3) ionic strength. Ternary complexes formed in a stepwise manner, where gly, ala, pro and en coordinate as secondary ligands and HPQ acts as a primary ligand. The proton-ligand dissociation constants, metal-ligand, ternary metal complex formation constants were also evaluated at different temperatures(20^0 C, 30^0 C and 40^0 C). Thermodynamic parameters (free energy (ΔG), enthalpy (ΔH) and entropy (ΔS) changes) were computed for the complexation reactions. The order of formation constants of binary as well as ternary chelates follows Irving-William order [Co(II)< Ni(II)<Cu(II)>Zn(II)].

(**Keywords :** equilibrium studies/thermodynamic parameters/bivalent transition metal ions/chelating agents/3 hydroxy-2phenylquinazolin-4-one)

Introduction

Cyclic hydroxamic acids containing $-\overset{O}{\overset{\|}{C}}-N\langle^{OH}$ functional group have numerous chemical applications. These are also known for biological activity[1,2], such as anti-helmentic agent, anti-microbial, bactericidal, analgesic, hypnotic, anti-convulsant, anti-inflammatory, CNS depressants and also have gained significant importance as anti-pyretic, anti-allergic, anti-ulcer, anti-cancer, anti-tumor, anti-HIV etc. These also act as good chelating agents. In the present investigation, the formation constants of 1:1 and 1:2 binary chelates of 3-hydroxy-2-phenylquinazolin-4-one (HPQ), one of the cyclic hydroxamic acid with Co(II), Ni(II), Cu(II) and Zn(II) and formation of mixed ligand complexes of above transition metal ions in the presence of other chelating agents like glycine (gly), α-alanine(ala), proline(pro), ethylenediamine (en) have been determined. Thermodynamic parameters computed for the complexation reactions studied in this investigation were free energy (ΔG), enthalpy (ΔH) and entropy (ΔS) changes. These have been calculated by using Vant Hoff isotherm, Gibbs-Helmholtz equation and Vant Hoff equations respectively.

Materials and Method

HPQ was prepared and purified by the method reported in literature[3,4]. The solution of the ligand HPQ was prepared in distilled ethyl alcohol. All the metal salts were obtained as nitrates[5] (AnalaR/ BDH quality). The other reagents KNO_3 (BDH), HNO_3, gly(E.Merck), ala, pro, and en(Sigma) of AR grade were used. Stock solutions (0.1M) of Co^{II}, Ni^{II}, Cu^{II} and Zn^{II} were prepared and standardized[6]. Doubly distilled water was used throughout. Commercial ethanol was distilled.[7]

Proton-ligand formation constants[8,9] were refined by using computer programmes PKAS, IRVING-ROSSOTTI, BEST. The formation constants of ternary systems were determined by Ramamoorthy and Santhappa[10,11]method and further refined by BEST[12,13] and SCOGS[14,15]. pH-meter

readings in 10% (v/v) ethanol-water were corrected by the method of Van Uitert and Haas[16].

Results and Discussion

Proton-ligand dissociation constants of HPQ : The p*K*a value for HPQ was determined for the first time by pH metric method. In the present investigation the titration curves for HPQ shows two buffer regions, first one in pH < 3 and the second one at 6.5. In the case of HPQ the release of protons in the lower buffer region corresponds to the dissociation of proton from the protonated tertiary nitrogen atom. The acid dissociation constant of tertiary nitrogen atom could not be determined because the protons from nitrogen atom dissociate at much lower pH and the metal ligand titration curves indicate that tertiary nitrogen is not involved in complex formation.

The n_H (average number of protons bound to the ligand) for HPQ indicates the liberation of one proton, which is due to the dissociation of hydroxamic group.

Formation constants for binary metal complexes : $\bar{n}$ (degree of formation or metal ligand formation number) values ($0.1<n<1.9$) obtained for M(II)-HPQ system indicate the formation of both 1:1 and 1:2 complexes in solution. The binary formation constants so obtained are presented in Table 1.

Table 1 – Stepwise stability constants of binary complexes of HPQ at different temperatures.

Medium : 10%(v/v) aqueous ethanol, Ionic strength : 0.1MKNO$_3$

Metal ions	Stability constants	Temperature		
		20^{0}C	30^{0}C	40^{0}C
H$^+$	pK_a	6.27	6.10	5.91
CO^{II}	$log\ K_1$	4.73	4.54	4.35
	$log\ K_2$	3.64	3.4	3.34
Ni^{II}	$log\ K_1$	5.12	4.93	4.74
	$log\ K_2$	4.82	3.67	3.52
Cu^{II}	$log\ K_1$	5.81	5.60	5.32
	$log\ K_2$	4.68	4.53	4.38
Zn^{II}	$log\ K_1$	4.91	4.71	4.52
	$log\ K_2$	3.93	3.72	3.57

It is a well-known fact that statistically coordination of a second ligand molecule is difficult when compared to the first ligand due to availability of less number of coordinating sites on the metal ion for the second ligand. The value of K follows the order $K_1 > K_2$.

The complexing tendency of the metal ion follows the order: Co(II) < Ni(II) < Cu(II) > Zn(II).All the systems studied are in the conformity with the Irving -William natural order of stabilites[17]. As a representative case, Ni(II)-HPQ distribution diagram is given in Fig. 1.
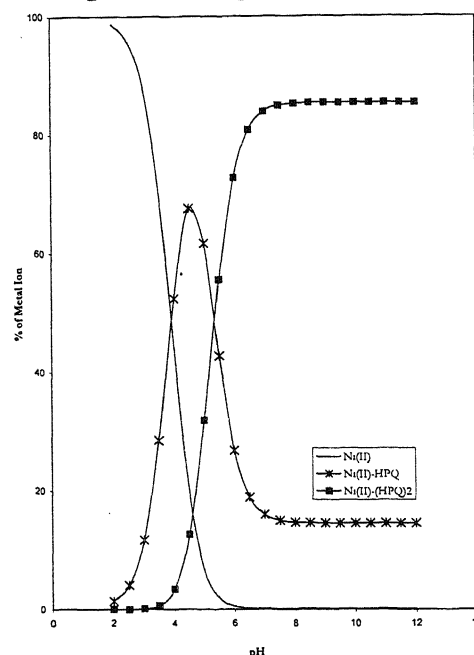
Fig. 1 – Distribution diagram of Ni(II)-HPQ complex.

Formation of ternary metal complexes : In the case where A is gly, ala, pro and en in presence of HPQ coordinated with transition metal ions [Co(II), Ni(II), Cu(II) and Zn(II)] in stepwise manner, the equilibria involved in ternary complex formation of the type [M(II)-HPQ-A] can be represented by the following equation (1 and 2) (charges are omitted for clarity)

$$M + HPQ \rightleftharpoons M\text{-}HPQ \quad (1)$$

$$[M\text{-}HPQ] + A \rightleftharpoons [M\text{-}HPQ\text{-}A] \quad (2)$$

(where A = gly, ala, pro and en)

Such a stepwise formation of ternary complex

is confirmed from the distribution diagram, that in the lower pH range the major species are the free metal ion and the [M-HPQ] species, whereas in the higher pH range the major species are [M-HPQ] and [M-HPQ-A], (Fig. 2). These findings indicate that HPQ acts as a primary ligand.
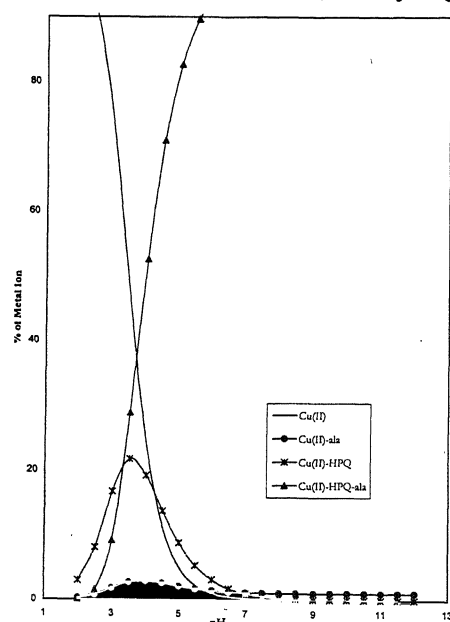
Fig. 2 – Distribution diagram of Cu(II)-HPQ-ala (1:1:1)

The formation of mixed ligand complexes in solution is further supported by (i) intensification of colour, (ii) non-superimposable nature of the theoretical composite curve over the experimental mixed ligand curve in the region of mixed ligand complex formation[18].

Perusal of the data (Table 2) indicates that the order of stability of [MAL] ternary complexes with respect to secondary ligands A are Pro>Gly>Ala>en. Glycine forms more stable complex than alanine owing to absence of alkyl side chain[19]. A comparison of statistical considerations (Δlog K, SUBS) and ligand basicity reveals that the order of stability of ternary complexes with respect to the donor atoms is found to be $N\text{-}O^- > N\text{-}N$. The order may be explained in terms of electrostatic interactions[20]. In the case of gly, ala and pro coordination occurs between mono positive $(M\text{-}HPQ)^+$ primary complex and uninegative gly, ala and pro (A^-) by following Eqn. 4.

$$[M\text{-}HPQ]^+ + A \rightleftharpoons [M\text{-}HPQ\text{-}A] \quad (3)$$

(where A^- = gly, ala and pro)
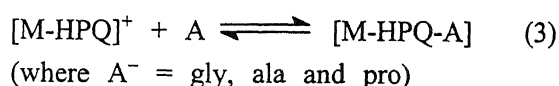
In the case of en, it is between $[M(HPQ)]^+$ and neutral ligand en (A) by following Eqn. 4,

$$[M\text{-}HPQ]^+ + A \rightleftharpoons [M\text{-}HPQ\text{-}A]^+ \quad (4)$$

(where A = en)
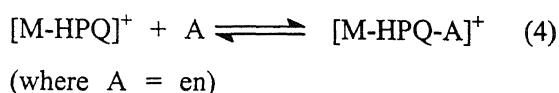
Therefore more electrostatic attraction is expected between mono positive primary complex $[M\text{-}HPQ]^+$ and uninegative ligands i.e., gly, ala and pro than between mono positive primary complex $[M\text{-}HPQ]^+$ and neutral ligand i.e., en.

The extent of favoured formation of the ternary complexes can be inferred from Δlog K values.[21] The negative Δlog K values (Table 2) reveal that the formation of ternary complexes is not favoured over that of binary complexes. This may be due to the availability of lesser number of coordinating sites for A (where A= gly, ala,

Table 2 – Stability constants for ternary complexes of M(II)-HPQ-A.
Temp. = 30°C, Medium=10%(v/v) aqueous ethanol, I = 0.1 $MKNO_3$

A	Co^{II}			Ni^{II}			Cu^{II}			Zn^{II}		
	$\log K^{ML}_{MLA}$	Δlog K	SUBS	$\log K^{ML}_{MLA}$	Δlog K	SUBS	$\log K^{ML}_{MLA}$	Δlog K	SUBS	$\log K^{ML}_{MLA}$	Δlog K	SUBS
gly	4.49	–0.15	0.469	5.09	–0.69	0.532	6.15	–2.00	0.643	5.19	0.11	0.542
ala	4.20	–0.11	0.433	4.53	–0.87	0.467	6.95	–1.18	0.717	5.10	–0.50	0.526
pro	4.30	–0.80	0.414	6.00	0.05	0.578	7.67	–1.16	0.739	5.36	–0.29	0.516
en	4.13	–2.13	0.439	4.32	–2.64	0.460	5.61	–4.85	0.597	4.70	–1.11	0.500

Table 3 – Thermodynamic parameters for the formation of 1:1 and 1:2 metal chelates of HPQ.

Medium : 10% (v/v) aqueous methanol, I = 0.1 M KNO_3
Temp: 30^0 C

M^{III}	1:1 Complex			1:2 Complex		
Ion	$-\Delta G$	$-\Delta H$	ΔS	$-\Delta G$	$-\Delta H$	ΔS
Co^{II}	911.06	723.37	148.04	750.94	695.91	43.41
Ni^{II}	960.69	667.21	231.48	782.95	706.80	60.07
Cu^{II}	1037.42	527.65	403.10	909.73	574.77	264.21
Zn^{II}	933.20	589.42	271.17	791.10	606.06	145.96

pro and en) on primary complex [M(II)-HPQ] than on the free transition metal ions.

Effect of Temperature : Formation constants obtained at different temperatures has been used in the evaluation of thermodynamic parameters accompanying the formation of metal complexes[22-24].

For all the chelates studied, the negative ΔH and the positive ΔS values (Tables 3 & 4) obtained indicate that both enthalpy and entropy factors are favouring the chelate formation. The decrease in the log$K$ values with the increase in the temperature shows that the reactions are exothermic. This probably resulted from the covalent interaction between the metal ions and carbonyl oxygen of the ligands. The positive entropy changes could be due to the displacement of water molecules from the hydration shells of interacting ions, which accompanies the essentially electrostatic interaction between the positively charged metal ion and negatively charged oxygen of the hydroxyl group of the ligand HPQ. The order of log K^{ML}_{MLA} values for the metal ions is found to be Cu(II) > Zn(II) > Ni(II) > Co(II).The $-\Delta G$ and $-\Delta H$ values also follow the same order. Thus the observed stabilities can be explained using their thermodynamic quantities.

Structural analysis of binary complex : Formation of binary complex of Co^{II}–HPQ is also supported by the spectral data. The ligand contains hydroxyl group at 3-position. The characteristic band of the hydroxyl group at 3400-3600 cm^{-1} is absent and instead a broad band at 3200-3100 cm^{-1} appears which can be attributed to a hydrogen bonded type of hydroxyl group with oxygen of amide carbonyl group[25]. The disappearance of this band in the complexes indicates deprotonation followed by coordination to the metal ion. In addition to this ligand display a band around 1700 cm^{-1} characteristic of carbonyl group. This shifts by 20-40 cm^{-1} towards lower wave numbers in the complexes indicating that the oxygen of carbonyl group is also involved in coordination[26]. The ^{1}H-NMR spectra of Co^{II}–HPQ display a down field signal at δ 10.2 indicating that the hydroxyl proton is hydrogen bonded. The disappearance of this signal in the complex confirms deprotonation and participation of oxygen in the M-L bond formation.

Table 4 – Formation cosntants log K^{ML}_{MLA} of Cu(II)-A-HPQ ternary complexes at different temperatures and thermodynamic parameters.

Medium : 10% (v/v) aqueous methanol,
Ionic strength = 0.1 M KNO_3

A	Temp.			Thermodynamic parameters		
	20^0C	30^0C	40^0C	$-\Delta G$	$-\Delta H$	ΔS
gly	6.33	6.15	5.98	1127.17	873.77	199.87
ala	7.13	6.95	6.79	1167.48	451.15	565.03
pro	7.85	7.67	7.51	1226.84	409.29	644.87
en	5.79	5.61	5.41	1038.50	557.22	379.87

Acknowledgements

The authors (P.N. and P.M.R.) are grateful to C.S.I.R. and U.G.C., New Delhi respectively for the award of Fellowships.

References

1. Shukla, J. S., Srivastava & Bina (1985) *Indian J. Pharm. Sci.* 47 (4) : 168.
2. Mamalis, P., Rix, M. J. & Sarsfield, A. A. (1965) *J. Chem. Soc.* 6278.

3. Tanaka, K., Matuo, Nakanishi, A., Kataoka, Y., Takase, K. & Otsuki, S. (1988) *Chem. Pharm. Bull.* **36(7)** : 2323.

4. Reddy, D. S. & Reddy, P. S. N. (1996) *Syn. Comm..* **26(15)** : 2843.

5. Vogel, A L (1985) *Text book of Quantitative Inorganic Analysis* , 4th Edition ELBS, Longman, London.

6. Flashka, H. A. (1964) *EDTA Titrations*, Pergamon Press, Oxford.

7. Vogel, A. L. (1984) *Text book of Practical Organic Chemistry,* ELBS, London.

8. Irving, H. M. & Rossotti, H. S. (1953) *J. Chem. Soc.* 3397.

9. Irving, H. M. & Rossotti, H. S. (1954) *J. Chem. Soc.* 2904.

10. Ramamoorthy, S. & Santhappa, M. (1971) *Indian J. Chem.* **9** : 381.

11. Ramamoorthy, S. & Santhappa, M. (1970) *J. Inorg. Nucl. Chem.* **32** : 1623.

12. Martell, A. E. & Motekaitis, R. J. (1988) *The Determination and Use of Stability Constants,* V C H Publishers Inc. 197-212.

13. Moitekaitis, R.J. & Martell, A.E.(1982) *Can. J. Chem.* **60** : 2403.

14. Legget, D. J. (ed) (1983) *Computational Methods for the Determination of Stability Constants,* Plenum, New York.

15. Sayce, I. G. (1985) *Talanta* **16** : 251.

16. Van Uitert, L. G. & Haas, C. G. (1952) *J. Amer. Chem. Soc.* **75** : 451.

17. Irving, H. & William, R. J. P. (1953) *J. Amer. Chem. Soc.* **8** : 92.

18. Carey, G. H. & Martell, A. E. (1976) *J. Amer. Chem. Soc.* **89** : 2859.

19. Ramanujam, V. V. & Selvarajan, V. M. (1984) *Proc. Indian Acad. Sci. (*Chem. Sci.) **93** (8) : 1251.

20. Sigel, H. (1975) *Ang. Chem. Int. Edn* **14** : 394

21. Thompson, C. & Lorass, J. A. (1963) *Inorg. Chem.* **2** : 89.

22. Hull, J. A., Davies, R. H. & Staveley, L. A. K. *J.* (1964) *Chem. Soc.* 5422.

23. Taqui Khan, M. M. & Martell, A. E. (1966) *J. Amer. Chem. Soc.* **88** : 668.

24. Trivedi, J , Patel, M. S. & Vyas, D. N. (1978) *J. Indian Chem. Soc.* **55** : 980.

25. Sammour, A., Fammy, A.. F. M. & Mohmoud. M. (1973) *Indian J. Chem.,* **13** : 222.

26. Sahai, R., Agarwal, R. S. & Kushawaha, S. S. S. (1982) *J. Indian Chem. Soc.* **7** : 853.

PROC. NAT. ACAD. SCI. INDIA, 75(A), II, 2005

Major steam distillate constituents of *Trachyspermum stictocarpum*

AJOY K. BAURI and SUBRATA CHATTOPADHYAY*

Bio-Organic Division, Bhabha Atomic Research Centre, Mumbai- 400085, India.

Received July 13, 2004; Accepted September 27, 2004

Abstract

The steam distillate of the spice, *T. stictocarpum* seeds was analyzed by GLC and GC-MS techniques. The terpenoid constituents of the essential oil was different than those present in another related spice, *T. ammi* seeds. Interestingly, the *T. stictocarpum* seeds were found to contain various bioactive oxygen heterocycles including medicinally important coumarins such as dihydropsoralin, seselin and bergapten.

(**Keywords** : wild ajowan/*Trachyspermum stictocarpum*/ Umbelliferae/GC-MS analysis)

Introduction

Plants in the genus *Trachyspermum* are valued for their medicinal activities[1], besides their extensive use as spices in domestic cooking. Various species of the plants are used in some of the ayurvedic preparations. Amongst the different *Trachyspermum* species[2], most of the scientific investigations have been carried out with *T. ammi* (ajowan). The seed extract of *T. ammi* exhibits antispasmodic and stimulant activities, and is prescribed as a household remedy for indigestion. Besides, the seed extract is reported to possess anti-bacterial, anti-fungal[3,4], antioxidant[5] and molluscidal activities[6]. The seeds are also used in pickle, certain types of biscuits, confectionary and pan mixtures due to their pleasant aroma. The steam volatiles of the *T. ammi* seeds have been investigated extensively and variations in the chemical constituents are reported[7,8] in different varieties.

The plant, *T. stictocarpum* (wild ajowan, aajmoda in Hindi and randhuni in Bengali) is cultivated for the seeds that are commonly used as a spice because of its pleasant aroma. The plant is an erect, branched up to 90 cm tall, cultivated mainly in north-eastern i.e. West Bengal, Bihar Assam, Orissa, Uttar Pradesh and north-western i.e. Gujarat, Rajasthan parts of India. The fruits are ovoid, aromatic cremocorps, 2-3 mm long, grayish-brown in colour, mericarps impressed with distinct ridges and tublar surface and one seeded[2]. The minor crops are grown in cold weather especially in the winter season in India. Several commercial types of the crop are available in the markets in different names, in accordance to their origin. Some of the best quality, comparatively small seeded varieties are produced chiefly in West Bengal. Its use in Indian traditional medicines is also documented[9]. So far no phytochemical investigation on the seeds of *T. stictocarpum* is reported in literature. Given the importance of the seeds as food-additive and in traditional medicine, the compositions of the steam distillate of the *T. stictocarpum* seeds were analyzed by GC-MS. This has led to the new finding of the presence of coumarins like seselin and bergapten that are known[10] to possess impressive anti-tumour and anti-cancer activities. Herein, the results are presented.

Materials and Method

T. stictocarpum syn. *Carum stictocarpum* (Lin.) seeds of good quality were procured from a local market in Mumbai. Other chemicals including solvents used were of analytical grade. The GLC analyses were performed with a Chemito chromatogram using a 3% OV-17 column, 40 ml/ min N_2 as the carrier gas, a temperature program

80-240 @ 4 ^{0}C/min and a flame ionization detector. The GC-MS analyses were carried out with a Fission MD-800 gas chromatogram-mass spectrum instrument using a 5% DB-5 splitless capillary column (30 M x 0.25 mm), 2 ml/min. He as the carrier gas and a temperature program 80-240 @ 4 ^{0}C/min. and a mass detector. The GC-MS data were analyzed by comparing the mass spectral data with those obtained from the respective authentic samples as well as library search available in Fission 800 series. The ^{1}H NMR spectra were recorded with a Bruker AC 200 (200 MHz) spectrometer.

Preparation of the steam distillate : The cleaned powdered seeds (200 g) along with distilled water (400 ml) was taken in a three-necked round bottom flask fitted with a steam generator. The apparatus was assembled for the downward distillation and the distillate obtained by passing steam was condensed and collected in a receiver. The distillation was complete in two hours. The distillate was extracted with ether, and analyzed by GLC.

Chromatographic fractionation of the steam distillate : The steam distillate (1.5 g) was loaded on a silica gel (200 g) column, which was eluted with solvent mixtures of increasing polarity as mentioned in Table 1. Five fractions of 250 ml. were collected and each fraction was individually analyzed by. The results obtained by analysis in details are given below.

Results and Discussion

In order to analyze the essential oil composition of the *T. stictocarpum* seeds, these were subjected to steam distillation to obtain the steam distillate in 2% w/w yield of the dry seeds. The essential oil was directly analyzed by GLC using a temperature programming. The terpenoids such as α-cadenene, ocimene, carvone, citral, jasmonene, dihydropsoralin, α-terpeineol were the major constituents, as revealed by comparison of the GLC data with those of authentic samples. In addition, minor components such as α-pinene, β-pinene, jasmone, jasmonol, dehydro-borneol, borneol, *p*-carveol, linalool, lavendulol and isocyclocitranal were also present in the essential oil.

However, some of the GLC peaks were unresolved, even when the analyte concentration was low. Hence, a part of the steam distillate was fractionated using a silica gel column and eluting with a gradient solvent system. Five fractions, each of 250 ml were collected, which were individually analyzed by GLC, while the major constituents

Table 1 – Chemical composition of the major constituents of the steam distillate of *T. stictocarpum* seeds

Fraction No.	Eluent	Yield (mg)	Composition
1	hexane	700 (46.7%)	α-pinene (1.1%), ocemene (2.0%), β-pinene (1.3%), carane (10.2%), α-cadenene (0.3%), β- cadenene (3.5%), β-germacrene (4.4%), δ-selinene (6.3%), isocaryophyllene (5.6%).
2	2.5% EtOAc/hexane	350 (35%)	isocyclocitranal (0.5%), *p*-carveol (1.0%), citral (2.0%), jasmonene (3.0%), carvone (3.6%), carvacrol (trace), linalool (trace), patchouli alcohol, methyl undecanoate, 6-(penta-1,3 dienyl)-6-(acetoxy methyl) δ-valerolactone.
3	5-10% EtOAc/hexane	150 (10%)	lavendulol (0.2%), α-terpeneol (1.4%), *p*-mentha-3-ene-9-ol (1.7%), jasmine (1.2%), jasmonol (1.3%).
4	15-20% EtOAc/hexane	80 (5.4%)	dehydroborneol (1.0%), borneol (1.1%), dihydropsoralin (1.5%), seselin (0.4%).
5	25% EtOAc/hexane	25 (1.7%)	4-hydroxy-6-methoxybenzopyran (trace), 5-hydroxybenzopyran, 6-hydroxy-4-methoxybenzofuran (0.65%), 5-hydroxycoumarin (0.22%), bergapten (0.68%).

were identified by GC-MS. The mass spectral fragmentation patterns of the constituents were compared with those available in the mass library. The details of analyses conditions are given in the Materials and Methods section. The major constituents of the fraction-1 were carane, selinene, isocaryophyllene, β-cadenene and β-germacrene. In addition, small amounts of α-pinene, β-pinene, ocimene and α-cadenen were also detected in this fraction. Likewise, citral, jasmonene, carvone and some alkyl derivatives of δ-valerolactones were the major constituents of fraction-2, while fraction-3 contained α-terpineol, menthol, jasmone and jasmonol. Surprisingly, besides the terpenoids such as dehydroborneol and borneol, fraction-4 also contained the coumarins, dihydropsorlin in substantial amount and a trace amount of seslin. Significant amounts of the coumarins and other benzopyran derivatives were also found in the last fraction. Of these, the major constituent, bergapten could be easily identified from its ^{1}H NMR spectrum. Identification of the other constituents are in progress. The chemical composition of the essential oil of *T. stictocarpum* seeds is summarized in Table 1.

Earlier, the esential oil of *T. ammi* seeds have been reported[8] to contain thymol (39.4%), γ-terpenine (30.97%) as the major constituents along with β-pinene (5.45%) and α-pinene (1.48%). Further, the presence of cumene and carvone were also reported in some varieties of the seeds. In comparison, the major constituents of the *T. stictocarpum* seeds were carane (10.2%), isocaryophyllene (5.6%), δ-selinene (6.3%), β-germacrene (4.4%), carvone (3.6%), β-cadenene (3.5%), jasmonene (3.0%). In addition, some other important terpenes present were citral (2.0%), ocimene (2.0%), jasmonol (1.3%) and jasmone (1.2%) and borneol (1.08%). However, most strikingly, the seeds were found to be rich source for various bioactive hydroxybenzopyrans, benzofurans and coumarins. These include compounds such as dihydropsoralin, seselin and bergapten, which are extremely valued in medicinal science for use against leucoderma, cancer and tumour.

References

1. Tare, V. (2000-2001) *J. Medicinal and Aromatic Plants Sci.* **22-23 (4A-1A)** : 120.
2. Barclay, E.L. & Watson, M.F (1998) *Kew Bull.* **53** : 897.
3. Singh, J. & Tripathi, N.N (1999) *Flavour and Fragrance J.* **14** : 1.
4. Singh, I. & Singh, V.P. (2000) *Phytomorphology* **50** : 151.
5. Mehta, R.L., Zayas, F.J. & Yang, S.-S. (1994) *J. Agric. Food Chem.* **12** : 1420.
6. Singh, S., Singh, V.K. & Singh, D.K. (1998) *Malaysian Appl. Biol* **27** : 45.
7. Choudhury, S., Ahmed, R. & Karjilal P.B (1998) *Essential Oil Res.* **10** : 588.
8. Nagalakshmi, S., Shanakarachyarya, N.B., Naik, J.P. & Rao, L.J.M. (2000) *J. Food Sci. Technol.* **37** : 277.
9. *Wealth of Indian Raw Materials* (1997) CSIR Publ., New Delhi, Vol 10, pp. 267-270.
10. Huang, L., Kashiwada, Y., Cosentino, L.M., Fan, S., Chen, C.-H., McPhail, A.T. Fujioka, T., Mihashi, K. & Lee, K.-H. (1994) *J. Med. Chem.* **37** : 3947.

PROC. NAT. ACAD. SCI. INDIA, 75(A), II, 2005

Heterobinuclear complex formation by transition metal ions with diethylenetriaminepentacetic acid

BIPIN K. SRIVASTAVA, V. SHANKAR and V. KRISHNA*

Department of Chemistry, University of Allahabad, Allahabad –211002 India..

E-mail: vkprochem@ yahoo.com

Received August 4, 2004; Accepted September 27, 2004

Abstract

The formation constant for ternary metal complexes $M^{I}M^{II}L$, where L= diethylenetriaminepentacetic acid (DTPA) and $M^{I}=Cu^{II}$, $M^{II}=Co^{II}$, Ni^{II}, Zn^{II} and Cd^{II} have been determined. The mixed metal complex formation of diethylenetriaminepentacetic acid with Cu^{II}-Co^{II}, Cu^{II}-Ni^{II}, Cu^{II}-Zn^{II}, and Cu^{II}-Cd^{II} has been studied. All the studies have been carried out by pH titrimetry at 37°C and I = 0.1M ($NaNO_3$) and computations have been made with the aid of SCOGS computer programme.

(Keywords : potentiometric study/heterobinuclear complex/ DTPA)

Introduction

Polyaminopolycarboxylate ligands, both linear and cyclic are currently used in medical applications to prepare metal complexes with radioisotopes for Magnetic Resonance Imaging[1]. Diethylenetriaminepentacetic acid has been widely used as antidote[2,3] compounds in heavy metal detoxication. It is an octadentate pentabasic acid and possesses the possibilities for the formation of mixed metal complexes. Heterobimetallic complexes involving more than one metal ion of the same or of different type may prove as better models for mixed metal system. Copper is an important trace element for plants and animals[4,5]. Such complexes are of importance in the study of biofluids particularly when hyper-accumulated metal ions are present for physiological or pathological reasons[6]. Mutual influences between metal ions may be of antagonist or of synergistic nature[7]. Also the mixed metal complexes are very common in enzymatic processes[8,9]. We have recently investigated[10,11] the heterobinuclear complexes of mercury (II) – DTPA with certain metal ions. In the present paper we report the potentiometric studies of the formation constants of heterobinuclear complexes of Cu^{II} with diethylenetriaminepentacetic acid and Co^{II}, Ni^{II}, Zn^{II}, Cd^{II}, as secondary metal ions.

Materials and Method

All the reagents were of A. R. grade. A stock solution (0.01M) of diethylenetriamine pentacetic acid (DTPA) was prepared by dissolving it into two equivalent NaOH and metal salt (Cu^{II}, Co^{II}, Ni^{II}, Zn^{II}, and Cd^{II} nitrate). Solutions were prepared in double distilled water and standardized by complexometric EDTA titration[12], pH was measured using a Century cp 901s pH meter (accuracy ± 0.01) at 37°C temperature. The reaction mixture were prepared keeping the total volume 50.0ml, I=0.1M($NaNO_3$) free acid concentration 0.002M(HNO_3), metal ion and ligand concentration 0.001M. The ratio 1:1:1 was kept of $M^{I}LM^{II}$. All the mixtures were then separately titrated with carbonate free 0.1M NaOH solution[13]. Ionic product of water (K.W.) and activity coefficient of hydrogen ion under the experimental conditions were obtained from literature[14,15].

Results and Discussion

The overall stability constants (β_{pqrst}) of ternary complexes are expressed as follows

$$pM_1 + qM_2 + rL_1 + sL_2 + t(\mathrm{OH}) \Leftrightarrow (M_1)_p\,(M_2)_q\,(L_1)_r\,(L_2)_s\,(\mathrm{OH})_t$$
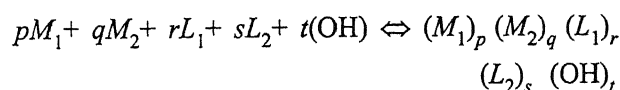
$$\beta_{pqrst} = \frac{[(M_1)_p (M_2)_q (L_1)_r (L_2)_s (OH)_t]}{[M_1]^p [M_2]^q [L_1]^r [L_2]^s [OH]^t}$$

where the stoichiometric numbers p, q, r, and s are either zero or positive integer and t is a negative integer for a protonated species. Positive integer for a hydroxo or a deprotonated species and zero for a neutral species. Complex formation equilibria have been derived on the basis of distribution curves of the complexes occuring at different pH. The β_{pqrst} values were evaluated using SCOGS computer programme[16]. The overall stability constant values are reported in Tables (1-2) and some representative distribution curves are shown in Fig. (1-4).

Table-1 – Proton ligand constants, M^{II}-ligand binary constants in aqueous solution at 37 ± 1°C and I = 0.1M $NaNO_3$.

	p	q	r	s	log β
(a) Proton - ligand formation constants :					
LH_5	0	0	1	–5	27.68
LH_4	0	0	1	–4	25.86
LH_3	0	0	1	–3	23.21
LH_2	0	0	1	–2	18.90
LH	0	0	1	–1	10.45
(b) Metal-ligand binary constants :					
CuL	1	0	1	0	21.38
CoL	0	1	1	0	19.15
NiL	0	1	1	0	20.17
ZnL	0	1	1	0	18.29
CdL	0	1	1	0	19.0

As is revealed from the species distribution curves, H_3L, H_2L and HL types of protonated species of the ligand are found to exist in decreasing order of the concentration with the gradual rise in pH. Deprotonation equilibria of the carboxyl groups of DTPA may be shown according to equation

$$H_3L^{2-} + OH^- \Leftrightarrow H_2L^{3-} + H_2O$$

$$H_2L^{3-} + OH^- \Leftrightarrow HL^{4-} + H_2O$$

$$HL^{4-} + OH^- \Leftrightarrow L^{5-} + H_2O$$
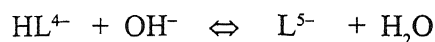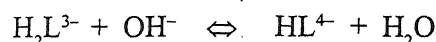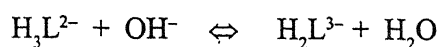
The octadentate ligand DTPA forms the binary complexes with Cu, Co, Ni, Zn, Cd, metal ions in aqueous solutions.

Table 2 – Stability constant values for the mixed-metal complexes of DTPA at 37 ± 1°C and I = 0.1M $NaNO_3$

Reactions	log β
$Cu^{II} + DTPA^{5-} + Co^{II} \Leftrightarrow [Cu^{II}\text{-DTPA-}Co^{II}]^-$	24.73
$Cu^{II} + DTPA^{5-} + Ni^{II} \Leftrightarrow [Cu^{II}\text{-DTPA-}Ni^{II}]^-$	26.60
$Cu^{II} + DTPA^{5-} + Zn^{II} \Leftrightarrow [Cu^{II}\text{-DTPA-}Zn^{II}]^-$	27.09
$Cu^{II} + DTPA^{5-} + Cd^{II} \Leftrightarrow [Cu^{II}\text{-DTPA-}Cd^{II}]^-$	26.99

Cu^{II} and the secondary metal ions M^{II} taken under study are existent in the free state and there is a gradual fall in their concentration with the rise in pH from ~2.25 to 4.5. The buffer region at pH >2.5 may be due to metal- induced
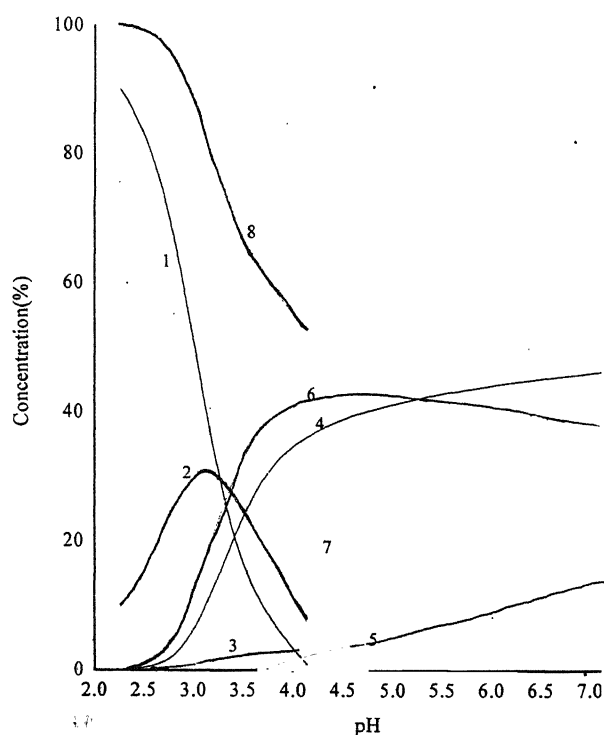
Fig. 1– Species distribution curves of Cu^{II}-DTPA-Co^{II} system, (1) H_3L, (2) H_2L, (3) HL, (4) Cu^{II}-DTPA, (5) Co^{II}-DTPA, (6) Cu^{II}-DTPA-Co^{II}, (7) Cu^{II}, (8) Co^{II}.
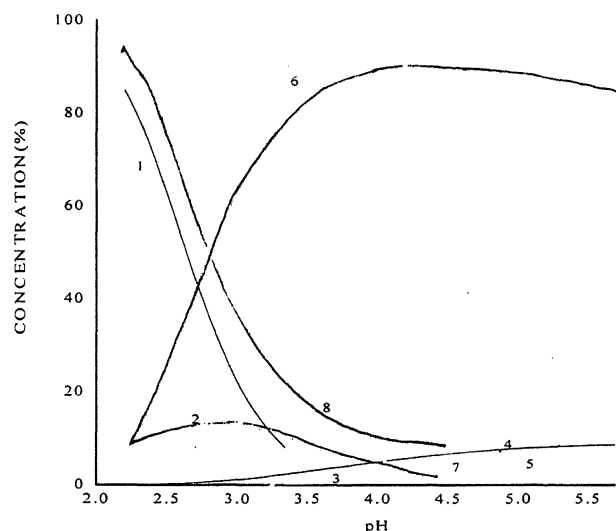
Fig. 2 – Species distribution curves of Cu^{II}-DTPA-Ni^{II} system, (1) H_3L, (2) H_2L, (3) HL, (4) Cu^{II}-DTPA, (5) Ni^{II}-DTPA, (6) Cu^{II}-DTPA-Ni^{II}, (7) Cu^{II}, (8) Ni^{II}.
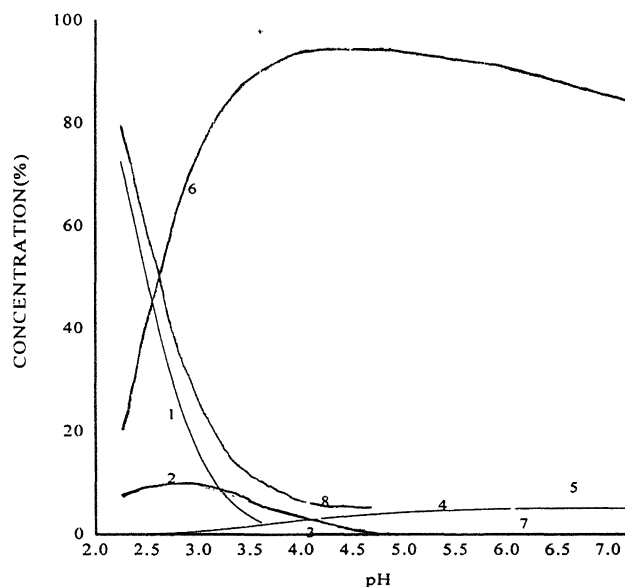
Fig. 3 – Species distribution curves of Cu^{II}-DTPA-Zn^{II} system, (1) H_3L, (2) H_2L, (3) HL, (4) Cu^{II}-DTPA, (5) Zn^{II}-DTPA, (6) Cu^{II}-DTPA-Zn^{II}, (7) Cu^{II}, (8) Zn^{II}.

deprotonation of the ligand. Both the metal ions i.e. Cu^{II} and M^{II} are found to co-ordinate with the ligand forming binary complexes Cu^{II}-L and M^{II}-L, which are making their first appearance at pH~2.25 and passing through a wide maxima in the pH range ~2.25 to 4.0 and 3.5 to7.5.

The formation of binary complex species is governed according to the following general equilibria :
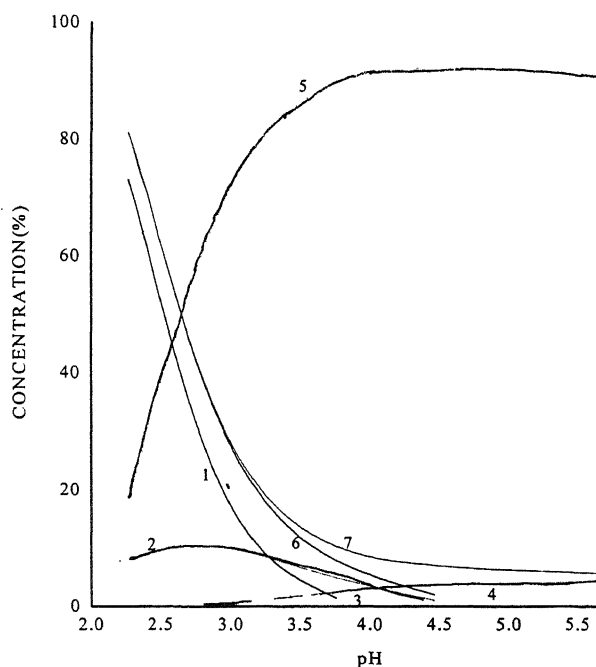
Fig.4 – Species distribution curves of Cu^{II}-DTPA-Cd^{II} system, (1) H_3L, (2) H_2L, (3) HL, (4) Cu^{II}-DTPA, (5) Cu^{II}-DTPA-Cd^{II}, (6) Cu^{II}, (7) Cd^{II}

$$DTPA^{5-} + Cu^{II} \Leftrightarrow [Cu^{II}\,DTPA]^{3-}$$

$$DTPA^{5-} + M^{II} \Leftrightarrow [M^{II}\,DTPA]^{3-}$$
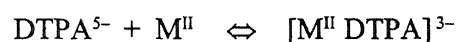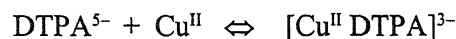
Speciation curves (Fig. 1-4) clearly show the remarkable presence of 1:1:1 heterobimetallic complex, $Cu^{II}LM^{II}$ in all the systems under study which is forming right from the very beginning of the titration – it shows that there is a simultaneous process of complex formation and the process of heterobinuclear complex formation follows the equilibrium.

$$Cu^{II} + DTPA^{5-} + M^{II} \Leftrightarrow [Cu^{II}\,DTPA\,M^{II}]^{-}$$

The larger and steep fall in the concentration of Cu^{II} in comparison to M^{II} indicates the involvement of the former in binary as well as ternary complexation. There is a gradual incline in the concentration of mixed metal complex in the pH range ~2.25 to 4.0 with the concomitant decline in the concentration of free metal ions as well as protonated ligand species. The completely deprotonated ligand which becomes available in greater quantity with rising pH interacts with the

other metal ion M^{II} forming the heterobimetallic complexes.

The binary complex is expected to involve six co-ordinate octahedral arrangement around Cu^{II} as this is the most preferred coordination for Cu^{II} metal ion[17], in the species Cu^{II} DTPA. The Cu^{II} is expected to be bound to two amino nitrogen and four carboxylic groups in a octahedral fashion and it has still some vacant coordination sites available for interaction with another metal ion and thus making the formation of heterobinuclear complex (Cu^{II} DTPAM^{II}) possible. The stability constants of heterobinuclear complexes follows the Irving -Williams order Co < Ni < Cd < Zn.

References

1. Swanson, D.P., Chilton, H.M. & Thrall, J.H. (1989) *Pharmaceuticals in Medical Imaging*, McMillan Publishing Co., Inc., New York.
2. Cantilena, L.R. & Klassen, C.D. (1982) *Toxicol. Appl. Pharmacol.* **63** : 173.
3. Behari, J.R. & Gregoriadis, G. (1992) *Int. J. Pharmaceutics* **79** : 213.
4. Gaudin, D. & Fellman, J. H. (1967) *Biochem. Biophys. Acta* **141** : 64.
5. Sigel, H. (1974) *Metal Ions in Biological Systems,* 3, Marcel Dekker, New York.
6. Amico, P., Arena, G., Daniele, P.G., Ostacoli, G., Rizzarelli, E. & Samaranto, S. (1985) *Environ. Inorg. Chem.* 285.
7. Williams, D.R. & Thomas C.C. (1976) *An Introduction to Bioinorganic Chemistry,* Springer, Illinois.
8. Eichhorn, G.L. (1973) *Inorganic Biochemistry,* Vol. 1 & 2, Elsevier, Amsterdam.
9. Zavier, A.V. (1986) *Frontiers in Bioinorganic Chemistry,* VCH, Verlagsgesellschaft, Weinheim.
10. Singh, K.P., Mishra, G.K. & Krishna, V. (2000) *Proc. Nat. Acad. Sci. India* **70A**(III) : 233.
11. Mishra, G.K., Singh, K.P. & Krishna, V. (2002) *J. Indian Chem. Soc.* **79** : 753.
12. Welcher, F. J. (1975) *The Analytical Uses of Ethylenediamine Tetra Acetic Acid.* D.Van Nostarand, New York, 164.
13. Schwaszenbach, G. & Biderman, W. (1948) *Helv.Chim. Acta* **31** : 331.
14. Wolleym, E. M., Hurkot, D.G. & Helper I. J. (1970) *J. Phys. Chem.* **70** : 3908.
15. Harned, H.S. & Owen, B.B. (1958) *The Physical Chemistry of Electrolytic Solution*, Reinhold, New York. 639.
16. Sayce, I.G. (1968) *Talanta* **15** : 1397.
17. Cotton, F. A. & Wilkinson, G. (1988) *Advanced Inorganic Chemistry*, 5th Edn. Reinhold, New York.

PROC. NAT. ACAD. SCI. INDIA, 75(A), II, 2005

The role of melt microstructure in the crystallization of borates

SANGEETA* and S.C. SABHARWAL

Crystal Technology Laboratory, TPPED, Bhabha Atomic Research Centre, Trombay, Mumbai-400 085, India.

**Corresponding author, FAX: +91 022 5505151; e-mail : sangita@magnum.barc.ernet.in*

Received July 13, 2004; Accepted September 27, 2004

Abstract

The solidification behaviors of some of the technologically important borates *viz.* BaB_2O_4, LiB_3O_5 and $Li_2B_4O_7$ have been investigated employing differential thermal analysis and powder X- ray diffraction technique. An analysis of the results of these studies and the bulk single crystal growth of these materials, show that the microstructure of the molten state is an important factor governing the nature of solidification. A new model for crystallization has been proposed and it explains an important and unresolved issue as to why certain materials can be easily crystallized while others cannot.

(**Keywords** : borates/ differential thermal analysis/ crystallization behavior)

Introduction

The borates form an important class of materials, which find applications in the areas of non-linear optics, acousto-electronics, radiation dosimetry etc.[1-4] Some of the important materials identified for these applications are BaB_2O_4, LiB_3O_5, $Li_2B_4O_7$, and they are required in the form of high quality single crystals. Indeed, the single crystal growth of these materials is found to be quite complicated due to variety of reasons and some important ones are as follows. BaB_2O_4 may be crystallized into two different crystallographic forms commonly referred as α- and β-phases to distinguish the high and low temperature phases, respectively. It is the β-phase that exhibits excellent non-linear optical properties and hence is of interest. BaB_2O_4 melts congruently at ~1100°C and when crystallized from melt it results in the growth of α-phase crystal. During slow cooling of the grown crystal to room temperature, structural re-ordering occurs around 925°C which gives rise to cracking. The β-phase is stable below 925°C and hence the growth of this phase must be carried out below this temperature. Consequently, the single crystal growth of β-BaB_2O_4 has been conventionally attempted below the phase transition temperature of 925°C[5] by the top seeded solution growth (TSSG) technique, using Na_2O as a flux. Here, the crystals are found to have the presence of a minute amount of sodium which gives rise to residual absorption, thermoluminescence and poor crystal hardness for optical damage[6]. It is therefore important to avoid the sodium contamination in the crystals. Consequently, efforts must be made to grow β-phase crystals from pure melts, which is not easily achievable. LiB_3O_5 decomposes on melting and hence its crystal growth from melt is not feasible. The crystals have been grown by TSSG technique from boron rich solutions. One of the problem reported here is the difficulty of seeding the solution[7]. Further, the grown crystals are often found to have the presence of impurity phases as inclusions, which adversely affects their optical quality. $Li_2B_4O_7$ melts are quite viscous and as a consequence they have a strong tendency to stabilize in the glassy state. The determination of the exact conditions that promote its single crystal growth is an important issue[8].

A detailed investigation carried out on the crystallization behaviors of the borates along the lines mentioned above has brought out a novel and an important commonality in their growth behaviors. The results, for the first time, bring out the role of melt microstructure in the crystallization of borates. The mechanism of crystallization process envisaged at the microscopic level also helps to understand as to why some materials can be crystallized with relative ease, while others cannot.

Materials and Method

The polycrystalline materials used for the present investigation were synthesized by the solid state sintering method. The constituent powders of 4N purity taken in the stoichiometric proportions were thoroughly mixed and raised to the sintering temperatures, as described elsewhere[6-9]. The powder X-ray diffraction patterns for the synthesized materials were recorded using Cu Kα source so as to ensure the formation of the desired crystalline phase or to study the effect of different thermal treatments to which the materials were subjected. The solidification behaviors of the materials were investigated employing the differential thermal analysis (DTA) technique. The growth of single crystals was studied by Czochralski pulling (CZ) and top seeded solution growth (TSSG) techniques, as applicable to a particular material.

Results and Discussion

Some of the important results obtained for the three borates on their solidification behaviors and the bulk crystal growth are summarized as follows.

1. *Solidification behavior of BaB_2O_4* : The DTA plots recorded under pure oxygen and argon atmospheres for BaB_2O_4 are reproduced in Fig. 1. The melting and freezing temperatures measured under oxygen were 1104°C and 952°C. The freezing temperature measured employing a lower cooling rate of 1° min^{-1} was 955°C. This result showed that the crystallization rate is not a strong function of the cooling rate at least over the range 1-10°C min^{-1}. As may be seen from Fig. 1, the freezing under pure argon occurred around 883°C. Thus the freezing point gets considerably lowered (~80°C) under argon atmosphere. The same was the case observed when pure nitrogen atmosphere was provided. The melt oxygen stoichiometry is thought to be responsible for the observed decrease in the freezing point. The results of the thermogravimetric measurements performed on BaB_2O_4 samples under oxygen and argon atmospheres are also in agreement with this
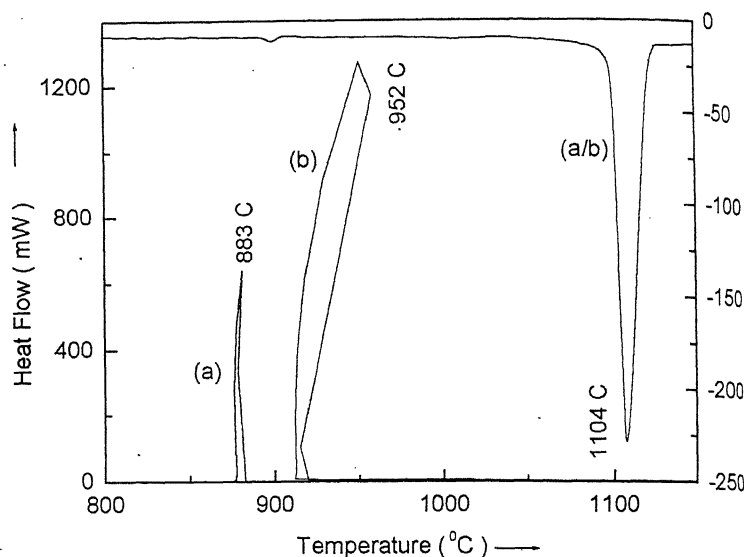
Fig. 1 – DTA plots recorded for BaB_2O_4 during heating and cooling cycles under (a) argon and (b) oxygen atmospheres.

inference. The percentage loss in the sample weight measured on heating up to the melting point under pure argon and oxygen atmospheres was 0.35 and 0.044, respectively. The weight loss on heating under argon is attributed to the selective loss of oxygen from the melt.

2. *Crystallization of LiB_3O_5 from boron rich solution* : The X-ray powder diffraction pattern recorded for the polycrystalline material is shown in Fig. 2(a). While, LiB_3O_5 is the major phase formed, the presence of some reflections corresponding to the strong lines of $Li_2B_4O_7$ phase[10,11] in the pattern also shows the presence of the impurity phase in small amount. The differential thermal analysis (DTA) plots recorded for the polycrystalline material are reproduced in Fig. 3. The material melts at 837°C, as may be seen from plot (a). When the maximum temperature is set at 860°C, one exotherm appeared at 770°C during the cooling cycle, as shown in plot (b). In a set of different experiments, the highest temperatures invoked were 870°C or higher. A typical plot obtained during the cooling cycle is shown in plot (c). The exotherm as observed in plot (b) is found to be absent here. In other words, the behavior observed during cooling cycle is a function of the highest temperature to which the
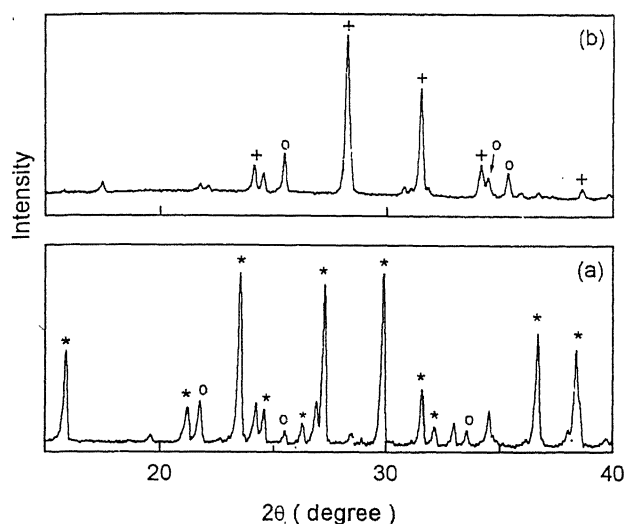
Fig. 2 – X-ray powder diffraction patterns of polycrystalline LiB_3O_5 materials (a) synthesized by solid state sintering at 750°C and (b) obtained after 1hour of thermal treatment at 900°C. Reflections corresponding to different phases are indexed as LiB_3O_5 (*), $Li_2B_4O_7$ (o) & $Li_2B_8O_{13}$(+).

material was raised during heating cycle. This result has been understood as follows. When the material is raised to just a few degrees above the melting point, the melt essentially contains the basic growth units of LiB_3O_5, which are $(B_3O_5)^{-1}$ groups. Consequently, on cooling the crystallization takes place, as revealed by the presence of exotherm in Fig. 3(b). On the other hand, when the melt is heated to a higher temperature of 870°C, the growth units of LiB_3O_5 in the melt get transformed to those corresponding to the phases formed on decomposition of LiB_3O_5 *viz.* $Li_2B_4O_7$ and $Li_2B_8O_{13}$. In order to ascertain the validity of this explanation, the XRD plots were recorded for the LiB_3O_5 materials after one-hour thermal treatments at 860°C and 900°C. In case of the material heated to 860°C, the presence of both LiB_3O_5 and $Li_2B_4O_7$ phases was revealed. However, on thermal treatment at 900°C, the transformation of LiB_3O_5 into $Li_2B_4O_7$ and $Li_2B_8O_{13}$ was clearly revealed by the XRD pattern shown in Fig.2(b). If the kinetics of reverse process was quite slow then during cooling the exotherm corresponding to the decomposed phases and not that of the LiB_3O_5 phase would be observed. Fig. 3(c) shows the absence of exotherm as observed in Fig. 3(b). The DTA plot of fig. 3(c) indeed resembles with that of recorded for $Li_2B_4O_7$ material (Fig. 5(b)), which confirms the picture envisaged.

Fig. 3 – DTA plots for LiB_3O_5 recorded during (a) heating and (b) cooling cycles, with highest temperature reached during the heating cycle equal to 860°C.The plot (c) shows the behavior during cooling cycle after the material was heated to 870°C for 4 hour.

From the above results it follows that to achieve nucleation or bulk crystal growth by flux technique, the solution should not be allowed to be over heated. The problem faced with the seeding of solution by the application of a Pt wire, as reported by Markgraf *et al.*[7] we attribute to the over heating of solution by 50°C above the
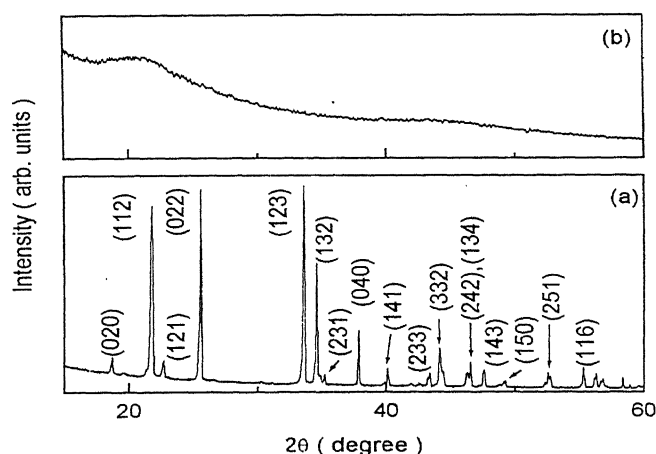
Fig. 4 – X-ray powder diffraction patterns of $Li_2B_4O_7$ material (a) synthesized by solid state sintering method, (b) obtained after heating to 950°C.

melting temperature. In order to confirm the analysis made, the bulk crystal growth of LiB_3O_5 was carried out by TSSG technique using boron oxide as a flux. Care was exercised not to raise the melt temperature more than 10°C above the saturation point. The seeding with a Pt wire could easily be achieved in this case. By employing a cooling rate of 0.1 deg h^{-1} and a pull rate of 1 mm d^{-1} good quality LiB_3O_5 crystals could be grown. The powder XRD pattern recorded for the crystal did not show the presence of any reflection due to impurity phase. The reflections corresponding to the phases $Li_2B_4O_7$[11] or $Li_2B_8O_{13}$[12] were completely missing. The DTA measurements reported on polycrystalline LiB_3O_5 (Fig. 3) were repeated using the grown crystals to ensure that the results obtained were characteristic of the particular phase and the presence of trace impurity in the polycrystalline material has no measurable effect. It is important to note that the results obtained were essentially the same as reported here for the polycrystalline material.

3. *Solidification behavior of $Li_2B_4O_7$* : A typical powder X-ray diffraction pattern recorded for the starting polycrystalline material synthesized by the solid state sintering method and reproduced in Fig. 4(a) confirms the formation of $Li_2B_4O_7$[11]. The DTA plot recorded over the temperature range
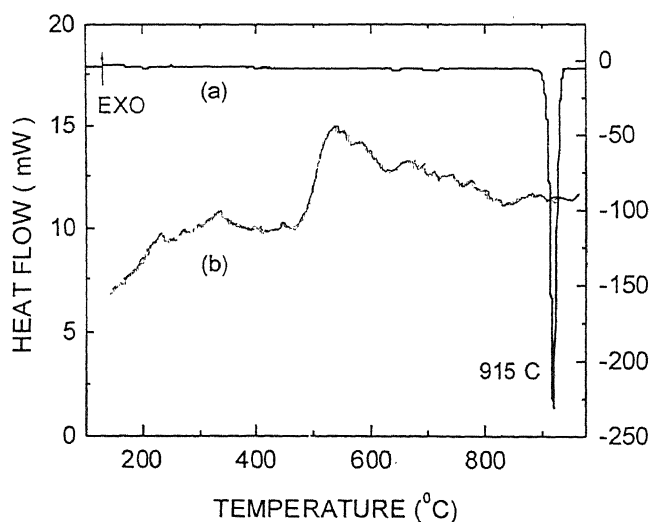
Fig. 5 – DTA plots recorded for $Li_2B_4O_7$ crystal during (a) heating and (b) cooling cycles. Maximum temperature reached: 950°C.

RT-950°C is shown in Fig.5. The plot (a) corresponds to the heating cycle and shows sharp melting at 915°C. The plot (b) was obtained during the cooling cycle employing a cooling rate of 10 deg. min^{-1}. However, the shape of this curve remained unaltered even for the lowest cooling rate of 1 deg. min^{-1} employed in our experiments. Here, the absence of an exotherm characteristic of liquid to crystalline phase transformation indicates the formation of amorphous state. In order to establish this point, the powder XRD pattern of the material having undergone a melting and cooling cycle was recorded. The plot obtained is reproduced in Fig. 4(b), which confirms the amorphous nature of the material.

The single crystal growth of $Li_2B_4O_7$ was carried out using a Pt crucible. The growth was investigated employing both low (15 deg. cm^{-1}) and high (70 deg. cm^{-1}) longitudinal temperature gradients. For seeding, a Pt wire was brought in contact with the melt and the melt temperature was gradually lowered till a small amount of the melt surrounding the wire got solidified. Presumably, this solidified mass was glassy in nature, and hence a fine necking operation was carried out prior to the commencement of bulk growth. The pulling rates used ranged between 0.5 mm h^{-1} and 2 mm h^{-1} and the rotation rates studied were in the range 5 to 60 rpm. In crystals grown at the rates higher than 0.5 mm h^{-1}, the presence of a defective central core, as also reported by Robertson and Young[13], was invariably noted. However, the application of a pull rate of 0.5 mm h^{-1}, a rotation rate of 10 rpm and higher longitudinal thermal gradient resulted in the growth of core free crystals. The powder XRD pattern recorded for the grown crystal matched very well with the plot shown in Fig. 4(a), thus confirming the formation of $Li_2B_4O_7$.

In the case of molten salt solutions, the role of viscosity has been generally invoked to explain the absence of nucleation in solutions undergoing transition to the glassy state. The role of high viscosity is envisaged as to affect the mass transport whereby the nucleation of any one of

the solution components is prevented. Consequently, the whole molten charge gets solidified before bulk crystallization can take place. However, for a pure melt like $Li_2B_4O_7$ in which case the mass transport is simply not a limiting factor, the viscosity factor alone cannot satisfactorily account for the observed results. The slow growth rates required to achieve transformation to crystalline phase suggest that the underline process must have a time dependant component. That is, on cooling some sort of reorganization in the melt takes place, which helps promoting the formation of crystalline phase. We believe that this time dependent component is related to the formation of growth units in the melt.

Proposed Mechanism for Crystallization Process

Voronko *et al.*[14] have studied the vibrational spectra of BaB_2O_4 and $CsBO_2$ both in crystalline and molten states by employing high-resolution Raman spectroscopy. In $CsBO_2$ melt while the presence of (B_3O_6) rings has been confirmed, the number of broken rings have been found to be negligible. In contrast, in BaB_2O_4 melt the chains of various lengths and not the (B_3O_6) rings have been found to be the dominant units. The $CsBO_2$ melt is observed to crystallize 5-10° below the melting point, while the BaB_2O_4 melt may be supercooled as much as 150°C before spontaneous crystallization occurs. Huang *et al.*[15] have carried out measurements for the fundamental properties like density, surface tension and viscosity of BaB_2O_4 melt within about 200°C around its melting point. Their investigation has also shown that BaB_2O_4 melt can be supercooled by at least 100° under oxygen atmosphere, which is in conformity with the results reported in the present investigation. An analysis of (i) the results on the effect of atmosphere surrounding the melt shown in the present study, (ii) the presence of borate chains in the molten state reported by Voronko *et al.*[14] and (iii) the time variation of the melt density observed by Huang *et al.*[15] shows that the breaking of the borate rings into chains of various lengths must be responsible for the large supercooling observed in this case. The results reported on $CsBO_2$ that it contains the rings same as BaB_2O_4 do confirm this inference. Concluding, the effect of atmosphere on solidification temperature has been understood in terms of the presence of molecules / species which have partially lost oxygen on melting. These impede the nucleation process by modifying the microstructure of the melt.

Zhong and Tang[16] have investigated relation of the starting compositions to the crystalline phases that form in the case of $Li_2O:B_2O_3$ solution. LiB_3O_5 contains the ringed complex anion $[B_3O_7]^{5-}$ consisting of one BO_4 tetrahedron and two BO_3 triangles. According to them, the combination of BO_4 and BO_3 in different ratios in the solution leads to the formation of various borate phases. The present results while supporting this view, have for the first time revealed the fact that the concentration of the building blocks of LiB_3O_5 also depends upon the thermal treatment of the solution. These blocks can be destroyed by heating the solution beyond 860°C whereby the growth of LiB_3O_5 phase can be completely suppressed.

If the basic building blocks of the crystalline solid exist in the melt then on cooling a transition to the corresponding crystalline state can take place with ease, otherwise, the kinetics of their formation would determine the rate of growth. Consequently, the growth rates higher than a critical value would yield an amorphous solid and the lower ones crystalline, as indeed observed by us for $Li_2B_4O_7$. The support to this model also comes from the following related observations reported in the literature: (i) The investigations reported on the physical properties of molten $Li_2B_4O_7$ in the literature show that the viscosity and density display a time dependant relaxation after the $Li_2B_4O_7$ material is completely melted and it takes a minimum of 15h for the melt to become stable, implying changes in the microstructure of the melt[17], (ii) The materials with stable melt structures show small amount of supercooling prior to solidification as for example $CsBO_2$ melt which is found to solidify 5-10° below the melting point,

(iii) The investigations in literature confirm the existence of a local ordering in $LiNbO_3$ melt that is similar to the crystal[18,19]. Notably, here the melt is found to solidify just about 30° below the melting point. The model for crystallization developed here explains as to why certain materials solidify with very small amount of supercooling and can be easily crystallized while others cannot.

References

1. Nakatani, H., Bosenberg, W.R., Cheng, L.K. & Tang, C.L. (1988) *Appl. Phys. Lett.* **53** : 2587.
2. Chen, C., Wu, Y., Jiang, A., Wu, B., You, G., Li, R. & Lin, S. (1989) *J. Opt. Soc. Am.* **B 6** :617.
3. Takeuchi, M., Odagawa, H., Tanaka, M., & Yamanouchi, K. (1997) *Jpn. J. Appl. Phys.* **36** : 3091.
4. Hubner, K., Prokert., K., Vizoco, S., & Bolorin, M. (1983) *Kernenergie* **26** : 118.
5. Feigelson, R.S., Raymaker, R.J. & Route, R.K. (1990) *Progress Crystal Growth & Characterization* **20** : 115.
6. Sangeeta, Sabharwal, S.C. (1998) *J. Crystal Growth* **187** : 253.
7. Markgraf, S.A., Furukawa, Y., & Sato, M. J. (1994) *J. Crystal Growth* **140** : 343.
8. Sabharwal, S.C., Tiwari, Babita & Sangeeta (2003) *J. Crystal Growth* **249:** 502.
9. Sangeeta, Tiwari, Babita & Sabharwal, S.C. (2004) *J. Crystal Growth* **273 :** 163.
10. Powder diffraction file No. **32-0549** *JCPDS-ICDD*, USA.
11. Powder diffraction file no. **40-0505** *JCPDF-ICDD*, USA.
12. Powder diffraction file No. **16-0200** *JCPDS-ICDD*, USA.
13. Robertson, D.S. & Young, I.M. (1982) *J. Materials Sci.* **17** : 1729.
14. Voronko, Yu.K., Gorbachev, A.V., Osiko, V.V., Sobal, A.A., Feigelson, R.S. & Route, R.K. (1993) *Phys. Chem. Solids* **54** : 1579.
15. Huang, X., Zhao, Y., Lu, K., & Tang, D. J. (1996) *J.Crystal Growth* **165** : 413.
16. Zhong, W. & Tang, D. (1996) *J. Crystal Growth* **166** : 91.
17. Y. Anzai, K. Terashima and S. Kimura (1993) *J. Crystal Growth* **134** : 235.
18. Andonov, P., Chieux, P. & Kimura, S. (1993) *J. Phys.: Condens. Matter* **5** : 4865.
19. Andonov, P., Fischer, H.E., Palleau, P. & Kimura, S. (2001) *Z. Naturforsch,* **56a** : 395.

PROC. NAT. ACAD. SCI. INDIA, 75(A), II, 2005

Synthesis and characterisation of metal complexes of tridentate Schiff base derived from benzimidazole-2-carboxaldehyde and thiosemicarbazide

N. PARVATHI* and K.L. OMPRAKASH

Department of Chemistry, Nizam College, Osmania University, Hyderabad-500 001, India.

Received December 10, 2001; Revised June 14, 2004; Re-revised October 11, 2004; Accepted December 14, 2004

Abstract

A novel new Schiff base is prepared by the condensation of benzimidazole-2-carboxaldehyde with thiosemicarbazide. The resultant ligand 2[1H-benzimidazole-2-ylmethylene] hydrazine carbothiamide (BMCT) is characterised by spectral studies. Chelates of BMCT with cobalt, nickel and copper metal ions have been isolated and characterised on the basis of their analytical, conductivity, infrared, magnetic and electronic spectral studies. The studies have indicated that ligand BMCT acts as a tridentate chelating agent coordinating through pyridyl nitrogen of benzimidazole, tertiary nitrogen of azomethine and through thiolo sulphur. The chelates of Co(BMCT) and Ni(BMCT) are 1:1 electrolytes with octahedral geometries, while Cu(BMCT) is 1:2 electrolyte, dimeric with square planar geometry. Cobalt and copper complexes are diamagnetic and Ni complex is paramagnetic.

(**Keywords** : IR/electronic spectral/magnetic/Schiff base/ octahedral legand fields/benzimidazole/2-carboxaldehyde/ thiosemicarbazide)

Introduction

A number of derivatives of benzimidazoles, thiosemicarbazide and their thiosemicarbazones act as potential chelating agents. Both these compounds also possess a wide spectrum application in medicine. Benzimidazoles show antibacterial[1], antihelmenthetic[2], fungicidal[3], antitumor[4] and anticancer[5] activities. A number of thiosemicarbazide and their thiosemicarbazones are known for their antitubercular[6], antitumor[7] and also for their activities against viruses, protozoa and smallpox[8]. In order to study the synergistic effect of benzimidazole and thiosemicarbazide moieties on the chelating tendencies of metal ions, a new multidentate heterocyclic schiff base is prepared.

The present paper deals with the isolation and characterisation of 2(1H-benzimidazole-2-ylmethylene) hydrazine carbothiamide and its cobalt, nickel and copper chelates. All the chemicals used were of AnalaR grade and solvents of reagent/spectroscopic grade. Benzimidazole-2-carboxaldehyde was prepared by following the procedure described in literature[9]. Co(II), Ni(II) and Cu(II) metal chlorides (AR) were used for the preparation of metal chelates.

Materials and Method

Synthesis of ligand : The ligand was synthesised by refluxing equimolar (.02) solution of benzimidazole-2-carboxaldehyde and thiosemicarbazide in methanol for 2 hours. The product was separated out as pale yellow coloured compound which is recrystallised from ethanol, m.p. 240°C.

Synthesis of metal complexes : The cobalt, neckel and copper complexes were prepared by refluxing equimolar (.05 moles) solutions of metal chlorides and the Schiff base in ehanol for 30 min. The resulting solid complexes were washed with methanol and acetone and dried in vaccum.

The percentage composition of metal ions in solid metal complexes were determined by using Atomic Absorption Sepectrophotometer (Perkin Elmer model 2380). Nitrogen, carbon, hydrogen and chlorides were determined by using microanalytical techniques. The molar conductances of complexes were determined using 10^{-3}M solution in methanol on Systronics Digital Conductivity Bridge (model 304). The mass spectra of the ligands were recorded on Mass Spectrophotometer

(model VG micromass 700) operating at 70eV. Magnetic susceptibilities were determined by using vibrating sample Magnetometer (Princeton Applied Research model 155). Electronic spectra of complexes (in methanol medium) were recorded on Varian Carry 2390 UV-Vis Near IR spectrophotometer in the range 1200nm-200nm. Infrared spectra (KBr disc) of ligands and metal complexes were recorded in the range 4000-400 cm^{-1} on Perkin Elmer (model 1430). The Far IR spectra of the complexes were recorded on Perkin Elmer (model 1430) in the working range 200-400 cm^{-1}. TGA data of complexes was determined using thermogravemetric analyser. The heating device consists of Hearous furnace and thermocouple system (Transistrol model) for the measurement and maintenance of temperature (upto 600°C) with a heating rate of 3°C per min.

Results and Discussion

(a) Characterisation of ligand :

Mass spectral data : The mass spectrum of the ligand exhibits a stable molecular ion peak at *m/e* 219 along with M^{+2} peak characteristic of sulphur containing compounds[10] and a fragment at M-17 (*m/e* = 202) corresponding to loss of NH_3 molecule. The chelating agent also shows fragments with *m/e* 159, 144, 131, 132, 118, 117, 91, 90 and 64 which arise due to the following three principal fragmentation patterns : (*a*) Fission between benzimidazole ring and azomethine carbon, (*b*) splitting at the bond between tertiary nitrogen of azomethine linkage and imido nitrogen of thiosemicarbazone moiety and (*c*) splitting between imido nitrogen and thionic carbon (characteristic of benzimidazole ring[11], azomethine linkage[12] and thiosemicarbazone moiety).

NMR spectra : The signals observed at δ10.85 (D_2O) exchangeable), 8.3 and 5.3 (broad and D_2O exchangeable) has been attributed to the imido proton[13], azomethine proton[14] and imino proton[15] respectively. The multiplet due to aromatic proton has been observed between 6.6 to 7.7[16]. The PMR spectrum showed a singlet at δ7.95 assignable to NH_2 proton.

(b) Characterisation of metal complexes :

All the complexes are stable in air and non-hygroscopic. They are soluble in polar organic solvents but insoluble in water and nonpolar organic solvents. The analytical data of the complexes, presented in Table 1, reveal that the metal to ligand ratio in Cu(II) and Ni(II) chelates is 1:1 and is 1:2 in Co[BMCT] complex. The solubility and conductance data indicated that Co[BMCT] and Ni[BMCT] complexes are 1:1 electrolytes where as Cu[BMCT] complex is 1:2 electrolyte.

Table 1 – Analytical and physiochemical data of BMCT and its complexes.

Compd./ (Colour)	Analysis % : Found (Calcd.)						Decom. temp.°C	μ_{eff} (BM)	Conductance (mhos cm^2 $mole^{-1}$)
	M	C	H	N	Cl	S			
BMCT ($C_9H_9N_5S$)	–	49.18 (49.31)	4.08 (4.10)	31.90 (31.96)	–	14.80 (14.61)	–	–	–
$[Cu_2(BMCT)_2]Cl_2$ Green $[Cu_2(C_9H_8N_5S)_2]Cl_2$	19.92 (20.04)	34.00 (34.07)	2.48 (2.52)	22.02 (22.08)	11.15 (11.19)	11.12 (10.09)	>250	Zero	170
$[Ni(BMCT)(H_2O)_3]Cl$ Reddish brown $[Ni(C_9H_8N_5S)(H_2O)_3]Cl$	16.10 (16.03)	24.56 (24.49)	3.98 (3.82)	19.22 (19.11)	9.60 (9.68)	8.63 (8.73)	>290	2.92	96
$[Co(BMCT)_2]Cl$ Dark brown $[Co(C_9H_8N_5S)_2]Cl$	11.23 (11.11)	40.58 (40.71)	2.98 (3.01)	26.28 (26.39)	6.58 (6.68)	12.76 (12.06)	>270	Zero	108

Table 2 – IR spectral data (cm^{-1}) of BMCT and its complexes.

[BMCT]	Cu[BMCT]	Ni[BMCT]	Co[BMCT]	Assignments
3430	3430	–	3430	νas NH_2
–	–	3400	–	νOH (coordinated water)
3280	3280	--	3280	νs NH_2
3150	3090	3080	3090	νN-H (imino)
3000	–	–	–	νN-H (imido)
1620	1600	1600	1600	νC=N (benzimidazole)
1600	1580	1580	1590	νC=N (azomethine)
–	1640	1640	1640	νC=N (thiosemicarbazide)
1550	–	–	–	δNH (imido) deformation
1510	1510	1510	1510	δNH (imino) in-plane def
1470,1450	1470,1420	1470,1450	1470,1440	
1310,1275	1320,1290	1320,1280	1310,1270	ν(C-N)+δNH_2+ν(C-S)
–	1170	1170	1170	ν(C-S)
820	–	–	–	ν(C=S)
735	735	735	735	δNH (imino) out-of-plane def
–	–	870	–	H_2O (rocking) coord. water
–	–	660	–	H_2O (wagging) coord. water
–	510,420	480,400	490,410	νM-N, √M-S

IR spectra : The IR spectral data of selected vibrational modes of the ligand and its metal complexes are presented in Table 2. The ligand BMCT exhibited two IR bands of strong intensity at 3430,3280 which may be assigned to asymmetric and symmetric stretching vibrations of free NH_2 group of thiosemicarbazone[17] which do not undergo any appreciable change on complex formation indicating non-coordination of NH_2 group. The band at 3090 in the complex spectra, which is assigned to νNH of benzimidazole ring, showed a –ve shift by 60 to 70cm^{-1} suggesting the involvement of pyridyl nitrogen of benzimidazole ring in complex formation. The sharp peaks at 1620 and 1600 in the ligand spectrum are assigned to stretching vibrational modes of C=N of pyridyl group as well as the azomethine linkage[18] have suffered a negative shift by 20cm^{-1} suggesting their involvement in metal ligand bond formation. A perusal of the complex spectrum further reveals that, the ligand undergoes thioenolisation and binds to the metal ion in the thiolato form. This is evident from (i) the disappearance of νC=S band at 820, (ii) appearance of νC-S (1170), (iii) appearance of νC=N band at 1640 due to the new linkage between imido nitrogen and thiol carbon, (iv) disappearance of νNH (3000) and δNH (1550) of imido group. These facts are compatible with the enolisation of the NH-C=S group in the ligands to N=C-SH in the presence of metal ion and coordination of the metal ion through S after deprotonation. The presence of thiol form is confirmed from the appearance of new band at 1170 due to νC-S[19,20]. The complex spectrum also revealed new bands at 440 and 410 – may be attributable to νM-N and νM-S vibrational frequencies[21,22,23].

Thermogravimetric data : The thermal data indicated that Co(BMCT) and Cu(BMCT) com-

Table 3 – Electronic spectral data of the complexes.

Complex	Bands (cm^{-1})	Assignments			10Dq	B'	β	Geometry
$[CO(BMCT)_2]Cl$	19000	$^1A_{1g}$	⇒	$^1T_{1g}$	20000	500	0.47	Octahedral
	26000	$^1A_{1g}$	⇒	$^1T_{2g}$				
$[Ni(BMCT)(H_2O)_3]Cl$	9300	$^3A_{2g}$ (F)	⇒	$^3T_{2g}$ (F)	9300	773.3	0.75	Octahedral
	15800	$^3A_{2g}$ (F)	⇒	$^3T_{1g}$ (F)				
	23700	$^3A_{2g}$ (F)	⇒	$^3T_{1g}$ (P)				
$[Cu_2(BMCT)_2]Cl_2$	15625	$^2B_{1g}$	⇒	$^2B_{2g}$	–	–	–	Square planar
	25000	$^2B_{1g}$	⇒	^2E_g	–	–	–	

plexes are stable upto 170°C and did not undergo any loss in weight confirming that these two complexes do not posses any kind of water molecules. The thermogram of Ni(BMCT) indicated presence of three water molecules which are found to decompose in the temperature range between 180-220°C:

From the elemental analysis IR spectral, thermal and conductance data the stoichiometric formulae of the complexes have been computed (Table 1).

Magnetic and electronic spectral data : Co(BMCT) and Cu(BMCT) complexes are found to be diamagnetic (μ_{eff}=0) and Ni(BMCT) is paramagnetic. The diamagnetic nature in cobalt complex indicates the existence of Co(III) in low spin octahedral environment[24]. Similarly the near-
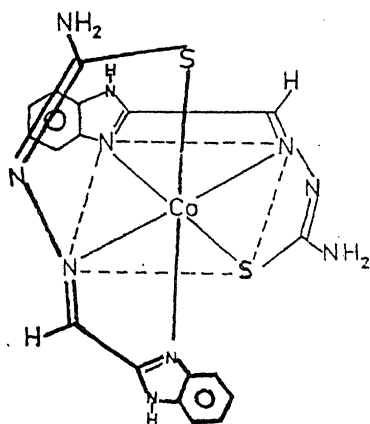
Fig. 1 – Tentative structure of $[CO(BMCT)_2]Cl$.
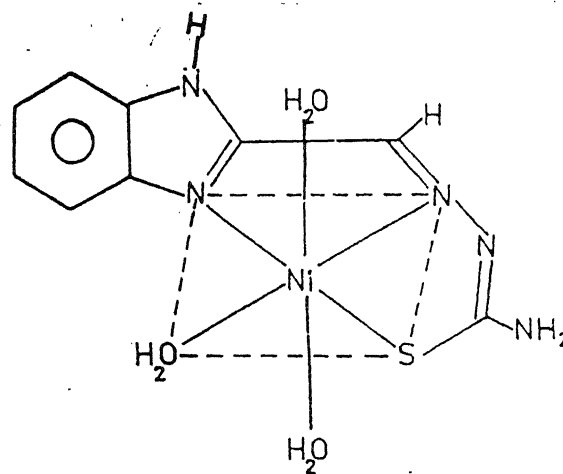
Fig. 2 – Tentative structure of $[Ni(BMCT)(H_2O)_3]Cl$.

ness of observed magnetic moments in Ni(BMCT) complex (μ=2.92) with that of spin only value (μ=2.83) indicates an octahedral geometry for it. Reports reveal that diamagnetic Cu(II) complexes invariably exist in binuclear or polynuclear forms[25-27]. It has been pointed out that strong spin-spin interaction (between two Cu(II) ions which are sufficiently close together and that results into diamagnetism) may take place by (a) the formation of σ or δ bond due to overlap of two *d*-orbitals where by the spins of the electrons are paired up. Therefore, the diamagnetic behavior observed in Cu(BMCT) complex may be attributed to a similar binuclear structure that may have resulted by the coordination of two tridentate chelating agents BMCT around the two Cu(II) ions as shown in Fig. 3. Such a binuclear structure facilitates the expected antiferromagnetic exchange interactions
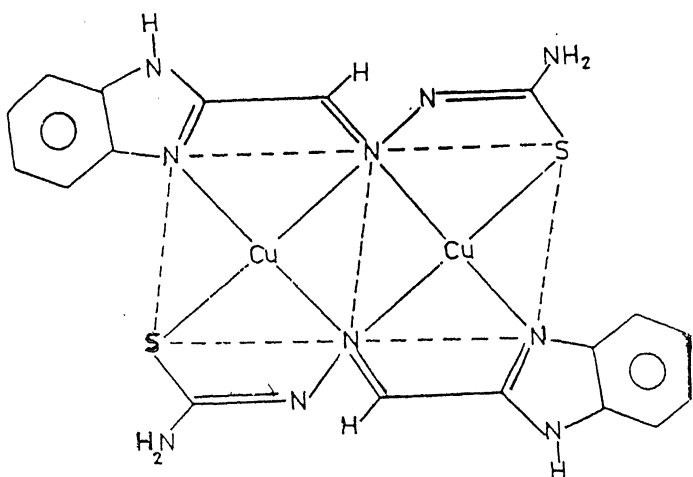
Fig. 3 – Tentative structure of dimeric complex of $[Cu_2(BMCT)_2]Cl_2$.

between two Cu(II) ions and explain the strong spin-spin interaction between the paramagnetic Cu(II) ion that result into complete quenching of magnetic moments. The fact that strong spin-spin interactions (as evident from the diamagnetic behaviour of complex) suggest that probably the Cu(II) ions in the binuclear complex might be sufficiently close to each other.

The electronic spectra of the complexes is given in Table 3 with due assignments. A perusal of number, position and assignments of bands indicated that the data is in conformity with the stereochemistries of the complexes proposed on the basis of magnetochemical data. The two bands observed in Co(III) indicates an octahedral geometry[28,29] in which the three donor atoms of the chelating molecule occupy the three equitorial positions of an octahedron while the other three vertical positions (perpendicular to the former) are occupied by the three donor atoms of the other ligand molecule. Thus each ligand maintains its co-planarity even after the complex formation. The three bands observed in Ni(BMCT) complex confirm an octahedral geometry to the complex. The two bands observed in binuclear Cu(II) complex suggest a square planar geometry[30].

On the basis of the above physicochemical data it may be concluded that the ligand act as a tridentate chelating agent coordinating through pyridyl nitrogen, azomethine nitrogen and through thiolo sulphur. Co(BMCT) and Ni(BMCT) complexes are ionic and monomeric containing octahedral ligand fields in the complex (Fig. 1 & 2). However, Cu(BMCT) is binuclear and associated with square planar ligand field (Fig. 3).

Acknowledgement

The present work has been done under the supervision of late Dr. K.L. Omprakash, Associate Professor, Department of Chemistry, Nizam College, Hyderabad. The valuable suggestions of Dr. Devdas Manwal, Associate Professor, Nizam College are gratefully acknowledged.

References

1. Omar Nabil, M. & Hussain, F. (1979) *Arch. Pharm. Chem. Scied.* 7(6) : 163.
2. Imtiaz, H.M. & Vinay Kumar, J. (1991) *J. Indian Chem. Soc.* **68** : 102.
3. Nakajima, S., Tanaka, I. & Toshio, A. (1958) *Yakugaku, Zasshi.* **78** : 1378.
4. Thomas, C. & Jerchell, D. (1971) *Ger. Offen.* 20319122.
5. Tadeo, I. (1975) *J. Cancer* **29** : 286.
6. Joshi, M.D., Jani, M.K. & Trivedi, P.B. (1991) *J. Indian Chem. Soc.* **68** : 107.
7. Dwyer, F.P., Mayhew, E. & Shulman (1965) *J. Cancer* **19** : 195.
8. Bawer, D.J., Vincent, L.S., Kempe, C.H. & Downie, A.W. (1963) *Lancet* **20** : 494.
9. Hensel, H.R. (1965) *Chem. Ber.* **98** : 1325.
10. Silverstein, R.M. & Bassler, G.C. (1967) *Spectrophotometric Identification of Compounds,* IInd edition, John Wiley & Sons, Interscience, New York.
11. Reddy, A.K. & Kheomitskiikost, A.N. (1969) *Zh. Org. Khim.* **5**(7) : 1153; Nishiwaki, T. (1968) *J. Chem. Soc.* **4** : 428.
12. Lewesson, S.O., Schroll, G. & Bowie, J.H. (1968) *Tetrahedron* **24** (4) : 1875.
13. Balakrishna, K. & Aravindashan, K.K. (1991) *J. Indian Chem. Soc.* **68** : 187.
14. Patil, S.R., Kantale, V.N. & Sen, D. (1982) *J. Indian Chem. Soc.* **59** : 1300.
15. Larima, L.I., Vakulskaya, J.I. & Najedeva, O. (1979) *Dokl. Akad. Nauk. USSR* 403.
16. King & Dust (1962) *Cand. J. Chem.* **40** : 882.

17. Burns, G.R. (1968) *Inorg. Chem.* **7** : 277; Haines, R.A. & Sun, K.W. (1968) *Cand. J. Chem.* **46** : 3241.

18. Freedman, H.H. (1961) *J. Am. Chem. Soc.* **83** : 2900; Harkins, T.R., Walter, J.L., Harris O.E. & Frieser, H. (1956) *J. Am. Chem. Soc.* **78** : 260.

19. Colthup, N.B. & Daly, L.H. (1964) *Introduction to Infrared and Raman Spectroscopy,* Academic Press, London, p. 311.

20. Srivastava, F.N. & Rashmi Rostogi, B. (1978) *J. Indian Chem. Soc.* **55** : 521.

21. Nakamato, K. (1964) *Infrared Spectra of Inorganic and Coordination Compounds,* John Wiley and Sons, Interscience, New York, p. 146.

22. Baldin, D.A., Lever, A.B.P. & Parish, R.V. (1969) *Inorg. Chem.* **8** : 107.

23. Ferraro, J.R. (1971) *Low Frequency Vibrations of Inorganic Coordination Compounds,* Plenum Press, New York.

24. Cotton, F.A. & Wilkinson, G. (1976) *Advanced Inorganic Chemistry,* John Wiley and Sons, Interscience, New York.

25. Khullar, I.P. & Agarwala, O. (1975) *Cand. J. Chem.* **53** : 1165.

26. Bhattacharya, P.K. (1982) *J. Indian Chem. Soc.* **69** : 505.

27. Harris, C.M. & Sinn, E. (1968) *J. Inorg. Nucl. Chem.* **30** : 2723.

28. Orgel, L.E. (1955) *J. Chem. Phys.* **23** : 1824.

29. Balhausen, C.J. & Maffit, W. (1956) *J. Inorg. Nucl. Chem.* **18** : 178.

30. Werden, B.C. Billing & Grey, H.B. (1963) *Inorg. Chem.* **2** : 197.

PROC. NAT. ACAD. SCI. INDIA, 75(A), II, 2005

Variations of moving load velocity at the boundary surface interface of two half spaces

RAJNEESH KUMAR and PRAVEEN AILAWALIA*

Department of Mathematics, Kurukshetra University, Kurukshetra, India.

**Department of Applied Sciences, I.E.E.T., Makhnumajra, Baddi, Distt. Solan, India.*

E-mail : rajneesh_kuk@rediffmail.com; praveen_2117@rediffmail.com.

Received October 21, 2003; Accepted June 17, 2004

Abstract

The steady state response of an orthotropic micropolar solid with an overlying elastic half-space subjected at the plane interface to a moving point load has been studied. The eigen-value approach using Fourier transforms has been employed and the transform has been inverted by using a numerical technique. The displacement and stress components in the physical domain are obtained numerically. The numerical results are illustrated graphically for a particular model.

(**Keywords** : steady state/orthotropic micropolar/eigen-value/ Fourier transform)

Introduction

In many engineering phenomenon, including the response of solids, geological materials and composites, the assumptions of an isotropic behaviour may not capture some significant features of the continuum response. The formulation and solution of anisotropic problems is far more difficult and cumbersome than its isotropic counterpart. In the recent years the elastodynamic response of anisotropic continuum has received the attention of several researchers. In particular, transversly isotropic and orthotropic materials, which may not be distinguished from each other in plane strain and plane stress, have been more regularly studied.

The theory of micropolar elasticity introduced and developed by Eringen[1] aroused much interested becasue of its possible utility in investigating the deformation properties of solids for which the classical theory is inadequate. The micropolar theory is believed to be particularly useful in investigating materials consisting of bar like molecules which exibit microrotation effects and which can support body and surface couples.

A review of literature on micropolar orthotropic continua shows that lesan[2-4] analysed the static problems of plane micropolar strain of a homogeneous and orthotropic elastic solid, torsion problem of homogeneous and orthotropic cylinders in the linear theory of micropolar elasticity and bending of orthotropic micropolar elastic beams by terminal couple. Nakamura *et al.*[5] applied finite element method for orthotropic micropolar elasticity. Recently Kumar and Choudhary[6-10] have discussed various problems for orthotropic micropolar continua.

The dynamical response to moving loads is an interesting subject in various technological and geophysical circumstances and some recent investigations are concerned with this problem. For instance, it is of great interest in solid dynamics where ground motions and stresses can be produced by blast waves (surface pressure waves due to explosions), or by supersonic aircraft. This type of investigation occurs in many branches of engineering, for e.g. in bridges and railways, beams subjected to pressure waves and piping systems subjected to two phase flow. Other applications are encountered within the context of contact mechanics like, the problem of high velocity rocket sleds sliding over steel guide rails. Most of the

moving load problems soled so far involve the use of potential functions. However, the use of eigen-value approach has the advantage of finding the solutions of equations in the coupled form directly in the matrix notations, wheras the potential functions approach requires decoupling of equations. Various authors[11-18] have discussed the problems of moving load in the theory of elastic solids. Kumar and co-workers[19-22] studied the steady state response to moving loads in micropolar theory of elasticity.

In the present paper we apply the eigen-value approach after using Fourier transformation to the moving load problem at elastic/orthotropic micropolar solid interface. The solutions are obtained in the transformed domain and are inverted by using a numerical technique.

Formulation and Solution of the Problem– We consider a normal point load moving along the interface of elastic/orthotropic micropolar solid. We consider a rectangular coordinate system (x,y,z) having origin on the surface $y=0$ and y-axis pointing vertically into the medium. Let us consider a pressure pulse $P(x+Ut)$ which is moving with a constant velocity in the negative x direction. After the load has been moving for some time and the transient effects have died away, the displacements will appear stationary in a coordinate system moving with the load.

If we restrict out attention to the plane deformation parallel to xy-plane with displacement vector $\vec{u}=(u_1, u_2, 0)$ and microrotation vector $\vec{\phi}=(0,0,\phi_3)$, the basic equations in the dynamic theory of the plane strain of homogeneous, orthotropic micropolar elastic solid in the absence of body forces and body couples, given by Eringen[23], can be recalled as

$$t_{kl,l} = \rho \frac{\partial^2 u_k}{\partial t^2}, \tag{1}$$

$$m_{k3,k} + \varepsilon_{kl_3} t_{kl} = \rho \frac{\partial^2 \phi_3}{\partial t^2}, \; k = l = 1,2. \tag{2}$$

The constitutive relations, given by Iesan[2], can be written as :

$$t_{11} = A_{11}\varepsilon_{11} + A_{12}\varepsilon_{22}, \; t_{12} = A_{77}\varepsilon_{12} + A_{78}\varepsilon_{21},$$

$$t_{21} = A_{78}\varepsilon_{12} + A_{88}\varepsilon_{21}, \; t_{22} = A_{12}\varepsilon_{11} + A_{22}\varepsilon_{22},$$

$$m_{13} = B_{66}\phi_{3,1}, \; m_{23} = B_{44}\phi_{3,2}, \tag{3}$$

where

$$\varepsilon_{kl} = u_{l,k} + \varepsilon_{lk3}\phi_3 \tag{4}$$

In these relations, we have used the following notations : t_{kl}-components of the force stress tensor, m_{k3}-components of the couple stress tensor, ε_{kl}-components of micropolar strain tensor, u_k-components of displacement vector, ϕ_3-component of microrotation vector, ε_{kl_3}-permutation symbol, $A_{11}, A_{12}, A_{77}, A_{78}, A_{88}, A_{22}, B_{44}, B_{66}$–characteristic constants of the material, ρ-the density and j-the microinertia.

From equations (1)-(4), we obtain the field equations of the plane strain for orthotropic micropolar elastic solid in the form :

$$\left(A_{11}\frac{\partial^2}{\partial x^2} + A_{88}\frac{\partial^2}{\partial y^2}\right)u_1 + (A_{12} + A_{78})\frac{\partial^2 u_2}{\partial x \partial y} - K_1\frac{\partial \phi_3}{\partial y} = \rho\frac{\partial^2 u_1}{\partial t^2}, \tag{5}$$

$$(A_{12} + A_{78})\frac{\partial^2 u_1}{\partial x \partial y} + \left(A_{77}\frac{\partial^2}{\partial x^2} + A_{22}\frac{\partial^2}{\partial y^2}\right)u_2 - K_2\frac{\partial \phi_3}{\partial x} = \rho\frac{\partial^2 u_2}{\partial t^2}, \tag{6}$$

$$\left(B_{66}\frac{\partial^2}{\partial x^2} + B_{44}\frac{\partial^2}{\partial y^2} - \aleph\right)\phi_3 + K_1\frac{\partial u_1}{\partial y} + K_2\frac{\partial u_2}{\partial x} = \rho j\,\frac{\partial^2 \phi_3}{\partial t^2} \tag{7}$$

$$t_{22} = A_{12}\frac{\partial u_1}{\partial x} + A_{22}\frac{\partial u_2}{\partial y}, \tag{8}$$

$$t_{21} = A_{78}\frac{\partial u_2}{\partial x} + A_{88}\frac{\partial u_1}{\partial y} + \phi_3(A_{88} - A_{78}), \tag{9}$$

$$m_{23} = B_{44}\frac{\partial \phi_3}{\partial y}. \tag{10}$$

where

$$K_1 = A_{78} - A_{88}, \; K_2 = A_{77} - A_{78}, \; \aleph = K_2 - K_1 \tag{11}$$

The equations of motion and stress-strain relations for an elastic solid are given by Ewing *et al.*[24] as,

$$\left(\lambda^0 + \mu^0\right)\nabla(\nabla.\vec{w}) + \mu^0\left(\nabla^2\vec{w}\right) = \rho^0\frac{\partial^2 \vec{w}}{\partial t^2}. \tag{12}$$

$$t^0_{kl} = \lambda^0\theta\delta_{kl} + 2\mu^0 e_{kl}. \tag{13}$$

where

$$\theta = w_{1,1} + w_{2,2} + w_{3,3}, \; e_{kl} = \frac{w_{k,l} + w_{k,l}}{2}; \; k = l = 1,2,3 \tag{14}$$

For two dimensional problem we assume,

$$\vec{w} = (w_1, w_2, 0) \tag{15}$$

Following Fung[25], a Galilean transformation

$$x^* = x + Ut, \; y^* = y, \; t^* = t \tag{16}$$

is introduced then the boundary conditions would be independent of t^* and assuming the dimensionless variables defined by the expressions.

$$x' = \frac{\omega^*}{c_1}x^*, \; y' = \frac{\omega^*}{c_1}y^*, \; u_1' = \frac{\omega^*}{c_1}u_1, \; u_2' = \frac{\omega^*}{c_1}u_2,$$

$$\phi_3' = \frac{A_{11}}{K_1}\phi_3, \; t_{kl} = \frac{t_{kl}}{A_{11}}, \; m_{k_3}' = \frac{c_1}{B_{44}\omega^*}m_{k_3},$$

$$w_1 = \frac{\omega^*}{c_1}w_1, \; w_2 = \frac{\omega^*}{c_1}w_2, \; t^0_{kl} = \frac{t^0_{kl}}{\lambda^0}, \tag{17}$$

where

$$\omega^{*2} = \frac{\aleph}{\rho j}, \; c_1^2 = \frac{A_{11}}{\rho} \tag{18}$$

in equations (5)-(7) and using (16) and (17) and applying Fourier transform defined by

$$\tilde{f}(\xi, y) = \int_{-\infty}^{\infty} f(x, y)\, e^{i\xi x}\, dx \tag{19}$$

on the resulting equations (after suppressing the primes), we obtain

$$D^2\tilde{u}_1 = b_{11}\tilde{u}_1 + a_{12}D\tilde{u}_2 + a_{13}D\tilde{\phi}_3, \tag{20}$$

$$D^2\tilde{u}_2 = b_{22}\tilde{u}_2 + a_{21}D\tilde{u}_1 + b_{23}\tilde{\phi}_3, \tag{21}$$

$$D^2\tilde{\phi}_3 = b_{33}\tilde{\phi}_3 + a_{31}D\tilde{u}_1 + b_{32}\tilde{u}_2, \tag{22}$$

where

$$b_{11} = \frac{\xi^2\left(A_{11} - \rho U^2\right)}{A_{88}}, \; b_{22} = \frac{\xi^2\left(A_{77} - \rho U^2\right)}{A_{22}},$$

$$b_{23} = -\frac{i\,\xi\,K_1\,K_2}{A_{11}A_{22}}, \; b_{33} = \frac{i\,\xi\,c_1^2\,K_2\,A_{11}}{\omega^{*2}K_1 B_{44}}$$

$$b_{33} = \frac{1}{B_{44}}\left[\xi^2\left(B_{66} - \rho U^2 j\right) + \frac{\aleph c_1^2}{\omega^{*2}}\right],$$

$$a_{12} = \frac{i\xi(A_{12} + A_{78})}{A_{88}}, a_{13} = \frac{K_1^2}{A_{88}A_{11}}, a_{21} = \frac{i\xi(A_{12} + A_{78})}{A_{22}}.$$

$$a_{31} = -\frac{A_{11}c_1^2}{B_{44}\omega^{*2}}, \; D = \frac{d}{dy} \tag{23}$$

The equations (20)-(22) may be written as

$$DW(\xi, y) = A(\xi)\, W(\xi, y) \tag{24}$$

where

$$W = \begin{pmatrix} V \\ DV \end{pmatrix}, \; A = \begin{pmatrix} O & I \\ A_1 & A_2 \end{pmatrix}, \; V = \begin{pmatrix} \tilde{u}_1 \\ \tilde{u}_2 \\ \tilde{\phi}_3 \end{pmatrix},$$

$$A_1 = \begin{pmatrix} b_{11} & 0 & 0 \\ 0 & b_{22} & b_{23} \\ 0 & b_{32} & b_{33} \end{pmatrix}, \; A_2 = \begin{pmatrix} 0 & a_{12} & a_{13} \\ a_{21} & 0 & 0 \\ a_{31} & 0 & 0 \end{pmatrix} \tag{25}$$

O and I are respectively zero and identity matrix of order 3.

To solve equation (24), we assume

$$W(\xi, y) = X(\xi)\, e^{qy} \tag{26}$$

which leads to eigen-value problem. The characteristic equation corresponding to matrix A is given by

$$|A - qI| = 0 \tag{27}$$

which on expansion provides us

$$q^6 + \lambda_1 q^4 + \lambda_2 q^2 + \lambda_3 = 0 \tag{28}$$

where

$$\lambda_1 = -(a_{12}a_{21} + a_{13}a_{31} + b_{11} + b_{22} + b_{33}),$$

$$\lambda_2 = a_{12}(a_{21}b_{33} - b_{23}a_{31}) + a_{13}(b_{22}a_{31} - a_{21}b_{32})$$
$$+ b_{22}b_{33} - b_{23}b_{32} + b_{11}(b_{22} - b_{33}),$$

$$\lambda_3 = b_{11}(b_{23}b_{32} - b_{22}b_{33}) \tag{29}$$

The eigen values of the matrix A are the characteristic roots of the equation (28). The vectors $X(\xi)$ corresponding to the eigen values q_s, can be determined by solving the homogeneous equation

$$[A - qI]X(\xi) = 0 \tag{30}$$

The set of eigen vectors $X_s(\xi)$, s = 1,2........6 may be obtained as

$$X_s(\xi) = \begin{pmatrix} X_{g1}(\xi) \\ X_{g2}(\xi) \end{pmatrix} \tag{31}$$

where

$$X_{g1}(\xi) = \begin{pmatrix} q_g \\ a_g \\ b_g \end{pmatrix}, \; X_{g2}(\xi) = \begin{pmatrix} q_g^2 \\ a_g q_g \\ b_g q_g \end{pmatrix},$$

$$q = q_g \; ; \; g = 1,2,3 \tag{32}$$

$$X_{R1}(\xi) = \begin{pmatrix} -q_R \\ a_R \\ b_R \end{pmatrix}, \; X_{R2}(\xi) = \begin{pmatrix} q_R^2 \\ -a_R q_R \\ -b_R q_R \end{pmatrix},$$

$$R = g + 3; \; q = -q_g; \; g = 1,2,3 \tag{33}$$

and

$$a_g = \frac{b_{11}b_{23} - q_g^2(b_{23} + a_{21}a_{13})}{\nabla_g},$$

$$b_g = \frac{q_g^2 a_{31} + a_g b_{32}}{q_g^2 - b_{33}},$$

$$\nabla_g = q_g^2 a_{13} + a_{12}b_{23} - b_{22}a_{13}. \tag{34}$$

The solution of equation (22) is given by

$$W(\xi, y) = \sum_{s=1}^{3} [B_s X_s(\xi) \exp(q_s y)$$
$$+ B_{s+3} X_{s+3}(\xi) \exp(-q_s y)] \tag{35}$$

where $B_{\Xi}(\Xi = 1,2...........6)$ are arbitrary constants.

The relation (35) represents the solution of the general problem in case of orthotropic micropolar elasticity and can be applied to a class of problem in the domain of Fourier transform.

The transformed displacements and micro-rotation satisfying the radiation conditions are given by

For $y \geq 0$,

$$\tilde{u}_1 = -q_1 B_4 e^{-q_1 y} - q_2 B_5 e^{-q_2 y} - q_3 B_6 e^{-q_3 y},$$

$$\tilde{u}_2 = +a_1 B_4 e^{-q_1 y} + a_2 B_5 e^{-q_2 y} + a_3 B_6 e^{-q_3 y}$$

$$\tilde{\phi}_3 = +b_1 B_4 e^{-q_1 y} + b_2 B_5 e^{-q_2 y} + b_3 B_6 e^{-q_3 y} \quad (36)$$

Adopting the same approach for elastic half-space, the solutions are given by

$$\tilde{w}_1 = M\left(A'_1\, p_1 e^{p_1 y} + A'_2\, p_2 e^{p_2 y}\right), \quad (37)$$

$$\tilde{w}_2 = A'_1\, d_1 e^{p_1 y} + A'_2\, d_2 e^{p_2 y}. \quad (38)$$

where

$$M = \xi c_{12}, \; d_\nu = i\left(\xi^2 c_{11} - p_\nu^2\right); \; \nu = 1,2$$

$$P_\nu^2 = \frac{-\lambda_4 \pm \sqrt{\lambda_4^2 - 4\lambda_5}}{2},$$

$$\lambda_4 = \xi^2 (c_{12}c_{21} - c_{22} - c_{11}),$$

$$\lambda_5 = c_{11}c_{22}, \; c_{11} = \frac{\lambda^0 + 2\mu^0 - \rho^0 U^2}{\mu^0},$$

$$c_{21} = \frac{\lambda^0 + \mu^0}{\lambda^0 + 2\mu^0}, \; c_{12} = \frac{\lambda^0 + \mu^0}{\mu^0}, \; c_{22} = \frac{\mu^0 - \rho^0 U^2}{\lambda^0 + 2\mu^0}. \quad (39)$$

Boundary Conditions :

Case (i) : Load in normal direction : For a concentrated normal force, we take $P(x+Ut) = F\delta(x^*)$, where $\delta(x^*)$ is Dirac delta function and F is the magnitude of applied force, therefore in moving coordinates the boundary conditions at the interface $y=0$ are,

(*i*) $t_{22} = t_{22}^0 - F\delta(x^*)$,

(*ii*) $m_{23} = 0$,

(*iii*) $u_2 = w_2$,

(*iv*) $u_1 = w_1$,

(*v*) $t_{21} = t_{21}^0$. (40)

Applying Fourier transform defined by (19) on the boundary conditions (40) and using (8)-, (10), (13), (15)-(17) and (36)-(38), we obtain the expressions for displacement components, force stress and couple stress for orthotropic micropolar half-space as,

$$\tilde{u}_2 = -\frac{F}{\Delta}\left[a_1\Delta_1 e^{-q_1 y} - a_2\Delta_2 e^{-q_2 y} + a_3\Delta_3 e^{-q_3 y}\right], \quad (41)$$

$$\tilde{t}_{22} = -\frac{F}{\Delta}\left[r_1\Delta_1 e^{-q_1 y} - r_2\Delta_2 e^{-q_2 y} + r_3\Delta_3 e^{-q_3 y}\right], \quad (42)$$

$$\tilde{m}_{23} = \frac{FK_1}{A_{11}\Delta}\left[b_1 q_1\Delta_1 e^{-q_1 y} - b_2 q_2 \Delta_2 e^{-q_2 y} + b_3 q_3 \Delta_3 e^{-q_3 y}\right] \quad (43)$$

where

$$\Delta = N(r_\vartheta s_\Omega - r_\Omega s_\vartheta) + (q_\Omega d_2 + M a_\Omega p_2)(r_\vartheta s_4 - r_4 s_\vartheta)$$
$$-(q_\Omega d_1 + M p_1 p_\Omega)(r_\vartheta s_5 - r_5 s_\vartheta) + G(q_\vartheta a_\Omega - q_\Omega a_\vartheta)$$
$$+(r_\Omega s_5 - r_5 s_\Omega)(d_1 q_\vartheta + M p_1 a_\vartheta) - (r_\Omega s_4 - r_4 s_\Omega)$$
$$(q_\vartheta d_2 + M p_2 a_\vartheta),$$

$$\Delta_g = N(b_\Omega q_\Omega s_\vartheta - b_\vartheta q_\vartheta s_\Omega) - H q_\vartheta q_\Omega (b_\Omega - b_\vartheta)$$
$$+J(b_\Omega q_\Omega a_\vartheta - b_\vartheta q_\vartheta a_\Omega),$$

$\vartheta = 2,1,1; \quad \Omega = 3,3,2$,

$$N = M(p_2 d_1 - p_1 d_2),\ G = r_4 s_5 - r_5 s_4 ,$$

$$H = s_5 d_1 - s_4 d_2 ,\ J = M(p_2 s_4 - p_1 s_5) ,$$

$$r_g = \frac{q_g}{A_{11}}\left(i\xi A_{12} - a_g A_{22}\right),$$

$$r_{4,5} = p_{1,2}\left[i\xi M - \left(\frac{\lambda^0 + 2\mu^0}{\lambda^0}\right)d_{1,2}\right];\ g = 1,2,3 ,$$

$$s_g = \frac{1}{A_{11}}\left[-i\xi a_g A_{78} + q_g^2 A_{88} + \frac{K_1}{A_{11}}(A_{88} - A_{78})b_g\right],$$

$$s_{4,5} = \frac{\mu^0}{\lambda^0}\left(i\xi d_{1,2} - M p_{1,2}^2\right). \quad (44)$$

Case II : Load in tangential direction

When tangential load is applied at the interface, the boundary conditions are given by,

(*i*) $t_{22} = t_{22}{}^0$,

(*ii*) $m_{23} = 0$,

(*iii*) $u_2 = w_2$,

(*iv*) $u_1 = w_1$,

(*v*) $t_{21} = t_{21}{}^0 - F\delta(x^*)$. (45)

Particular Case :

Taking

$$A_{11} = A_{22} = \lambda + 2\mu + K,\ A_{77} = A_{88} = \mu + K,$$

$$A_{12} = \lambda,\ A_{78} = \mu,\ B_{44} = B_{66} = \gamma,$$

with

$$-K_1 = K_2 = \aleph / 2 = K,$$

we obtain the corresponding expressions for the isotropic micropolar medium. These results tally with the one obtained if we solve the problem for an isotropic micropolar medium.

Inversion of the Transform

To obtain the solution of the problem in the physical domain, we must invert the transform in (41)–(43). These expressions are functions of y and the parameter of Fourier transform ξ, hence are of the form $\tilde{f}(\xi, y)$. To get the function $f(x,y)$ in the physical domain we invert the Fourier transform using,

$$f(x,y) = \frac{1}{2\pi}\int_{-\infty}^{\infty} \tilde{f}(\xi, y)e^{-i\xi x}\, d\xi \quad (46)$$

$$= \frac{1}{2\pi}\int_{-\infty}^{\infty}\left[\mathrm{Cos}(\xi x) f_e - i\mathrm{Sin}(\xi x) f_0\right] d\xi \quad (47)$$

where f_e and f_0 are respectively even and odd parts of the function $\tilde{f}(\xi, y)$. The method for evaluating this integral is described by Press *et al.*[26] which involves the use of Rhomberg's integration ith adaptive step size. This also uses the results from successive refinements of the extended trapezoidal rule followed by extrapolation of the results to the limit when the step size tends to zero.

Numerical Results and Discussion

For numerical computations, we take the following values of relevant parameters for orthotropic micropolar solid as,

$A_{11} = 13.97 \times 10^{10}$ dyne/cm^2 ,

$A_{77} = 3.0 \times 10^{10}$ dyne/cm^2 ,

$A_{88} = 3.2 \times 10^{10}$ dyne/cm^2 ,

$A_{22} = 13.75 \times 10^{10}$ dyne/cm^2 ,

$A_{12} = 8.13 \times 10^{10}$ dyne/cm^2 ,

$A_{78} = 2.2 \times 10^{10}$ dyne/cm^2 ,

$B_{44} = 0.056$ dynes , $B_{66} = 0.057$ dynes

For the comparison with micropolar isotropic solid, following Gauthier[27], we take the following values of relevant parameters for the case of aluminium epoxy composite as,

$\rho=2.19$ gm/cm^3 , $\lambda=7.59\times10^{10}$ dyne/cm^2

$\mu=1.89\times10^{10}$ dyne/cm^2, $K=0.0149\times10^{10}$ dyne/cm^2,

$\gamma=0.0268\times10^{10}$ dyne, j=0.00196 cm^2

The physical constants for granite as elastic solid are given by Bullen[28] as,

$\lambda^0=0.884\times10^{11}$ dyne/cm^2 ,

$\mu^0=1.2667\times10^{11}$ dyne/cm^2 ,

ρ^0 = 2.6 gm/cm^3

The values of normal displacement $U_2 = (u_2/F)$, normal force stress $T_{22}=(t_{22}/F)$ and tangential couple stress $M_{23}=(m_{23}/F)$ for an orthotropic micropolar solid (MOS) and isotropic micropolar solid (MIS) have been studied for different load velocities and the variations of these components with distance x have been shown by (*a*) solid line (——) for MOS and dashed line (------) for MIS ($U<c_1$), (b) solid line with centered symbols (*x*—*x*—*x*) for MOS and dashed line with centered symbols (*x*---*x*---*x*) for MIS ($U=c_1$) and (*c*) solid line with centered symbols (o—o—o) for MOS and dashed line with centered symbol (o---o---o) for MIS ($U<c_1$). These variations are shown in Fig. (1-6). The computations are carried out for y=1.0 in the range $0\leq x\leq10.0$.

Discussions for Various Cases

Case (*i*) : *Normal load* : The variation of normal displacement is similar in nature for MOS and MIS for different load velocities. It is observed that the values of normal displacement initially increases and then starts oscillating with increase in distance x. Very near to the point of application of source, the values of normal displacement are large for MIS (for $U<c_1$ and $U>c_1$) as compared to the values for MOS, whereas for $U=c_1$, the values of normal displacement are large for MOS in comparison to the values for MIS. The variation of normal displacement for both the solids vanishes with increase in distance x. The variations of normal displacement for MOS and MIS are shown in Fig. 1.
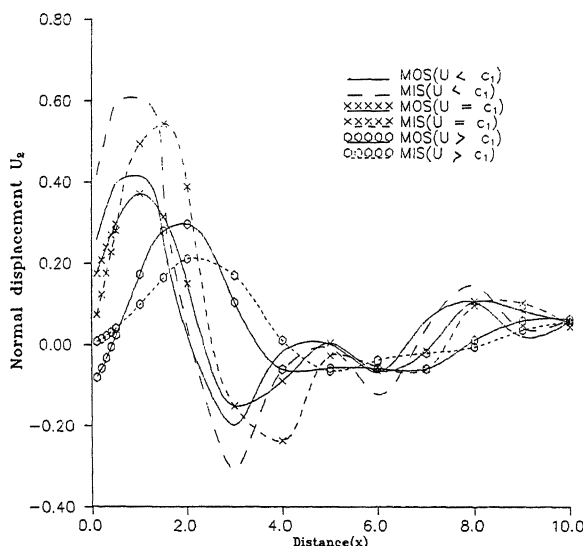
Fig. 1 – Variation of normal displacement $U_2(=u_2/F)$ with distance x. (load in normal direction)

The variation of normal force stress is similar to the variation of normal displacement with difference in magnitude. However, the values of normal force stress for both the solids increases initially similar to that of the variation of normal displacement. The variation of normal force stress for both the solids and for $U>c_1$ decreases in the initial range and then increases to further oscillate with distance x. It is also seen that the range in which the values of normal force stress lie, is slightly more for MIS as compared to MOS. These variations of normal force stress are shown in Fig. 2.

The variation of tangential couple stress, depicted in Fig. 3, shows that the values for MIS lie in a very short range as compared to the values for MOS. Also it can be seen that, near the point of application of source, the values of tangential couple steress are more for MIS (for different load velocities) in comparison to the values for MOS. For MOS the variation of tangential couple stress is more for $U<c_1$ and $U=c_1$. The variations in case of MOS decreases for $U>c_1$ but the local maxima and local minima of the variations arises for $U>c_1$.
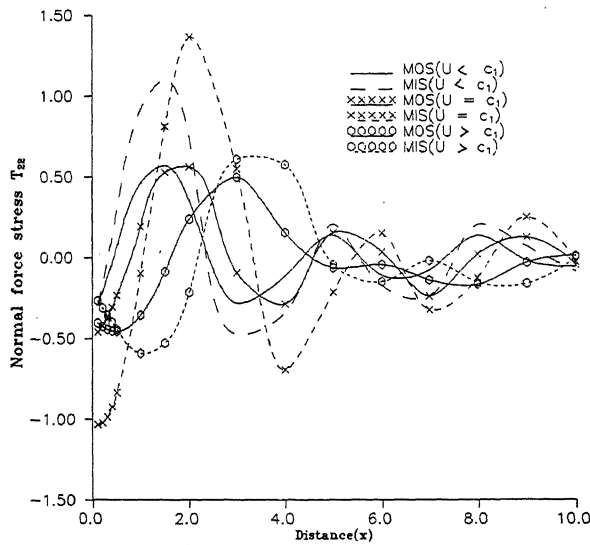
Fig. 2 – Variation of normal force stress $T_{22}(=t_{22}/F)$ with distance x. (Load in normal direction)
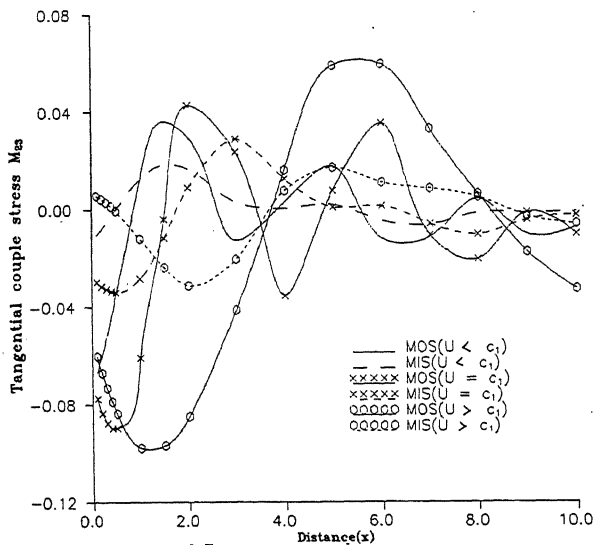
Fig. 3 – Variation of tangential couple stress $M_{23}(=m_{23}/F)$ with distance x. (Load in normal direction)

Case (ii) : Tangential load : The variation of normal displacement for both the solids is similar, as discussed in the case of normal point load. However, it is quite interesting to note that, separately for both MOS and MIS, the oscillations of the values of normal displacement decrease as the magnitude of load velocity increases. Also near the point of application of source, the values of normal displacement for MIS and MOS, increase with increase in magnitude of load velocity. These variations for different load velocities are shown in Fig. 4.

Similar to normal point load, the values of normal force stress for MOS lie in a short range as compared to MIS. The variation of normal force stress for MIS are opposite in nature for $U=c_1$ and $U>c_1$. However, for MOS the variation is very similar for $U<c_1$ and $U=c_1$. The variations of normal force stress in case of tangential load are shown in Fig. 5.
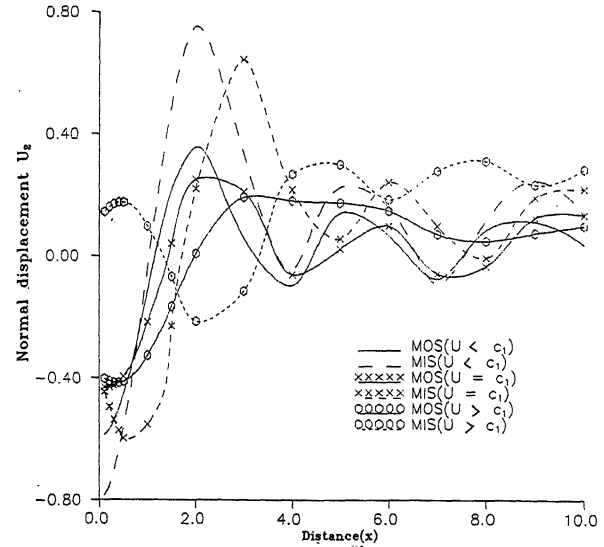
Fig. 4 – Variation of normal displacement $U_2(=u_2/F)$ with distance x. (Load in tangential direction)
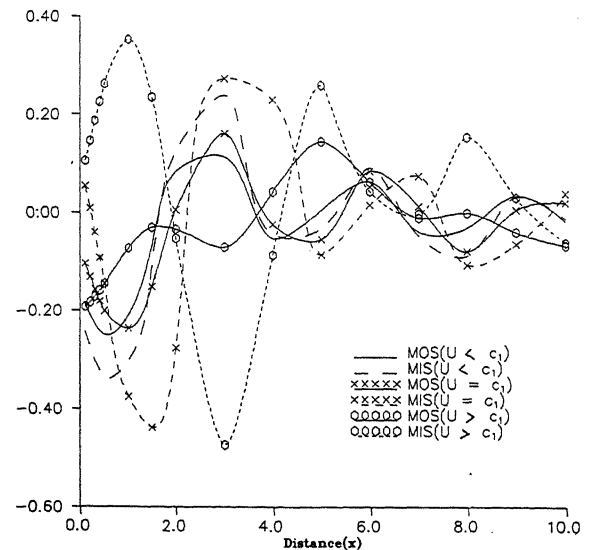
Fig. 5 – Variation of normal force stress $T_{22}(=t_{22}/F)$ with distance x. (Load in tangential direction)

The values of tangential couple stress for MIS, which are oscillating to much more extent, lie in

a short range as compared to the values for MOS. The values of tangential couple stress for MOS and different load velocities decreases, initially, but the decrease in values is very sharp for $U=c_1$ and this decrease is minimum for $U>c_1$. The trend which is decreasing in nature, is opposite for MIS and for $U>c_1$, where the values starts with an initial rise. The variations of tangential couple stress are shown in Fig. 6.
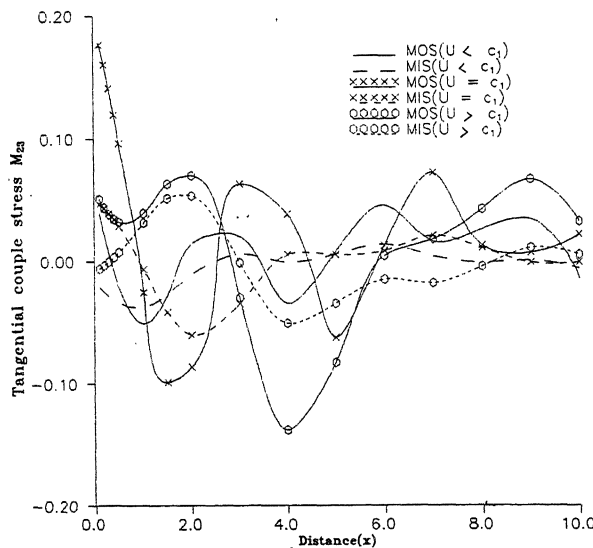
Fig. 6 – Variation of Tangential couple stress $M_{23}(=m_{23}/F)$ with distance x. (Load in tangential direction).

Conclusion

It can be observed that the varying load velocities have a significant effect on the quantities. The values of normal force stress, in both the cases, lies in a short range for MOS as compared to MIS. It is also observed that the values of normal force stress in both the cases and both MOS and MIS, increases initially but the values for both the solids and for $U>c_1$ starts with initial decrease. When tangential load is applied at the interface, the variations of normal displacement which are oscillatory in nature, decrease with increase in magnitude of load velocity. In case of normal load, the values of normal displacement, near the point of application of source, decrease with increase in magnitude of load velocity, whereas, the nature is opposite in the case of tangential load. For both the cases, the values of tangential couple stress for MIS lies in a short range as compared to MOS. The anisotropy property of the solid also has a significant effect on the quantities.

References

1. Eringen, A.C. (1966) *J. Math. Mech.* **15** : 909.
2. Iesan, D. (1973) *Archives of Mechanics* **25** : 547.
3. Iesan, D. (1974) *ZAMM* **54** : 773
4. Iesan, D. (1974) *An. St. Uni. Iasi.* **20** : 411.
5. Nakamura, S., Benedict, R. & Lakes, R. (1984) *Int. J. Engg. Sci.* **22** : 319.
6. Kumar, R. & Choudhary, S. (2002) *Archives of Mechanics* **54** : 185.
7. Kumar, R. & Choudhary, S. (2002) *J. Vibration. Control.* **8** : 1053.
8. Kumar, R. & Choudhary, S. (2002) *Proc. Indian Acad. Sci. (Earth Plant. Sci.)* **111**(2) : 133.
9. Kumar, R. & Choudhary, S. (2003) *Meccanica* **38** : 349.
10. Kumar, R. & Choudhary, S. (2004) *Sadhana* **29**(1) : 83.
11. Payton, R.G. (1964) *Qrtrly. Appld. Maths* **21** : 299.
12. Eason, G. (1965) *Int. J. Engg. Sci.* **2** : 581.
13. Gakenheimer, D.C. & Miklowitz, J. (1969) *J. Appl. Mech.* 369(3) *Trans. ASME,* **91,** Series E. 505.
14. Kennedy, T.C. & Hermann, G. (1973) *J. of Appl. Mech.* p. 137.
15. Halpern, M.R. & Christiano, P. (1986) *Earthquake, Engg. & Structural Dynamics* **14** : 439.
16. Nath, S. & Sengupta, P.R. (1991) *J. Pure. Appl. Math.* **30** : 317.
17. Katz, J. (2001) *J. of Sound and Vibration* **246** (5) : 757.
18. Verrujit, A. & Cordova, C.C. (2001) *J. Appl. Mechanics* **68** : 915.
19. Kumar, R. & Gogna, M.L. (1992) *Int. J. Engg. Sci.* **30** : 811.
20. Kumar, R. & Deswal, S. (2000) *Proc. Indian Acad. Sci. (Math. Sci.)* **110** (4) : 499.
21. Kumar, R. & Deswal, S. (2002) *Ganita* **8** (4) : 621.
22. Kumar, R. Ailawalia, P. (2003) *Int. J. Appl. Mech. Engg.* **8**(4) : 621.
23. Eringen, A.C. (1968) *Theory of Micropolar Elasticity in Fracture,* Vol. II, Academic Press, p. 621.

24. Ewing, W.M., Jardetzky, & Press, F. (1957) *Elastic Waves in Layered Media,* Mcgraw Hill.

25. Fung, Y.C. (1968) *Foundations of Solid Mechanics,* Prentice Hall, New Delhi.

26. Press, W.H., Teukolsky, S.A., Vellerling, W.T. & Flannery, B.P. (1986) *Numerical Recipies,* Cambridge University Press.

27. Gauthier, R.D. (1982) *Mechanics of Micropolar Media,* Ed. Brulin, O. & Hsieh, R.K.T., World Scientific, Singapore.

28. Bullen, K.E. (1969) *An Introduction to theory of Seismology,* Cambridge University Press, Cambridge.

PROC. NAT. ACAD. SCI. INDIA, 75(A), II, 2005

Thermoelastic interactions in an infinite elastic solid with time-dependent distributed heat sources without energy dissipation

S.K. ROY CHOUDHURI and NUPUR BANDYOPADHYAY

Department of Mathematics, Burdwan University, Burdwan-713 104, India.

E-mail : skrc_math@yahoo.com (S.K. Roy Choudhuri)

E-mail : nupurbandyopadhyay@yahoo.co.in (Nupur Bandyopadhyay)

Tel. : (091)342-2557741; Fax : (091) 342-2530452

Received January 27, 2004; Revised July 12, 2004; Accepted August 9, 2004

Abstract

The theory of generalized thermo-elasticity of type II without energy dissipation is employed to solve the problem of determination of temperature, deformation and stress in an infinite isotropic elastic solid having time-dependent distributed heat sources. The solutions are derived by the use of Laplace transform on time and Fourier transform on space. Discontinuities of temperature field, deformation and stress are studied at the modified elastic and thermal wave fronts and compared with the previous results deduced from classical theory and generalized thermo-elasticity theory with thermal relaxation. It reveals that the thermo-elasticity theory without energy dissipation removes some of the finite discontinuities in deformation, temperature and stress which were not observed in the corresponding problems studied by previous authors, using other generalized thermo-elasticity theories.

(Keywords : thermoelastic interactions / Green-Naghdi Model / infinite solid).

Introduction

Paria[1] investigated a problem of an infinite isotropic elastic solid having distributed instantaneous heat sources using the classical coupled thermo-elastic theory. The solutions obtained consist of two parts- a wave part travelling with the speed of dilatational (elastic) wave and a part diffusive in nature. His solutions for deformation and temperature were observed to be continuous at the elastic wave front. Later, Roy Choudhuri and Sain[2] studied the same problem using the generalized dynamical theory of thermo-elasticity (L-S theory) with thermal relaxation time of Lord and Shulman[3]. It was seen that the solutions for deformation, temperature and stress suffer finite jump discontinuities at the elastic and thermal wave fronts and that the magnitudes of the discontinuities decay exponentially with distance at the wave fronts. Further the thermoelastic interactions in the case of continuously distributed heat sources in an infinite elastic solid was studied by Bhatta[4], where the displacement field was found to be continuous but temperature and stress fields suffer finite discontinuities at both the wave fronts.

In the present paper the authors have studied the same problem using the thermo-elasticity theory of type II of Green and Naghdi[5] without energy dissipation (G-N theory). This thermo-elastic model possesses several significant characteristics that differ from the traditional classical development in thermo-elastic material behavior- (i) it does not sustain energy dissipation, (ii) the entropy flux vector (or equivalently the heat flow vector) in the theory is determined in terms of the same potential that also determines the stress, (iii) it permits transmission of heat flow as thermal waves at finite speed. The authors in this paper consider an infinite elastic solid having (i) distributed instantaneous heat sources and (ii) continuously distributed heat sources. Using G-N theory, the solutions for deformation, temperature, and stress are derived. The solutions consist of two waves (i) the elastic wave travelling with speed $v_1 = 1/\lambda_1$ and (ii) the thermal wave travelling with speed $v_2 = 1/\lambda_2$ and that $v_1 < v_2$ implying that the elastic wave follows the thermal wave.

The displacement field is continuous at both the wave fronts in case (i), but the temperature field and stress suffer finite jumps at these locations. The discontinuities of stress and temperature field at the wave fronts are studied in case (i) and compared with Paria's[1] result and the result derived by Roy choudhuri and Sain[2]. In case (ii), displacement, temperature and stresses are all continuous at the elastic and thermal wave fronts in contrast to the results derived by Bhatta[4] in a similar problem of an infinite solid with continuously distributed heat sources using L-S theory wherein the deformation is continuous but the temperature and stress fields are both discontinuous at both the wave fronts.

It reveals that G-N theory without energy dissipation removes the discontinuity in deformation, which were not observed in the solution of the corresponding problem (case(i)) studied by Roy Choudhuri and Sain[2] using L-S theory and also eliminates the finite discontinuities in temperature and stress observed in the corresponding problem studied by Bhatta[4] (case (ii)). Again in the problems considered by Roy Choudhuri and Sain[2] and Bhatta[4], the amount of discontinuities in temperature and stress in case (i) and (ii) are seen to decay exponentially with distance at both the wave fronts where no such exponential decay case happens in the present problem using G-N theory.

Though transient boundary value problems relating to elastic half-space[6] and surface waves in generalized thermo-elasticity[7,8] have been studied, it is believed that this particular problem of an infinite elastic solid with time-dependent distributed heat sources considering G-N thermoelastic model without energy dissipation is not dealt with before. It may be mentioned that this particular problem under consideration is the extension of the papers considered by Paria[1], Roy Choudhuri and Sain[2] and Bhatta[4] in the thermoelasticity theory of type II (G-N theory).

Problem Formulation, Basic Equations and its Transform solution

We consider an infinite elastic solid unstrained and unstressed initially, but has a uniform reference temperature throughout. It is then subjected to distributed heat sources over the plane $x = 0$ and the solid occupies the whole space $-\infty < x < \infty$.

From the symmetry of the problem, the displacement vector $\bar{u}$ has only one component in the x direction, $\bar{u} = [u(x, t), 0, 0]$ and the temperature increase $\theta = \theta(x, t)$ where x denotes the spatial coordinate and t the time.

The stress-strain-temperature relations in linear thermo-elasticity are

$$\tau_{ij}=\lambda\Delta\delta_{ij}+2\mu e_{ij}-\gamma\theta\delta_{ij} \quad \text{with} \quad 2e_{ij}=u_{i,j}+u_{j,i}\,;\; ii=1,2,3 \qquad (1)$$

where u_i is the component of the displacement vector $\bar{u}$, τ_{ij} is the stress tensor, e_{ij} is the strain tensor, Δ = div $\bar{u}$ = e_{ii} = dilatation, δ_{ij} is the Kronecker delta, θ is the temperature above the uniform reference temperature T_0. Here, $\gamma = \alpha_t(3\lambda + 2\mu)$, where α_t is the coefficient of linear thermal expansion of the material and λ, μ are Lame' constants.

The fundamental equations of the theory of thermoelasticity (type II) without energy dissipation proposed by Green and Naghdi[5] (in absence of body forces) are

$$\mu\nabla^2\bar{u}+(\lambda+\mu)\bar{\nabla}(div\bar{u})-\gamma\bar{\nabla}\theta=\rho\ddot{\bar{u}} \qquad (2)$$

$$\rho C_v\ddot{\theta}+\gamma T_0 div\ddot{\bar{u}} = \rho Q+K^*\nabla^2\theta,\; K^*>0 \qquad (3)$$

where ρ is the constant mass density, C_v is the specific heat, K^* is a material constant characteristic of the theory, Q is the heat source term.

For the present problem, the equations (2), (3) and (1) reduce to

$$(\lambda+2\mu)\frac{\partial^2 u}{\partial x^2} - \gamma\frac{\partial\theta}{\partial x} = \rho\frac{\partial^2 u}{\partial t^2} \qquad (4)$$

$$\rho C_v\frac{\partial^2\theta}{\partial t^2} + \gamma T_0\frac{\partial^3 u}{\partial x\partial t^2} = \rho Q+K^*\frac{\partial^2\theta}{\partial x^2} \qquad (5)$$

$$\tau_{11} = (\lambda+2\mu)\frac{\partial u}{\partial x} - \gamma\theta \tag{6}$$

Case (i) : For instantaneous heat sources distributed over the plane $x = 0$, we may represent it as $Q(x, t) = Q_0\,\delta(x)\,\delta(t)$ where $\delta(x)$ is Dirac's delta function defined by

$$\int_{-\infty}^{\infty}\delta(x)dx = 1; \qquad \delta(x)=0 \text{ for } x\neq 0$$

Case (ii) : For continuous heat sources distributed over the plane $x = 0$, we may represent it as $Q(x, t) = Q_0\delta(x)H(t)$ where $H(t)$ is the Heavy side function defined by $H(t) = 1,\ t > 0$.

$= 0, \quad t \le 0$

Introducing the variables

$$\xi = \frac{c_1 x}{\kappa},\ \tau = \frac{c_1^2 t}{\kappa},\ \kappa = \frac{K^*}{\rho C_v},\ Z = \frac{\theta}{T_0}$$

$$U = \frac{(\lambda+2\mu)c_1}{\kappa\gamma T_0}u,\ \omega^* = \frac{c_1^2}{\kappa}$$

$$c_1^2 = \frac{\lambda+2\mu}{\rho},\ \varepsilon = \frac{\gamma^2 T_0}{(\lambda+2\mu)C_\varepsilon},\ \varepsilon' = \varepsilon\omega^*,$$

$$C_\varepsilon = \rho C_v,\ \frac{Q}{Q_0} = Q^*$$

the above equations then reduce to the simplified forms as

$$\frac{\partial^2 U}{\partial\xi^2} - \frac{\partial Z}{\partial\xi} = \frac{\partial^2 U}{\partial\tau^2} \tag{7}$$

$$\omega^*\frac{\partial^2 Z}{\partial\tau^2} + \varepsilon'\frac{\partial^3 U}{\partial\xi\partial\tau^2} = \hat{Q}_0 Q^* + \frac{\partial^2 Z}{\partial\xi^2} \tag{8}$$

$$\sigma_{11} = \frac{\tau_{11}}{\gamma T_0} = \frac{\partial U}{\partial\xi} - Z \tag{9}$$

where $\hat{Q}_0 = \dfrac{Q_0}{C_v T_0\omega^*}$

We note that $\dfrac{1}{\sqrt{\omega^*}} = \dfrac{\sqrt{\dfrac{K^*}{\rho C_v}}}{c_1}$ is the non-dimensional thermal wave speed of G-N theory. We denote the Laplace transforms of $U(\xi,\tau)$, $Z(\xi,\tau)$ by $\overline{U}(\xi,s)$, $\overline{Z}(\xi,s)$ where s is the Laplace transform parameter. Thus

$$\overline{U}(\xi,s) = \int_0^\infty U(\xi,\tau)e^{-s\tau}\,d\tau$$

$$\overline{Z}(\xi,s) = \int_0^\infty Z(\xi,\tau)e^{-s\tau}\,d\tau$$

Applying Laplace transform to equations (7), (8) and (9), we obtain

$$\left(\frac{\partial^2}{\partial\xi^2} - s^2\right)\overline{U} = \frac{\partial\overline{Z}}{\partial\xi} \tag{10}$$

$$\varepsilon' s^2\frac{\partial\overline{U}}{\partial\xi} = \left(\frac{\partial^2}{\partial\xi^2} - \omega^* s^2\right)\overline{Z} + \hat{Q}_0\overline{Q^*} \tag{11}$$

$$\overline{\sigma_{\xi\xi}} = \frac{\partial\overline{U}}{\partial\xi} - \overline{Z} \tag{12}$$

We denote Fourier transforms of $\overline{U}(\xi,s)$, $\overline{Z}(\xi,s)$ by $\overline{U}_1(\varsigma,s)$, $\overline{Z}_1(\varsigma,s)$ where ς is the Fourier transform parameter. Thus

$$\overline{U}_1(\varsigma,s) = \frac{1}{\sqrt{2\pi}}\int_{-\infty}^{\infty}\overline{U}(\xi,s)e^{i\varsigma\xi}d\xi$$

$$\overline{Z}_1(\varsigma,s)=\frac{1}{\sqrt{2\pi}}\int_{-\infty}^{\infty}\overline{Z}(\xi,s)e^{i\varsigma\xi}d\xi$$

Applying Fourier transform to equations (10), (11) and (12), we obtain

$$\left(\varsigma^2+s^2\right)\overline{U}_1 = i\varsigma\,\overline{Z}_1 \tag{13}$$

$$\left(\varsigma^2+\omega^*s^2\right)\overline{Z}_1 - i\varepsilon' s^2\varsigma\overline{U}_1 = \hat{Q}_0\overline{Q_1^*} \tag{14}$$

$$\overline{\sigma_{\xi\xi_1}} = -i\varsigma\overline{U}_1 - \overline{Z_1} \tag{15}$$

Solving for $\overline{U}_1$, $\overline{Z_1}$, we obtain

$$\overline{U}_1(\varsigma,s)=\frac{i\varsigma\hat{Q}_0\overline{Q_1^*}}{M}$$

$$\overline{Z_1}(\varsigma,s)=\frac{\hat{Q}_0\left(\varsigma^2+s^2\right)\overline{Q_1^*}}{M} \quad \text{where}$$

$$M=\varsigma^4+(1+\varepsilon'+\omega^*)s^2\varsigma^2+\omega^*s^4$$

$$=(\varsigma^2+\varsigma_1^2)\,(\varsigma^2+\varsigma_2^2) \quad \text{and}$$

$$\varsigma_1^2+\varsigma_2^2 = (1+\varepsilon'+\omega^*)s^2, \quad \varsigma_1^2\varsigma_2^2=\omega^*s^4$$

Then $\varsigma_{1,2}^2$ are the roots of the quadratic equation

$$\varsigma^4-\left(1+\varepsilon'+\omega^*\right)s^2\varsigma^2+\omega^*s^4=0$$

given by $\varsigma_i = s\lambda_i$, $i=1,2$ where

$$\lambda_1=\left[\frac{\left(1+\varepsilon'+\omega^*\right)+\sqrt{\left(1+\varepsilon'+\omega^*\right)^2-4\omega^*}}{2}\right]^{1/2},$$

$$\lambda_2=\left[\frac{\left(1+\varepsilon'+\omega^*\right)-\sqrt{\left(1+\varepsilon'+\omega^*\right)^2-4\omega^*}}{2}\right]^{1/2},$$

Clearly λ_1, λ_2 are both real, since $(1+\varepsilon'+\omega^*)^2-4\omega^* = \varepsilon'^2+(1+\omega^*)_2^2\,\varepsilon'+(1-\omega^*)^2 > 0$

We write

$$\overline{U}_1(\varsigma,s)=\frac{i\hat{Q}_0\overline{Q_1^*}}{\varsigma_2^2-\varsigma_1^2}\left[\frac{\varsigma}{\varsigma^2+\varsigma_1^2}-\frac{\varsigma}{\varsigma^2+\varsigma_2^2}\right]. \tag{16}$$

$$\overline{Z}_1(\varsigma,s)=\hat{Q}_0\overline{Q_1^*}\left[\frac{A}{\varsigma^2+\varsigma_1^2}+\frac{B}{\varsigma^2+\varsigma_2^2}\right] \tag{17}$$

$$\overline{\sigma}_{\xi\xi_1}(\varsigma,s)=\hat{Q}_0\overline{Q_1^*}\left[\frac{C}{\varsigma^2+\varsigma_1^2}+\frac{D}{\varsigma^2+\varsigma_2^2}\right] \tag{18}$$

$$A=\frac{s^2-\varsigma_1^2}{\varsigma_2^2-\varsigma_1^2}, \quad B=-\frac{s^2-\varsigma_2^2}{\varsigma_2^2-\varsigma_1^2}$$

$$C=\frac{-s^2}{\varsigma_2^2-\varsigma_1^2}, \quad D=\frac{s^2}{\varsigma_2^2-\varsigma_1^2}$$

Case (i) : For instantaneous heat sources distributed over the plane $\xi=0$, we have $Q^*(\xi,\tau) = \delta(\xi)\,\delta(\tau)$

First by applying Laplace transform on time and then applying Fourier transform on space, we obtain

$$\overline{Q_1^*}(\varsigma,s) = \frac{1}{\sqrt{2\pi}}$$

Case (ii) : For continuously heat sources distributed over the plane $\xi=0$, we have $Q^*(\xi,\tau) = \delta(\xi)\,H(\tau)$

First by applying Laplace transform on time and then applying Fourier transform on space, we obtain

$$\overline{Q_1^*}(\varsigma,s) = \frac{1}{\sqrt{2\pi}}\frac{1}{s}$$

Since the results for case (i) can be obtained by taking time derivative of the results for case (ii), we consider first case (ii).

Case (ii) :

$$\overline{U}_1(\varsigma, s) = \frac{i\hat{Q}_0}{s\left(\varsigma_2^2 - \varsigma_1^2\right)\sqrt{2\pi}}\left[\frac{\varsigma}{\varsigma^2+\varsigma_1^2} - \frac{\varsigma}{\varsigma^2+\varsigma_2^2}\right] \quad (19)$$

$$\overline{Z}_1(\varsigma, s) = \frac{\hat{Q}_0}{s\sqrt{2\pi}}\left[\frac{A}{\varsigma^2+\varsigma_1^2} - \frac{B}{\varsigma^2+\varsigma_2^2}\right] \quad (20)$$

$$\overline{\sigma}_{\xi\xi_1}(\varsigma, s) = \frac{\hat{Q}_0}{s\sqrt{2\pi}}\left[\frac{C}{\varsigma^2+\varsigma_1^2} - \frac{D}{\varsigma^2+\varsigma_2^2}\right] \quad (21)$$

Inverse Fourier transform then gives the following solutions in the Laplace transform domain :

Case (ii) :

$$\overline{U}(\xi, s) = \frac{\hat{Q}_0}{2\left(\varsigma_2^2 - \varsigma_1^2\right)s}\left[e^{-\varsigma_1\xi} - e^{-\varsigma_2\xi}\right] \quad \text{for } \xi > 0 \quad (22)$$

$$\overline{Z}(\xi, s) = \frac{\hat{Q}_0}{2\varsigma_1\varsigma_2 s}\left[A\varsigma_2\, e^{-\varsigma_1\xi} + B\varsigma_1\, e^{-\varsigma_2\xi}\right] \quad \text{for } \xi > 0 \quad (23)$$

$$\overline{\sigma_{\xi\xi}}(\xi, s) = \frac{\hat{Q}_0 s}{2\varsigma_1\varsigma_2\left(\varsigma_2^2 - \varsigma_1^2\right)}\left[-\varsigma_2\, e^{-\varsigma_1\xi} + \varsigma_1\, e^{-\varsigma_2\xi}\right] \quad \text{for } \xi > 0 \quad (24)$$

The form of the solutions for ς_i given by $\varsigma_i = s\lambda_i, (i = 1, 2)$, where λ_1, λ_2 are both real suggest that the solutions for U, Z, $\sigma_{\xi\xi}$ consist of two waves-one travelling with speed $v_1 = \frac{1}{\lambda_1}$ and the other with speed $v_2 = \frac{1}{\lambda_2}$. Since $\lambda_1 > \lambda_2$, the speed of the slower wave (modified dilatational wave) is v_1 and that of the predominantly faster wave (modified thermal wave) is v_2.

Substituting the values of $\varsigma_i = s\lambda_i$, $i = 1,2$, we have the following solutions for case (ii) in the transform domain :

$$\overline{U}(\xi, s) = \frac{\hat{Q}_0}{2\left(\lambda_2^2 - \lambda_1^2\right)}\left[\frac{1}{s^3}\exp(-s\lambda_1\xi) - \frac{1}{s^3}\exp(-s\lambda_2\xi)\right] \quad (25)$$

$$\overline{Z}(\xi, s) = \frac{\hat{Q}_0}{2\lambda_1\lambda_2}\left[\frac{\lambda_2(1-\lambda_1^2)}{\lambda_2^2-\lambda_1^2}\frac{1}{s^2}\exp(-s\lambda_1\xi) - \frac{\lambda_1(1-\lambda_2^2)}{\lambda_2^2-\lambda_1^2}\frac{1}{s^2}\exp(-s\lambda_2\xi)\right] \quad (26)$$

$$\overline{\sigma_{\xi\xi}}(\xi, s) = \frac{\hat{Q}_0}{2\lambda_1\lambda_2\left(\lambda_2^2-\lambda_1^2\right)} \cdot \left[-\frac{\lambda_2}{s^2}\exp(-s\lambda_1\xi) + \frac{\lambda_1}{s^2}\exp(-s\lambda_2\xi)\right] \quad (27)$$

Laplace inversions of these expressions yield the following solutions :

Case (ii) :

$$U(\xi, \tau) = \frac{\hat{Q}_0}{4\left(\lambda_2^2-\lambda_1^2\right)}\left[(\tau-\lambda_1\xi)^2 H(\tau-\lambda_1\xi) - (\tau-\lambda_2\xi)^2 H(\tau-\lambda_2\xi)\right] \quad (28)$$

$$Z(\xi, \tau) = \frac{\hat{Q}_0}{2\lambda_1\lambda_2}\left[\frac{\lambda_2(1-\lambda_1^2)}{\lambda_2^2-\lambda_1^2}(\tau-\lambda_1\xi)H(\tau-\lambda_1\xi) - \frac{\lambda_1(1-\lambda_2^2)}{\lambda_2^2-\lambda_1^2}(\tau-\lambda_2\xi)H(\tau-\lambda_2\xi)\right] \quad (29)$$

$$\sigma_{\xi\xi}(\xi,\tau) = \frac{\hat{Q}_0}{2\lambda_1\lambda_2(\lambda_2^2-\lambda_1^2)}[-\lambda_2(\tau-\lambda_1\xi)$$

$$H(\tau-\lambda_1\xi)+\lambda_1(\tau-\lambda_2\xi)H(\tau-\lambda_2\xi)] \quad (30)$$

As the results for case (i) can be derived from those of case (ii), the solutions for case (i) are found as

Case (i) :

$$U(\xi,\tau) = \frac{\hat{Q}_0}{4(\lambda_2^2-\lambda_1^2)}[(\tau-\lambda_1\xi)H(\tau-\lambda_1\xi)$$

$$-(\tau-\lambda_2\xi)H(\tau-\lambda_2\xi)] \quad (31)$$

$$Z(\xi,\tau) = \frac{\hat{Q}_0}{2\lambda_1\lambda_2}\left[\frac{\lambda_2(1-\lambda_1^2)}{\lambda_2^2-\lambda_1^2}H(\tau-\lambda_1\xi)\right.$$

$$\left.-\frac{\lambda_1(1-\lambda_2^2)}{\lambda_2^2-\lambda_1^2}H(\tau-\lambda_2\xi)\right] \quad (32)$$

$$\sigma_{\xi\xi}(\xi,\tau) = \frac{\hat{Q}_0}{2\lambda_1\lambda_2(\lambda_2^2-\lambda_1^2)}[-\lambda_2 H(\tau-\lambda_1\xi)$$

$$+\lambda_1 H(\tau-\lambda_2\xi)] \quad (33)$$

Discussion

Case (i) : The solutions for deformation, temperature field and stress in G-N theory[5] without energy dissipation reveal that they consist of two wave fronts – one propagating with finite speed $v_1 = \frac{1}{\lambda_1}$ and the other with $v_2 = \frac{1}{\lambda_2}$ and $v_1 < v_2$. The former is the modified elastic wave propagating with $v_1 = \frac{1}{\lambda_1}$ and the later is the modified thermal wave propagating with finite speed $v_2 = \frac{1}{\lambda_2}$ and that the elastic wave follows the thermal wave. Moreover the displacement field is continuous at both the wave fronts whereas the temperature and stresses suffer finite jumps at these locations in contrast to the result derived by Paria[1] using (classical thermo-elasticity) wherein both the deformation and temperature are continuous at the elastic wave front and the solution consist of a diffusive part and wave part corresponding to elastic wave. Using L-S theory[3], with thermal relaxation Roy Choudhuri and Sain[2] derived result wherein deformation, temperature and stress fields are all discontinuous at both the wave fronts and that the amount of the discontinuity decays exponentially with distance at the wave fronts. It is observed that G-N theory removes the finite discontinuity in deformation which were not observed in the corresponding problem considered by Roy Choudhuri and Sain[2], using L-S theory of thermal relaxation time.

The finite jumps in the present problem in temperature and stress are given by

Case (i) :

$$(Z^+ - Z^-)_{\xi=\tau v_1} = \frac{\hat{Q}_0}{2\lambda_1}\frac{(1-\lambda_1^2)}{\lambda_1^2-\lambda_2^2}$$

$$(Z^+ - Z^-)_{\xi=\tau v_2} = \frac{\hat{Q}_0}{2\lambda_2}\frac{(1-\lambda_2^2)}{\lambda_2^2-\lambda_1^2}$$

$$(\sigma_{\xi\xi}^{\ +} - \sigma_{\xi\xi}^{\ -})_{\xi=\tau v_1} = \frac{\hat{Q}_0}{2\lambda_1(\lambda_2^2-\lambda_1^2)}$$

$$(\sigma_{\xi\xi}^{\ +} - \sigma_{\xi\xi}^{\ -})_{\xi=\tau v_2} = \frac{\hat{Q}_0}{2\lambda_2(\lambda_1^2-\lambda_2^2)}$$

Case (ii) : The solutions for deformation, temperature and stress field consist of two waves-modified elastic wave and the modified thermal wave. The deformation, temperature and the stress are all continuous at both the wave fronts in contrast to the results derived by Bhatta[4] in a

similar problem using L-S theory where, though the displacement is continuous at both the wave fronts but temperature, stress suffer finite discontinuities at these locations.

References

1. Paria, G. (1968) *Indian J. of Mech. and Math.*, Part **1**, Special Issue, p. 41.
2. Roy Choudhuri, S.K. & Sain, G. (1982) *Indian J. Pure Appl. Math.* **13** (11) : 1340.
3. Lord, H. W. & Shulman, Y. (1967) *J. Mech. Phys. Solids* **15** : 299.
4. Bhatta, N. (1981) *Proc. Indian Natn. Sci. Acad.* **47A** (4) : 499.
5. Green, A.E. & Naghdi, P.M. (1993) *J. Elasticity* **31** : 189.
6. Popov, E. B. (1967) *P. M. M.* **31** : 328.
7. Puri, P. (1973) *Int. J. Eng. Sci.* **2** : 735.
8. Agarwal, V.K. (1978) *J. Elasticity* **8** : 171.

PROC. NAT. ACAD. SCI. INDIA, 75(A), II, 2005

Relative order of meromorphic functions

B.K. LAHIRI* and DIBYENDU BANERJEE

*B-1/146, Kalyani-741235, India.

Department of Mathematics, Visva-Bharati University, Santiniketan, West Bengal-731 235, India.

E-mail : indrajit@cal2.vsnl.net.in

Received January 16, 2003; Accepted July 14, 2004

Abstract

In this paper we improve some theorems proved earlier and establish the consistency of the definition of relative order of meromrophic functions when the related functions are entire.

(**Keywords** : meromorphic functions/relative order)

Introduction

If f and g be entire functions, let

$$F(r) = \max\{|f(z)| : |z| = r\} \quad \text{and}$$

$$G(r) = \max\{|g(z)| : |z| = r\}.$$

If f is not constant then $F(r)$ is strictly increasing and continuous function of r and its inverse

$$F^{-1} : (|f(0)|, \infty) \to (0, \infty)$$

exists and is such that

$$\lim_{s\to 0} F^{-1}(s) = \infty.$$

According to Bernal[1] the definition of the relative order of f with respect to g is as follows:

Definition 1 : Let f and g be two non-constant entire functions. Then the *relative order* of f with respect to g, denoted by $\rho_g(f)$, is defined as follows :

$$\rho_g(f) = \inf\{\mu > 0 : F(r) < G(r^{\mu}) \text{ for all } r > r_0(\mu) > 0\}$$

$$= \limsup_{r\to\infty} \frac{\log G^{-1} F(r)}{\log r}.$$

Definition 1 coincides with the classical definition of order of f if $g(z) = e^z$.

If f is meromorphic, we[2] defined the relative order of f with respect to g as follows :

Definition 2[2] : Let f and g be two non-constant functions such that f be meromorphic and g be entire. The *relative order* of f with respect to g is defined by

$$\rho_g(f) = \inf\{\mu > 0 : T_f(r) < T_g(r^{\mu}) \text{ for all large } r\}$$

$$= \limsup_{r\to\infty} \frac{\log T_g^{-1} T_f(r)}{\log r} \quad \text{(see Theorem4[2]).}$$

Here $T_f(r) = T(r,f)$ etc. denote the Nevanlinna characteristic function[3].

It is known[2] that if $g(z) = e^z$ then Definition 2 coincides with the classical definition of order of a meromorphic function f.

In this paper, we prove the consistency of the Definition 2 when f is entire and obtain improvements of some of the theorems proved in

literature[2]. Throughout we shall assume f, g etc. to be non-constant and if they are entire then $F(r)$, $G(r)$ etc. will denote respectively their maximum modulus on $|z| = r$.

Property (A) and known Lemmas

Definition 3[1] : An entire function g is said to have the *property (A)* if for any $\sigma > 1$ and for all large r

$$[G(r)]^2 \leq G(r^\sigma)$$

holds.

Examples of entire functions are known[1] which have the *property (A)* as well as which do not have the *property (A)*.

Lemma 1[1] : Let g be an entire function which has the property (A). Then for any positive integer n and for all $\sigma > 1$ and for all large r

$$[G(r)]^n \leq G(r^\sigma)$$

holds.

Lemma 2[1] : If f be an entire function and $0 < \mu < \lambda$, then

$$\lim_{r\to\infty} \frac{F(r^\lambda)}{F(r^\mu)} = \infty.$$

Lemma 3[3] *(p 18)* : If f is entire then

$$T_f(r) \leq \log F(r) \leq 3\, T_f(2r) \text{ for all large } r.$$

Lemma 4[4,5] : Let f be a meromorphic function. Then for all large r

$$T_f(r) < C\, \{T_{f'}(2r) + \log r\}$$

where f' denotes the derivative of f and C is a constant.

Lemma 5[1] : If f is entire transcendental and $s > 1$ then for any positive integer n

$$\lim_{r\to\infty} \frac{F(r^s)}{r^n\, F(r)} = \infty.$$

Consistency Theorem

Theorem 1 : If f be entire and g has the property (A), then Definition 2 coincides with Definition 1.

Proof : We assume the Definition 2 for $\rho_g(f)$ and suppose first that $0<\rho_g(f)<\infty$. Then for $\varepsilon < 0$ arbitrary there exists $r_0(\varepsilon)>0$ such that

$$T_f(r) < T_g\left(r^{\rho_g(f)+\varepsilon/2}\right) \text{ for } r \geq r_0. \quad (1)$$

So for all large r

$$\begin{aligned}\log F(r) &\leq 3\, T_f(2r), \text{ by Lemma 3}\\ &< 3T_g((2r)^{\rho_g(f)+\varepsilon/2}), \text{ by (1)}\\ &\leq 3\log G\left((2r)^{\rho_g(f)+\varepsilon/2}\right), \text{by Lemma 3}\\ &< 3\log G\left(r^{\rho_g(f)+\varepsilon}\right)\\ &= \log\left[G\left(r^{\rho_g(f)+\varepsilon}\right)\right]^3\\ &\leq \log G\left(\left(r^{\rho_g(f)+\varepsilon}\right)^\sigma\right), \text{ by Lemma 1}\end{aligned}$$

for every $\sigma > 1$. Thus for all large r

$$G^{-1} F(r) < r^{\sigma(\rho_g(f)+\varepsilon)}$$

i.e. $$\frac{\log G^{-1} F(r)}{\log r} < \sigma(\rho_g(f)+\varepsilon).$$

Since $\sigma>1$ was arbitrary,

$$\frac{\log G^{-1} F(r)}{\log r} \leq \rho_g(f)+\varepsilon \text{ for all lage } r. \quad (2)$$

Choose now $0 < \lambda < \rho_g(f)$. Then from Definition 2, there exists a sequence $r_n \to \infty$ such that

$$T_f(r_n) > T_g\left(r_n^{\lambda_2}\right) \tag{3}$$

for all large n, where $\lambda<\lambda_2<\rho_g(f)$.

Now for all large n

$$\begin{aligned}
\log F(r_n) &\geq T_f(r_n), \text{ by Lemma 3} \\
&> T_g\left(r_n^{\lambda_2}\right), \text{ by (3)} \\
&> T_g\left(2r_n^{\lambda_1}\right), \text{ where } \lambda<\lambda_1<\lambda_2 \\
&> 1/3 \log G\left(r_n^{\lambda_1}\right), \text{ by Lemma 3} \\
&= 1/3 \log G\left(\left(r_n^{\lambda}\right)^{\sigma}\right), \text{ where } \sigma=\lambda_1/\lambda \\
&\geq 1/3 \log \left[G\left(r_n^{\lambda}\right)\right]^3, \text{ by Lemma 1} \\
&= \log G\left(r_n^{\lambda}\right).
\end{aligned}$$

So $\dfrac{\log G^{-1} F(r_n)}{\log r_n} > \lambda$ for all large n. (4)

Combining (2) and (4), we obtain

$$\rho_g(f) = \limsup_{r\to\infty} \frac{\log G^{-1} F(r)}{\log r}$$

which is Definition 1.

Suppose now that

$\rho_g(f) = \limsup\limits_{r\to\infty} \dfrac{\log T_g^{-1} T_f(r)}{\log r} = \infty$. Let M (>1) be arbitrary. Then there exists $r_0>0$ such that for all $r \geq r_0$

$$\frac{\log T_g^{-1} T_f(r)}{\log r} > 2M+1$$

i.e. $T_f(r) > T_g(r^{2M+1})$.

Now for all large r

$$\begin{aligned}
\log F(r) &\geq T_f(r), \text{ by Lemma 3} \\
&> T_g\left(r^{2M+1}\right) \\
&\geq \frac{1}{3}\log G\left(\frac{1}{2}r^{2M+1}\right), \text{ by Lemma 3} \\
&> \frac{1}{3}\log G\left(r^{2M}\right), \text{ since } G(r) \text{ is increasing} \\
&= \frac{1}{3}\log G\left(\left(r^{M}\right)^2\right) \\
&\geq \frac{1}{3}\log\left[G\left(r^{M}\right)\right]^3, \text{ by Lemma 1 by taking } \sigma = 2 \text{ and } n = 3 \\
&= \log G\left(r^{M}\right).
\end{aligned}$$

$\therefore$ $G^{-1}F(r) > r^M$ for all larger r and this gives

$$\limsup_{r\to\infty} \frac{\log G^{-1} F(r)}{\log r} = \infty.$$

The case when $\rho_g(f)=0$ can be treated analogously. This proves the theorem.

Theorems on Derivatives

The following theorem is known.

Theorem 2[2] (see Theorem 7[2]) : Let f be a transcendental meromorphic function and g be an entire function with the property (A). Then $\rho_g(f)= \rho_g(f')$ where dash denotes the derivative.

We now prove Theorem 2 when f is a rational meromorphic function. The following lemma is needed.

Lemma 6 : Let f be a rational meromorphic function. Then for all large values of r,

$$T_{f}'(r) < T_f(r) + K \log r + O(1)$$

where K is a constant depending on f only.

Proof of Lemma 6 : We can write $f(z)$ as

$$f(z) = \frac{\phi(z)}{\psi(z)}$$

where $\phi(z)$ and $\psi(z)$ are polynomials. Taking logarithmic differentiation, we see that

$$f' = f\left[\frac{\phi'}{\phi} - \frac{\psi'}{\psi}\right].$$

$$\therefore \quad T_{f'}(r) \le T_f(r) + T_{\phi'/\phi - \psi'/\psi}(r)$$

$$\le T_f(r) + T_{\phi'/\phi}(r) + T_{\psi'/\psi}(r) + \log 2$$

$$= T_f(r) + \lambda \log r + \mu \log r + O(1) + \log 2$$

where λ and μ are degrees of the polynomials ϕ and ψ respectively

$$= T_f(r) + K \log r + O(1).$$

This proves the lemma.

From Lemmas 4 and 6 we obtain for all large r

$$T_f(r) \le C' T_{f'}(2r),\ C' > 1$$

because f is rational and

$$T_{f'}(r) \le T_f(r) + K_1 T_f(r)$$

$$< K' T_f(2r), \text{ where } K' > 1.$$

From this stage onwards, the proof of Theorem 2 when f is rational follows in the same lines as the proof of Theorem 7[2].

The following theorem has therefore been proved.

Theorem 2 : Let f be a meromorphic function and g be an entire function with the property (A). Then $\rho_g(f) = \rho_g(f')$ where dash denotes the derivative.

We now prove the following theorem.

Theorem 3 : If f be meromorphic and g be entire transcendental having the property (A), then $\rho_g(f) = \rho_{g'}(f)$.

The following lemma is required.

Lemma 7 : Let g be entire transcendental and $\overline{G}(r) = \max_{|z|=r} |g'(z)|$. Then

$$G(r^{\lambda}) < \overline{G}(r) < G(2r),\ r > 1 \text{ and } \lambda \in (0,1).$$

Proof : We may write $g(z) = \int_0^z g'(t)dt$, where the line of integration is the segment from $z=0$ to $z = re^{i\theta_0}$, $r > 0$. Let $z_1 = re^{i\theta_1}$, be such that $|g(z_1)| = \max_{|z|=r} |g(z)|$.

$$\text{Then } G(r) = |g(z_1)| = \left| \int_0^{z_1} g'(t)dt \right|$$

$$\le r \max \{|g'(z)| : |z| = r\}$$

$$= r\overline{G}(r) \qquad (5)$$

Let C denote the circle $|t - z_0| = r$, where z_0, $|z_0| = r$ is defined so that $|g'(z_0)| = \max_{|z|=r} |g'(z)|$. So

$$\overline{G}(r) = \max_{|z|=r} |g'(z)| = |g'(z_0)|$$

$$= \left| \frac{1}{2\pi i} \oint_C \frac{g(t)}{(t-z_0)^2}\, dt \right|$$

$$\leq \frac{G(2r)}{r}. \tag{6}$$

From (5) and (6)

$$\frac{G(r)}{r} \leq \overline{G}(r) \leq \frac{G(2r)}{r}, r > 0. \tag{7}$$

Let $\lambda \in (0,1)$ and $s = \frac{1}{\lambda}$. Let n be a positive integer such that $n\lambda \geq 1$. Since g is transcendental, from Lemma 5.

$$G\left(r^s\right) > r^n G(r) \quad \text{for all large } r.$$

If we replace r by r^λ, then from above

$$G\left(r^{s\lambda}\right) > r^{n\lambda}\, G\left(r^\lambda\right) \geq rG\left(r^\lambda\right)$$

i.e. $\quad G(r) > rG\left(r^\lambda\right).$

From (7)

$$G\left(r^\lambda\right) < \frac{G(r)}{r} \leq \overline{G}(r) \leq \frac{G(2r)}{r} < G(2r), r > 1$$

i.e. $G\left(r^\lambda\right) < \overline{G}(r) < G(2r)$ where $r > 1$.

This proves the lemma.

Proof of Theorem 3 : We can assume that $\rho_g(f)$ and $\rho_{g'}(f)$ are finite. By the definition of $\rho_g(f)$, for all large r

$$T_f(r) < T_g\left(r^{\mu_1}\right) \text{ where } \rho_g(f) < \mu_1$$

$$\leq \log G\left(r^{\mu_1}\right), \text{ by Lemma 3}$$

$$= \frac{1}{3} \log \left[G\left(r^{\mu_1}\right)\right]^3$$

$$\leq \frac{1}{3} \log G\left(\left(r^{\mu_1}\right)^\sigma\right), \text{ for any } \sigma > 1, \text{ by Lemma 1}$$

$$< \frac{1}{3} \log \overline{G}\left(r^{\frac{\mu_1\sigma}{\lambda}}\right), \text{ by Lemma 7}$$

$$< \frac{1}{3} \log \overline{G}\left(\frac{1}{2} r^{\frac{\mu\sigma}{\lambda}}\right), \text{ where } \mu_1 < \mu$$

$$\leq T_{g'}\left(r^{\frac{\mu\sigma}{\lambda}}\right), \text{ using Lemma 3, since } g' \text{ is entire.}$$

So for all large r

$$T_{g'}^{-1}\, T_f(r) < r^{\frac{\mu\sigma}{\lambda}}, \text{ since } g \text{ is transcendental}$$

and this gives

$$\limsup_{r\to\infty} \frac{\log T_{g'}^{-1}\, T_f(r)}{\log r} \leq \frac{\sigma}{\lambda}.\mu.$$

Since this is true for any $\sigma > 1$ and $\lambda \in (0,1)$, we obtain

$$\rho_{g'}(f) \leq \mu.$$

Now $\mu > \mu_1 > \rho_g(f)$ is arbitrary, so we have ultimately

$$\rho_{g'}(f) \leq \rho_g(f). \tag{8}$$

To obtain the converse inequality, we see from the definition of $\rho_{g'}(f)$ that for all large r

$$T_f(r) < T_{g'}\left(r^{\lambda_1}\right), \text{ where } \rho_{g'}(f) < \lambda_1$$

$$\leq \log \overline{G}\left(r^{\lambda_1}\right), \text{ using Lemma 3, since } g' \text{ is entire}$$

$$< \log G\left(2r^{\lambda_1}\right), \text{ by Lemma 7}$$

$$\leq \log G\left(r^{\lambda_2}\right), \text{ where } \lambda_1 < \lambda_2 \text{ and } G(r) \text{ is strictly increasing}$$

$$= \frac{1}{3} \log \left[G\left(r^{\lambda_2}\right)\right]^3$$

$$\leq \frac{1}{3} \log G\left(\left(r^{\lambda_2}\right)^{\sigma}\right), \text{ by Lemma 1}$$

$$< \frac{1}{3} \log G\left(\frac{1}{2} r^{\lambda\sigma}\right), \text{ where } \lambda_2 < \lambda \text{ and } G(r) \text{ is strictly increasing}$$

$$\leq T_g\left(r^{\lambda\sigma}\right), \text{ by Lemma 3.}$$

$$\therefore \quad T_g^{-1} T_f(r) < r^{\lambda,\sigma} \text{ for all large } r.$$

$$\therefore \quad \limsup_{r\to\infty} \frac{\log T_g^{-1} T_f(r)}{\log r} \leq \lambda\sigma.$$

Since $\lambda > \rho_{g'}(f)$ is arbitrary, letting $\sigma \to 1+$, we obtain

$$\rho_g(f) \leq \rho_{g'}(f). \tag{9}$$

Combining (8) and (9), we obtain

$$\rho_g(f) = \rho_{g'}(f)$$

and this proves the theorem.

Note 1 : Starting from the function f', we can similarly show that

$$\rho_g(f') = \rho_{g'}(f').$$

Combining Theorem 2', Theorem 3 and Note 1 we obtain the following theorem.

Theorem 4 : If f be meromorphic and g be entire transcendental having the property (A) then

$$\rho_g(f') = \rho_{g'}(f) = \rho_{g'}(f') = \rho_g(f).$$

Note : If one or more of the above expressions be infinite, the modification of the proof is evident.

Relative Order of the Sum of Meromorphic Functions

The following theorem has been proved in literature[2].

Theorem 5 (see Theorem 5[2]) : Let f_1 and f_2 be meromorphic functions having orders $\rho_g(f_1)$ and $\rho_g(f_2)$ respectively, where g has the property (A). Then

(1) $\rho_g(f_1 \pm f_2) \leq \max\{\rho_g(f_1), \rho_g(f_2)\}$ and

(2) $\rho_g(f_1 \cdot f_2) \leq \max\{\rho_g(f_1), \rho_g(f_2)\}$.

The same inequality holds for the quotient. The equality holds in (2) if $\rho_g(f_1) \neq \rho_g(f_2)$.

Here we prove that in (1) the equality holds when $\rho_g(f_1) \neq \rho_g(f_2)$.

Proof : Let $f = f_2 \pm f_1$, $\rho = \rho_g(f)$, $\rho_1 = \rho_g(f_1)$, $\rho_2 = \rho_g(f_2)$ and suppose that $\rho_1 < \rho_2$.

For arbitrary $\varepsilon > 0$ and for all large r, we have

$$T_{f_i}(r) < T_g\left(r^{\rho_i + \varepsilon}\right) \tag{10}$$

and for a sequence of values of $r = r_n \to \infty$

$$T_{f_i}(r_n) > T_g\left(r_n^{\rho_i - \varepsilon}\right), \; i = 1,2. \tag{11}$$

Choose $\rho_1 < \mu < \lambda < \rho_2$. Now for all large r, we have by (10), Lemma 3 and Lemma 1

$$T_{f_1}(r) < T_g\left(r^{\mu}\right) \leq \log G\left(r^{\mu}\right) = \frac{1}{6}\log\left[G\left(r^{\mu}\right)\right]^{\sigma}$$

$$= \frac{1}{6}\log G\left(\left(r^{\mu}\right)^{\sigma}\right), \text{ for any } \sigma > 1$$

$$= \frac{1}{6}\log G\left(r^{\mu\sigma}\right). \tag{12}$$

Also by (11) there exists a sequence $\{r_n\}$, $r_n \to \infty$ such that

$$T_{f_2}(r_n) > T_g(r_n^{\lambda_1}) \text{ where } \lambda < \lambda_1 < \rho_2$$

$$\geq T_g(2r_n^{\lambda})$$

$$\geq \frac{1}{3}\log G(r_n^{\lambda}), \text{ using Lemma 3} \quad (13)$$

If $\sigma > 1$ is chosen such that $\mu\sigma<\lambda$, which is clearly possible, then by Lemma 2

$$\lim_{r\to\infty} \frac{G(r^{\lambda})}{G(r^{\mu\sigma})} = \infty.$$

So $\log G(r^{\lambda}) > \log G(r^{\mu\sigma})$ for all large r. (14)

From (12), (13) and (14)

$$2T_{f_1}(r_n) < T_{f_2}(r_n), \text{ for } n = 1,2,3,\ldots\ldots \quad (15)$$

Now $T_{f_2}(r) = T_{f\pm f_1}(r)$

$$\leq T_f(r) + T_{f_1}(r) + \log 2.$$

So for all large n

$$T_f(r_n) \geq T_{f_2}(r_n) - T_{f_1}(r_n) - \log 2$$

$$> \frac{1}{2}T_{f_2}(r_n) - \log 2 \quad \text{by (15)}$$

$$> \frac{1}{3}T_{f_2}(r_n)$$

$$> \frac{1}{3}T_g(r_n^{\lambda_1}) \quad \text{by (11),}$$

where $\lambda<\lambda_1<\rho_2$

$$> \frac{1}{9}\log G\left(\frac{r_n^{\lambda_1}}{2}\right) \text{ using Lemma 3.}$$

Now $G\left(\frac{r_n^{\lambda_1}}{2}\right) = G\left(\frac{r_n^{\lambda\sigma}}{2}\right)$ where $\sigma>1$ is so chosen that $\lambda_1 = \lambda\sigma$

$$> G\left(\left(\frac{r_n^{\lambda}}{2}\right)^{\sigma}\right)$$

$$\geq \left[G\left(\frac{r_n^{\lambda}}{2}\right)\right]^9, \text{ by Lemma 1.}$$

Therefore $\frac{1}{9}\log G\left(\frac{r_n^{\lambda_1}}{2}\right) > \log G\left(\frac{r_n^{\lambda}}{2}\right)$

$$> T_g\left(\frac{r_n^{\lambda}}{2}\right), \text{ by Lemma 3.}$$

This implies by the preceding step

$$T_f(r_n) > T_g\left(\frac{r_n^{\lambda}}{2}\right) \quad \text{for all large } n.$$

So $\dfrac{\log T_g^{-1}T_f(r_n)}{\log r_n} > \lambda - \dfrac{\log 2}{\log r_n}$

for all large n and this gives $\rho \geq \lambda$. Since $\lambda \in (\rho_1, \rho_2)$ is arbitrary, we have $\rho \geq \rho_2$.

By Theorem 5 above we have already $\rho \leq \rho_2$. Hence $\rho = \rho_2$.

So $\rho_g(f_2 \pm f_1) = \rho_g(f_2) = \max\{\rho_g(f_1), \rho_g(f_2)\}$.

References

1. Bernal, L. (1988) *Collectanea Mathematica*, 209.
2. Lahiri, B.K. & Banerjee, Dibyendu (1999) *Proc. Nat. Acad. Sci. India* **69**(A), III : 339.
3. Hayman, W.K. (1964) *Meromorphic Functions*, Oxford Univ. Press.
4. Dai, Chongi & Jin, Lu (1987) *Kodai Math. J.* **10** : 74.
5. Yang, Lo (1982) *Value Distribution and its New Research*, Beijing.

PROC. NAT. ACAD. SCI. INDIA, 75(A), II, 2005

Energy of trees with edge independence number two

H.B. WALIKAR and H.S. RAMANE*

Department of Mathematics,Karnatak University's Kittur Rani Chennama Post Graduate Centre, Post Bag No. 3, Belgaum – 590 001, India.

(E-mail: walikarhb@yahoo.co.in)

**Department of Master of Computer Applications, Gogte Institute of Technology, Udyambag, Belgaum – 590 008, India.*

(E-mail: hsramane@yahoo.com)

Received January 27, 2004; Revised July 12, 2004; Accepted August 9, 2004

Abstract

The energy of a graph G is defined as the sum of the absolute values of the eigenvalues of G. In this paper we consider the energy of trees with edge independence number two.

(**Keywords** : energy of a graph/tree/edge independence number)

Introduction

Let G be a undirected graph[1] without loops and multiple edges with p vertices. Let $V(G) = \{v_1, v_2, \dots, v_p\}$ be the vertex set of G. The adjacency matrix of a graph G is the $p{\times}p$ matrix $A(G) = [a_{ij}]$, in which $a_{ij} = 1$ if v_i is adjacent to v_j and $a_{ij} = 0$, otherwise. The characteristic polynomial of $A(G)$ is the characteristic polynomial of G and is denoted by $\phi(G:\lambda)$. Thus $\phi(G:\lambda) = det(\lambda I - A(G))$ where I is a unit matrix of order p. The roots of the equation $\phi(G:\lambda) = 0$, denoted by $\lambda_1, \lambda_2, \dots, \lambda_p$ are the eigenvalues[2] of G. The energy[3] of a graph G is defined as the sum of the absolute values of the eigenvalues of G and is denoted by $E(G)$. Thus $E(G) = |\lambda_1| + |\lambda_2| + \dots + |\lambda_p|$. It is a generalization of a formula valid for total pi-electron energy of certain nonsaturated hydrocarbons as calculated with the Huckel Molecular Orbital (HMO) method in quantum chemistry[4]. Various bounds on $E(G)$ were derived[5-9].

Gutman[9] established the energy of a graph in terms of integral expression as

$$E(G) = \frac{1}{\pi} \int_{-\infty}^{\infty} \left[p - \lambda \frac{d}{d\lambda} \log_e \phi(G : i\lambda) \right] d\lambda \quad (1)$$

where p is the number of vertices of a graph G, $\phi(G:\lambda)$ denotes the characteristic polynomial of G and $i = \sqrt{-1}$

Further the energy of a bipartite graph is defined as[10]

$$E(G) = \frac{1}{\pi} \int_{-\infty}^{\infty} \frac{d\lambda}{\lambda^2} \log_e (1 + a_2\lambda^2 + a_4\lambda^4 + \dots + a_{2k}\lambda^{2k}), \quad (2)$$

where

$$\phi(G:\lambda) = \lambda^p - a_2\lambda^{p-2} + a_4\lambda^{p-4} - \dots + (-1)^k a_{2k}\lambda^{p-2k} \quad (3)$$

is the characteristic polynomial of the corresponding bipartite graph G, p is the number of vertices of G and

$$k = \begin{cases} (p/2), & \text{if } p \text{ is even} \\ (p-1)/2, & \text{if } p \text{ is odd.} \end{cases}$$

If the characteristic polynomial is written as in equation (3), then

$a_{2j} = a_{2j}(G) \geq 0$ for all $j = 1, 2, \dots, k$.

Let G and H be the bipartite graphs with the same number of vertices. Suppose coefficients a_{2j} of these two graphs fulfill the inequalities

$$a_{2j}(G) \geq a_{2j}(H) \text{ for all } j = 1, 2, \ldots, k \tag{4}$$

then from equation (2) it follows that

$$E(G) \geq E(H) \tag{5}$$

Further if the characteristic polynomial of G and H are not same then the relation (4) implies that $E(G) > E(H)$[11].

An independent set of edges of G has no two of its edges incident to a common vertex and the maximum cardinality of such a set is the edge independence number of G denoted by $\beta_1(G)$. The distance $d_G(u, v)$ in G between two vertices u and v is the length of shortest path in G. The greatest distance between any two vertices in G is the diameter[12] of G and is denoted by $diam(G)$.

Theorem[13] *1* : Let T be the tree with p vertices and $M_k = \{e_1, e_2, \ldots, e_k\}$ be the set of k-independent edges of a tree T, $1 \leq k \leq \lfloor p/2 \rfloor$ and $Q_n(M_k) = \{S \mid S \subseteq M_k \text{ and } |S| = n\}$, $1 \leq n \leq k$. In addition $Q_0(M_k)$ is an empty set. Let T_k be the graph obtained from T by removing the k-independent edges $e_1, e_2, \ldots, e_k$ and $T_k - S$ is the graph obtained from T_k by removing the end vertices of the edges which belongs to S then

$$\phi(T:\lambda) = \sum_{n=0}^{k} \left[(-1)^n \sum_{S \in Q_n(M_k)} \phi(T_k - S : \lambda) \right] \tag{6}$$

Note that $\phi(K_0 : \lambda) = 1$, where K_0 is a graph without vertices and edges. □

Among all trees with p vertices the path P_p has maximum energy and star S_p has minimum energy[14]. Thus $E(S_p) \leq E(T) \leq E(P_p)$, where T is tree with p vertices.

The Fig. 1 depicts P_6 and S_7.
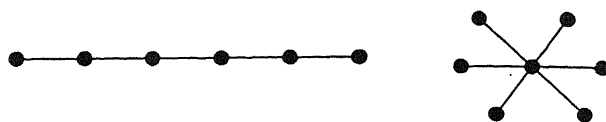
Fig. 1 – P_6 and S_7.

In this paper we discuss the energy of trees with edge independence number two.

Trees with $\beta_1(T) = 2$

Proposition 2 : If $\beta_1(T) = 2$ then, $3 \leq diam(T) \leq 4$.

Proof : If $diam(T) \leq 2$ then $T = K_1$ or K_2 or $K_{1,p-1}$. Therefore $\beta_1(T) \leq 1$, a contradiction to the fact that $\beta_1(T) = 2$. Thus $diam(T) \geq 3$.

Next we prove that $diam(T) \leq 4$.

If possible assume that $diam(T) = k \geq 5$. Let u and v be the peripheral vertices of the longest path $uu_1u_2u_3u_4 \ldots u_{k-2}u_{k-1}v$ in T. Then the edges $e_1 = uu_1$, $e_2 = u_2u_3$, $e_3 = u_4u_5$, ..., $e_{k/2} = u_{k-2}u_{k-1}$ are independent edges in T if k is even, so that $\beta_1(T) = (k/2) > 2$ as $k \geq 5$, a contradiction and the edges $e_1 = uu_1$, $e_2 = u_2u_3$, $e_3 = u_4u_5$,..., $e_{(k+1)/2} = u_{k-1}v$ are independent edges in T if k is odd, so that $\beta_1(T) = (k+1)/2 > 2$, again a contradiction to $\beta_1(T) = 2$. Thus $diam(T) \leq 4$. □

Proposition 3 : If $\beta_1(T) = 2$ then T is one of the following trees in Fig. 2 and Fig. 3.
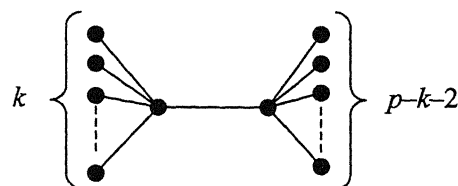
Fig. 2 – $A_p(k)$
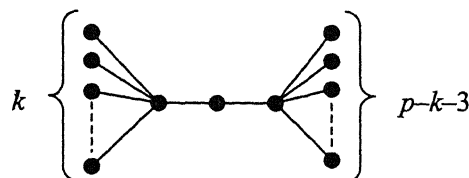
Fig. 3 – $B_p(k)$

Proof : By Proposition 2, if $\beta_1(T) = 2$ then $3 \le diam(T) \le 4$. We consider here two cases.

Case 1 : If $diam(T) = 3$ then there is a longest path say uu_1u_2v in T. Then all the remaining vertices of T are adjacent to u_1 or u_2 only, which gives the tree $A_p(k)$ as shown in Fig. 2.

Case 2 : If $diam(T) = 4$, then there is a longest path say $uu_1u_2u_3v$ in T. Then all the remaining vertices of T are adjacent to either u_1 or u_3 but not to u_2, for otherwise, if there is a vertex say w (other than u_1 and u_3) adjacent to u_2 then the edges uu_1, u_2w and u_3v are independent in T, so that $\beta_1(T) = 3$, a contradiction. Thus the tree with $diam(T) = 4$ is $B_p(k)$ as in Fig. 3. □

Energy of Trees with $\beta_1(T) = 2$

To find the energy of trees with $\beta_1(T) = 2$, we need the characteristic polynomials of these trees. The characteristic polynomials of trees listed in the Proposition 3, cån be computed by using Theorem 1. They are as follows.

$$\phi(A_p(k) : \lambda) = \lambda^p - (p-1)\lambda^{p-2} + k(p-k-2)\lambda^{p-4} \quad (7)$$

and $$\phi(B_p(k) : \lambda) = \lambda^p - (p-1)\lambda^{p-2} + [(k+1)(p-k-3) + k]\lambda^{p-4}. \quad (8)$$

With the help of characteristic polynomials given above and using inequalities (4) and (5) we prove the results of this section.

Proposition 4 : Let $A_p(k)$ be the tree as in Fig. 2, then for any two integers p and k,

$$E(A_p(1)) < E(A_p(2)) < E(A_p(3)) < \ldots < E(A_p(\lfloor (p/2) - 1 \rfloor)).$$

Proof : From the characteristic polynomial of $A_p(k)$ (see Eqn. (7)) we have

$$a_4(A_p(k)) = k(p - k - 2).$$

This integer valued function has maximum value if $k = \lfloor (p/2) - 1 \rfloor$ and it is increasing in $1 \le k \le \lfloor (p/2) - 1 \rfloor$. With this observation, and by the inequalities (4) and (5) the proof follows. □

Proposition 5 : Let $B_p(k)$ be the tree as in Fig. 3, then for any two integers p and k,

$$E(B_p(1)) < E(B_p(2)) < E(B_p(3)) < \ldots < E(B_p(\lfloor (p-3)/2 \rfloor)).$$

Proof : From the characteristic polynomial of $B_p(k)$ (see Eqn. (8)) we have

$$a_4(B_p(k)) = (k + 1)(p - k - 3) + k.$$

This integer valued function has maximum value if $k = \lfloor (p-3)/2 \rfloor$ and it is increasing in $1 \le k \le \lfloor (p-3)/2 \rfloor$. With this observation and by the inequalities (4) and (5) we get the required result. □

Proposition 6 : For any two integers p and k, $E(A_p(k + 1)) < E(B_p(k))$.

Proof : By the nature of the characteristic polynomials of $A_p(k)$ and $B_p(k)$ (Eqn. (7) and (8)), we have the coefficients

$$a_4(A_p(k)) = k(p - k - 2)$$

$$\therefore \quad a_4(A_p(k+1)) = (k+1)(p-k-3) \quad (9)$$

and $$a_4(B_p(k)) = (k+1)(p-k-3) + k. \quad (10)$$

From above coefficients (9) and (10) it is clear that $a_4(A_p(k+1)) < a_4(B_p(k))$.

Hence from above inequality and the inequalities (4) and (5) we have

$$E(A_p(k+1)) < E(B_p(k)). \quad □$$

Proposition 7 : For any two integers p and k, $E(A_p(k)) < E(B_p(k))$.

Proof : Follows from Propositions 4 and 6. □

References

1. Harary, F. (1998) *Graph Theory*, Narosa Publishing House, New Delhi, p.9
2. Cvetkovic, D. M., Doob, M. & Sachs, H. (1980) *Spectra of Graphs*, Academic Press, New York, p.12

3. Gutman, I. (1978) *Ber. Math. Stat. Sekt. Forschungszentrum Graz* **103** : 1.

4. Gutman, I., Polansky, O. E. (1986) *Mathematical Concepts in Organic Chemistry*, Springer-Verlag, Berlin.

5. Gutman, I. (1977) *Chem. Phys. Letters* **50** : 488.

6. McClelland, B. J. (1971) *J. Chem. Phys.* **54** : 640.

7. Walikar, H. B., Ramane, H. S. & Hampiholi, P. R. (1999) in *Graph Connections*, Eds. Balkrishnan, R., Mulder, H. M., Vijaykumar, A., Allied Publishers, New Delhi, p. 120.

8. Gutman, I., Pavlovic, L. (1999) *Bull. Acad. Serbe Sci. Arts (Cl. Math. Natur)* **118** : 35.

9. Gutman, I. (1974) *Chem. Phys. Letters* **24** : 283.

10. Coulson, C. A. (1954) *J. Chem. Soc. London* 3111.

11. Graovac, A., Gutman, I. & Trinajstic, N. (1977) *Topological Approach to the Chemistry of Conjugated Molecules*, Lecture Notes in Chemistry No. 4, Springer-Verlag, Berlin.

12. Diestel, R. (2000) *Graph Theory*, Springer, New York, p. 8

13. Walikar, H. B., Ramane, H. S. (Preprint).

14. Gutman, I. (1977) *Theoret. Chim. Acta (Berl.)* **45** : 79.

PROC. NAT. ACAD. SCI. INDIA, 75(A), II, 2005

Thermal instability of couple-stress fluid permeated with suspended particles in hydromagnetics in porous medium

PARDEEP KUMAR and POONAM SHARMA

Department of Mathematics, ICDEOL, Himachal Pradesh University, Shimla, India.

Received November 14, 2003; Revised April 13, 2004; Accepted September 10, 2004

Abstract

The effect of suspended particles on the thermal instability of couple-stress viscoelastic fluid in hydromagnetics in porous medium is considered. The medium permeability and suspended particles hasten the onset of convection whereas the magnetic field and couple-stress postpone the onset of convection, for the case of stationary convection. The principle of exchange of stabilities is found to hold good for couple-stress fluid permeated with suspended particles in the absence of magnetic field. The magnetic field introduces oscillatory modes in the system which were non-existent in its absence.

(**Keywords** : thermal instability/couple-stress fluid/suspended particles/magnetic field/porous medium)

Introduction

The theoretical and experimental results of the onset of thermal instability (Benard convection) in a fluid layer under varying assumptions of hydrodynamics and hydromagnetics has been treated in detail by Chandrasekhar[1]. A destabilizing effect of suspended particles on the onset of Benard convection have been shown by Scanlon and Segel[2]. In recent years the study of non-Newtonian fluids through porous media have attracted the attention of number of scholars because of their importance in modern technology and industries and the investigations on such fluids are desirable. Stokes[3] has formulated the theory of couple-stress fluid. One of the applications of couple-stress fluid is its use to the study of the mechanisms of lubrication of synovial joints, which has become the object of scientific research. A human joint is a dynamically loaded bearing, which has articular cartilage as the bearing and synovial fluid as the lubricant. Normal synovial fluid is a viscous, non-Newtonian fluid and is generally clear or yellowish. Walicki and Walicka[4] have modelled synovial fluid as a couple-stress fluid in human joints. Several workers[5,6] have worked on the problem of couple-stress fluid under varying physical conditions. Hence, the object of the present paper is to study the effect of suspended (or dust) particles on the couple-stress fluid heated from below in porous medium in the presence of a uniform horizontal magnetic field.

Formulation of the Problem and Perturbation Equations

Here we consider an infinite horizontal layer of an electrically conducting couple-stress fluid permeated with suspended particles and bounded by the planes $z = 0$ and $z = d$ in a porous medium. This layer is heated from below so that, the temperatures and densities at the bottom surface $z = 0$ are T_0, r_0 and at the upper surface $z = d$ are T_d, p_d respectively and that a uniform temperature gradient $\beta\left(=\left|dT/dz\right|\right)$ is maintained. A uniform horizontal magnetic field $\vec{H}(H,0,0)$ and gravity field $\vec{g}(0,0,-g)$ pervade the system.

Let δp, $\delta\rho$, θ, $\vec{q}\,(u,v,w)$, $\vec{q}_d(l,r,s)$, N and $\vec{h}\,(h_x,h_y,h_z)$ denote respectively the perturbations in fluid pressure p, density ρ, temperature T, couple-stress fluid velocity (0,0,0), suspended particles velocity (0,0,0), suspended particles number density N_0 and magnetic field $\vec{H}(H,0,0)$. Then the linearized hydromagnetic perturbation equations of the couple-stress fluid-particle layer in porous medium (Scanlon and Segel[2], Stokes[3], Joseph[7]) are

$$\frac{1}{\in}\frac{\partial \vec{q}}{\partial t} = -\frac{1}{\rho_0}\nabla \delta p + g\alpha\theta\vec{\lambda} - \frac{1}{k_1}\left(\upsilon - \frac{\mu'}{\rho_0}\nabla^2\right)\vec{q} +$$

$$\frac{KN_0}{\rho_0 \in}(\vec{q}_d - \vec{q}) + \frac{\mu_e}{4\pi\rho_0}\left(\nabla \times \vec{h}\right) \times \vec{H}, \quad (1)$$

$$\nabla \cdot \vec{q} = 0, \quad (2)$$

$$mN_0 \frac{\partial \vec{q}_d}{\partial t} = KN_0(\vec{q} - \vec{q}_d), \quad (3)$$

$$(E + h \in)\frac{\partial \theta}{\partial t} = \beta(w + hs) + \chi\nabla^2\theta, \quad (4)$$

$$\in \frac{\partial \vec{h}}{\partial t} = (\vec{H} \cdot \nabla)\vec{q} + \in \eta \nabla^2 \vec{h}, \quad (5)$$

$$\nabla \cdot \vec{h} = 0, \quad (6)$$

where $E = \in + (1 - \in)\frac{\rho_s C_s}{\rho_0 C_v}$, $h = \frac{mN_0 C_{pt}}{\rho_0 C_v}$ and

$$\chi = \frac{q'}{\rho_0 C_v} \text{ and } \upsilon, \mu', \in,$$

k_1, α, μ_e, η and q' stand for kinematic viscosity, couple-stress viscosity, medium porosity, medium permeability, coefficient of thermal expansion, magnetic permeability, electrical resistivity and "effective" thermal conductivity of the pure fluid, respectively. mN is the mass of particles per unit volume, $\vec{\lambda}=(0,0,1)$ and $K=6\pi\mu\eta'$, η' being particle radius, the Stokes' drag coefficient. The distance between particles is assumed quite large compared with their diameter so that interparticle reactions are ignored. The effects of pressure, gravity and Darcian force on the suspended particles are negligibly small and therefore ignored.

Eliminating $\vec{q}_d$ in equation (1) with the help of equation (3), writing the scalar components of resulting equation and eliminating u, v, h_x, h_y, s, δp between them, by using (2) and (6), we obtain,

$$n'\left(\nabla^2 w\right) + \frac{\in}{k_1}\left(\upsilon - \frac{\mu'}{\rho_0}\nabla^2\right)\nabla^2 w -$$

$$\in g\alpha\left(\frac{\partial^2\theta}{\partial x^2} + \frac{\partial^2\theta}{\partial y^2}\right) - \frac{\mu_e \in H}{4\pi\rho_0}\frac{\partial}{\partial x}\left(\nabla^2 h_z\right) = 0, \quad (7)$$

$$\left(\frac{m}{K}\frac{\partial}{\partial t} + 1\right)\left[\overline{E + h \in}\frac{\partial}{\partial t} - \chi\nabla^2\right]\theta =$$

$$\beta\left[\frac{m}{K}\frac{\partial}{\partial t} + 1 + h\right]w, \quad (8)$$

$$\in\left[\frac{\partial}{\partial t} - \eta\nabla^2\right]h_z = H\frac{\partial w}{\partial x}, \quad (9)$$

where $n' = \frac{\partial}{\partial t}\left[1 + \frac{mN_0 K/\rho_0}{m\frac{\partial}{\partial t} + K}\right]$.

Dispersion Relation

Here we analyse the disturbances into normal modes and assume that the perturbation quantities are of the form

$$[w, \theta, h_z] = [W(z), \Theta(z), K(z)]exp(ik_x x + ik_y y + nt), \quad (10)$$

where k_x, k_y are wave numbers along the x- and y- directions respectively, $k\left(= \sqrt{k_x^2 + k_y^2}\right)$ is the resultant wave number and n is, in general, a complex constant.

Using expression (10), equations (7)-(9) in non-dimensional form become

$$\left[\frac{\sigma'}{\in} + \frac{1}{P_l}\left\{1 - F\left(D^2 - a^2\right)\right\}\right]\left(D^2 - a^2\right)W$$

$$+\frac{g\alpha d^2 a^2 \Theta}{\upsilon} - \frac{ik_x \mu_e H d^2}{4\pi\rho_0 \upsilon}\left(D^2 - a^2\right)K = 0, \quad (11)$$

$$\left[\frac{\tau\upsilon}{d^2}\sigma + 1\right]\left[D^2 - a^2 - \overline{E + h\in}p_1\sigma\right]\Theta$$

$$= \frac{-\beta d^2}{\chi}\left[H' + \frac{\tau\upsilon\sigma}{d^2}\right]W, \quad (12)$$

$$\left[D^2 - a^2 - p_2\sigma\right]K = -\frac{ik_x H d^2}{\in\eta}W, \quad (13)$$

where we have expressed the co-ordinates x,y,z in the new unit of length d, time t in the new unit of length $\frac{d^2}{\chi}$ and put $a=kd$, $\sigma=\frac{nd^2}{\upsilon}$, $p_1 = \frac{\upsilon}{\chi}$ is the Prandtl number, $p_2 = \frac{\upsilon}{\eta}$ is the magnetic Prandtl number, $P_l = \frac{k_1}{d^2}$ is the dimensionless medium permeability, $F = \frac{\mu'/\rho_0 d^2}{\upsilon}$ is the dimensionless couple-stress viscosity, $\sigma' = \frac{n' d^2}{\upsilon}$, $H' = h + 1$, $\tau = \frac{m\chi}{Kd^2}$ and $D = \frac{d}{dz}$.

Eliminating Θ and K between equations (11)-(13), we obtain

$$\left[1 + \frac{\upsilon\tau\sigma}{d^2}\right]\left[D^2 - a^2 - \overline{E + h\in}\,p_1\sigma\right]\left[\left\{\frac{\sigma'}{\in} + \frac{1}{P_l}\right.\right.$$

$$\left.\left.\left(1 - F\left(D^2 - a^2\right)\right)\right\}\left\{D^2 - a^2 - p_2\sigma\right\} - \frac{k_x^2}{\in}Q\right]$$

$$\left(D^2 - a^2\right)W = Ra^2\left[H' + \frac{\upsilon\tau\sigma}{d^2}\right]\left[D^2 - a^2 - p_2\sigma\right]W. \quad (14)$$

We now assume that the fluid layer is confined between two free boundaries. This case is of artrificial nature, but due to mathematical simplicity it enables us to find analytical solutions. The appropriate boundary conditions, in non-dimensional form, are

$$W = 0,\ D^2 W = 0,\ D^4 W = 0,\ \Theta = 0,\ K = 0$$
$$\text{at } z = 0 \text{ and } z = 1. \quad (15)$$

Using the boundary conditions (15), it can be shown that all the even order derivatives of W must vanish on the boundaries and hence the proper solution of W characterizing the lowest mode is

$$W = W_0 \sin \pi z\ , \quad (16)$$

where W_0 is a constant. Substituting the proper solution (16) in equation (14), we obtain the dispersion relation

$$R_1 = \frac{(1+x)\left(1 + x + \overline{E + h\in}\,i\sigma_1 p_1\right)\left(1 + \frac{i\upsilon\tau\pi^2\sigma_1}{d^2}\right)\left[\frac{i\sigma_1'}{\in} + \frac{1}{P}\left\{1 + \pi^2 F\overline{1+x}\right\}\left\{1 + x + i\sigma_1 p_2\right\} + \frac{Q_1 x\cos^2\theta}{\in}\right]}{x\left[H' + \frac{i\upsilon\tau\pi^2\sigma_1}{d^2}\right]\left[1 + x + i\sigma_1 p_2\right]}, \quad (17)$$

where $x = \frac{a^2}{\pi^2}$, $i\sigma_1 = \frac{\sigma}{\pi^2}$, $P = \pi^2 P_l$, $R_1 = \frac{R}{\pi^4}$, $i\sigma_1' = \frac{\sigma'}{\pi^2}$, $Q_1 = \frac{Q}{\pi^2}$ and $k_x = k\cos\theta$.

The Stationary Covnection

When the instability sets in as stationary convection, marginal state will be characterized by $\sigma = 0$. Putting $\sigma = 0$, the dispersion relation (17) reduces to

$$R_1 = \frac{(1+x)\left[\frac{1}{P}\left\{1 + \pi^2 F\overline{1+x}\right\}\left\{1 + x\right\} + \frac{Q_1 x\cos^2\theta}{\in}\right]}{xH'}. \quad (18)$$

Equation (18) yields

$$\frac{dR_1}{dQ_1} = \frac{(1+x)\cos^2\theta}{H' \in}, \tag{19}$$

$$\frac{dR_1}{dF} = \frac{\pi^2(1+x)^3}{xH'P}, \tag{20}$$

$$\frac{dR_1}{dP} = -\frac{(1+x)^2\{1+\pi^2 F\overline{1+x}\}}{xH'P^2}, \tag{21}$$

$$\frac{dR_1}{dH'} = -\frac{(1+x)\left[\frac{1}{P}\{1+\pi^2 F\overline{1+x}\}\{1+x\} + \frac{Q_1 x\cos^2\theta}{\in}\right]}{xH'^2}. \tag{22}$$

It is clear from equations (19)-(22) that for stationary convection, the couple-stress and magnetic field postpone the onset of convection whereas the medium permeability and the suspended particles hasten the onset of convection, in couple-stress fluid permeated with suspended particles, heated from below in porous medium in presence of a uniform horizontal magnetic field.
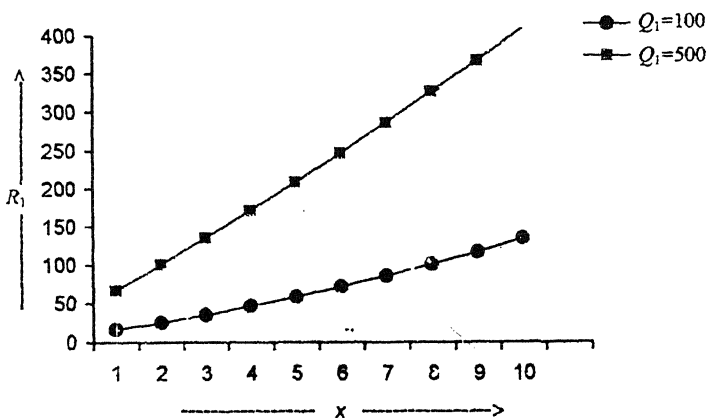
Fig. 1 – Variation of R_1 with x for a fixed $\in$=0.4, θ=45°, P=10, F=10, H'=20, for different values of Q_1=(100,500).

Graphs have been plotted between R_1 and x for various values of Q_1, F, P and H'. It is evident from Fig. (1-4) that the magnetic field, couple-stress parameter postpone the onset of convection while medium permeability and suspended particles hasten the onset of convection.
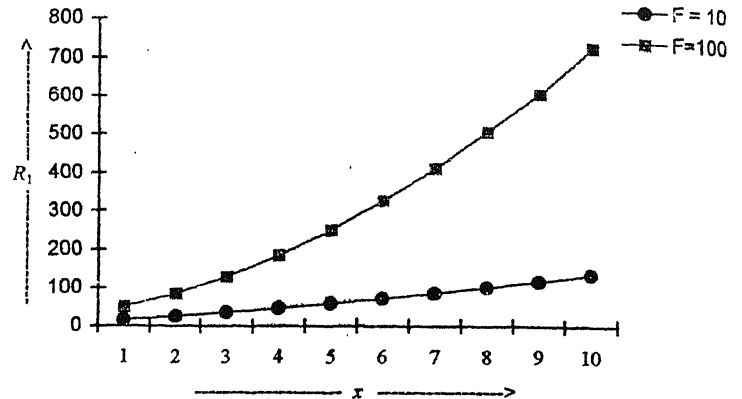
Fig. 2 – Variation of R_1 with x for a fixed $\in$ = 0.4, θ = 45°, P = 10, Q_1 = 100, H' = 20 for different values of F(=10,100).
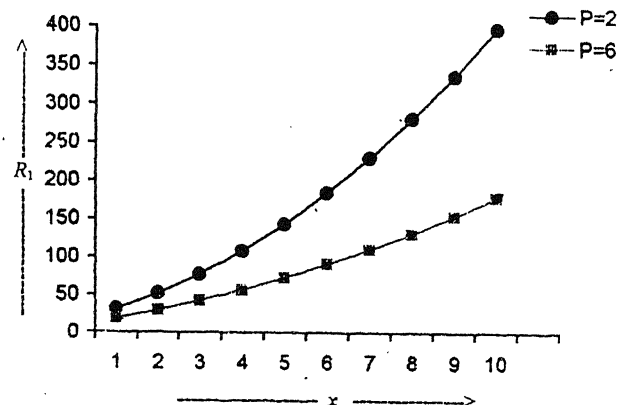
Fig. 3 – Variation of R_1 with x for a fixed $\in$ = 0.4, θ = 45°, F = 10, Q_1 = 100, H' = 20 for different values of P(=2, 6).
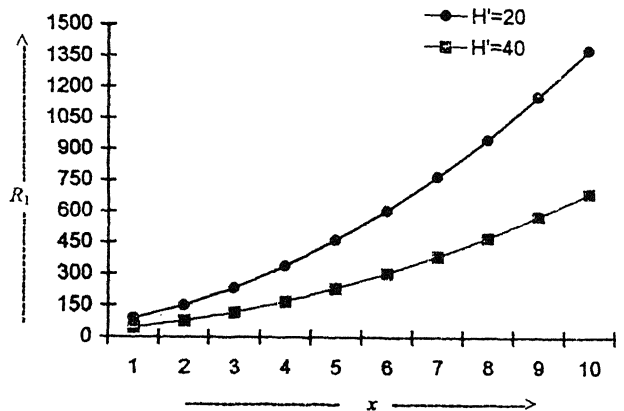
Fig. 4 – Variation of R_1 with x for a fixed $\in$ = 0.4, θ = 45°, F = 100, Q_1 = 100, P = 5 for different values of H'(=20, 40).

Stability of the System and Oscillatory Modes

Multiplying equation (11) by W^*, the complex conjugate of W, and using (12) and (13) together with the boundary conditions (15), we obtain

$$\frac{F}{P_l} I_1 + \left(\frac{\sigma'}{\in} + \frac{1}{P_l}\right) I_2 - \frac{g\alpha\chi a^2}{\upsilon\beta} \left[\frac{d^2 + \upsilon\tau\sigma^*}{H'd^2 + \upsilon\tau\sigma^*}\right].$$

$$\left[I_3 + \overline{E + h \in} p_1 \sigma^* I_4\right] + \frac{\mu_e \eta \in}{4\pi\rho_0\upsilon}\left[I_5 + p_2 \sigma^* I_6\right] = 0, \tag{23}$$

where

$$I_1 = \int_0^1 \left(\left|D^2 W\right|^2 + 2a^2 |DW|^2 + a^4 |W|^2\right) dz,$$

$$I_2 = \int_0^1 \left(|DW|^2 + a^2 |W|^2\right) dz,$$

$$I_3 = \int_0^1 \left(|D\Theta|^2 + a^2 |\Theta|^2\right) dz, \qquad I_4 = \int_0^1 |\Theta|^2 dz,$$

$$I_5 = \int_0^1 \left(\left|D^2 K\right|^2 + 2a^2 |DK|^2 + a^4 |K|^2\right) dz,$$

$$I_6 = \int_0^1 \left(|DK|^2 + a^2 |K|^2\right) dz, \tag{24}$$

which are all positive definite.

Putting $\sigma = i\sigma_i, f = \frac{mN_0}{\rho_0}$ and equating the imaginary parts of equation (23), we obtain

$$i\sigma_i \left[\left\{1 + \frac{f}{1 + p_1^2 \tau^2 \sigma_i^2}\right\} \frac{I_2}{\in} + \frac{g\alpha\chi a^2}{\upsilon\beta\left(H'^2 d^4 + \upsilon^2 \tau^2 \sigma_i^2\right)}\right.$$

$$\left\{d^2 \upsilon\tau h I_3 + \left(H' d^4 + \upsilon^2 \tau^2 \sigma_i^2\right)(E + h \in) p_1 I_4\right\}$$

$$\left. - \frac{\mu_e \eta \in}{4\pi\rho_0\upsilon} p_2 I_6\right] = 0. \tag{25}$$

Equation (25) yield that $\sigma_i = 0$ or $\sigma_i \neq 0$, which means that the modes may be non-oscillatory or oscillatory. In the absence of magnetic field, equation (25) reduces to

$$i\sigma_i = \left[\left\{1 + \frac{f}{1 + p_1^2 \tau^2 \sigma_i^2}\right\} \frac{I_2}{\in} + \frac{g\alpha\chi a^2}{\upsilon\beta\left(H'^2 d^4 + \upsilon^2 \tau^2 \sigma_i^2\right)}\right.$$

$$\left.\left\{d^2 \upsilon\tau h I_3 + \left(H' d^4 + \upsilon^2 \tau^2 \sigma_i^2\right)(\in + h \in) p_1 I_4\right\}\right] = 0, \tag{26}$$

and the quantity inside the brackets is positive definite. Thus $\sigma_i = 0$, which means that oscillatory modes are not allowed and the principle of exchange of stabilities is valid for the couple-stress fluid permeated with suspended particles, heated from below in porous medium. The magnetic field introduces oscillatory modes (as σ_i may not be zero) in the system which were non-existent in their absence.

Acknowledgements

The authors are grateful to the referee for his critical comments, which led to a significant improvement of the paper.

References

1. Chandrasekhar, S. (1981) *Hydrodynamic and Hydromagnetic Stability,* Dover Publications, New York.
2. Scanlon, J.W. & Segel, L.A. (1973) *Phys. Fluids* **16** : 1573.
3. Stokes, V.K. (1966) *Phys. Fluids* **9** : 1709.
4. Walicki, E. & Walicka, A. (1999) *Appl. Mech. Engng.* **4** : 363.
5. Sharma, R.C. & Sharma, S. (2001) *Indian J. Phys.* **B75** : 137.
6. Rathod, V.P. & Thippeswamy, G. (1999) *Math. Edu. India* **33** : 40.
7. Joseph, D.D. (1976) *Stability of Fluid Motions,* Vol. II, Springer Verlag, Berlin.

PROC. NAT. ACAD. SCI. INDIA, 75(A), II, 2005

On generalised Ricci-recurrent Lorentzian Para-Sasakian manifold

MOHD. NAZRUL ISLAM KHAN

Azad Institute of Engineering & Technology, Department of Applied Sciences, Natkur, Post-Chandrawal, Bangla Bazar Road, Lucknow-226002, India.

E-mail : nazrul73@rediffmail.com

Received September 20, 2004; Accepted September 30, 2004

Abstract

The present paper deals with a generalised Ricci-Recurrent Lorentzian Para-Sasakian manifold and also when it admits cyclic Ricci-tensor.

(**Keywords :** Ricci-recurrent/ Eienstien manifold/ Lorentzian Para-Sasakian manifold/ Lorentzian metric)

Introduction

Generalised Ricci-recurrent manifold was introduced and studied by De *et al.*[1] It is a type of Riemannian manifold M of dimension greater than 2, whose Ricci-tensor S of type (0,2) satisfies the condition

$$(\Delta_X S)(Y,Z) = A(X)S(Y, Z) + B(X)g(Y,Z) \quad (1)$$

where A and B are 1-forms. Let P, Q be two vector fields such that

$$g(X, P) = A(X) \quad (2)$$

$$g(X, Q) = B(X) \quad (3)$$

for every vector field X.

If the manifold is n-dimensional then it is denoted by GR_n. When the 1-form B vanishes identically then the manifold reduces to a Ricci-recurrent manifold[2]. Guha[3] studied generalised Ricci-recurrent Sasakian manifolds.

In this paper it is shown that in a generalised Ricci-recurrent Lorentzian Para-Sasakian manifold the vector fields P and Q defined in (2) and (3) are in opposite direction and if generalised Ricci-recurrent Lorentzian Para-Sasakian manifold admits a cyclic Ricci-tensor then the manifold is an Einstein manifold.

Preliminaries

A differential manifold M^n of dimension n is called Lorentzian Para-Sasakian[4-6], if it admits $a(1,1)$ tensor field ϕ, a contravarient vector field ξ, a covariant vector field η and a Lorentzian metric g which satisfy

$$\eta(\xi) = -1 \quad (4)$$

$$\phi^2 = I + \eta \otimes \xi \quad (5)$$

$$g(\phi X, \phi Y) = g(X, Y) + \eta(X)\eta(Y) \quad (6)$$

$$g(X, \xi) = \eta(X) \quad (7)$$

$$\nabla_X \xi = \phi X \quad (8)$$

$$(\nabla_X \phi)Y = [g(X, Y) + \eta(X)\eta(Y)]\xi + [X + \eta(X)\xi]\eta(Y) \quad (9)$$

where ∇ denotes the operator of covariant differentiation with respect to the Lorentzian metric g.

It can be easily seen that in a LP-Sasakian manifold M^n, the following relations hold

$$\phi\xi = 0, \quad \eta(\phi X)=0 \quad (10)$$

$$\text{rank } \phi = n-1 \quad (11)$$

Also, in a LP-Sasakian manifold M^n as the (ϕ,η,ξ,g) - structure, the following relations[6] hold.

$$R(\xi,X)Y = g(X,Y)\xi - \eta(Y)X \quad (12)$$

$$R(\xi, X)\xi = X + \eta(X)\xi \quad (13)$$

$$R(X,Y)\xi = \eta(Y)X - \eta(X)Y \quad (14)$$

$$S(X, \xi) = (n-1)\eta(X) \quad (15)$$

for any vector field X, Y, Z where $R(X,Y)Z$ is the Riemannian curvature tensor and S is the Ricci-curvature Tensor.

Generalised Ricci-recurrent Lorentzian Para-Sasakian Manifold

Let M^n be a generalised Ricci-recurrent LP-Sasakian manifold. We know that

$$(\nabla_X S)(Y,Z) = XS(Y,Z) - S(\nabla_X Y,Z) - S(Y,\nabla_X Z) \quad (16)$$

where $X,Y,Z \in TM$

From (1) and (16) we get,

$$A(X)S(Y,Z) + B(X)g(Y,Z) = XS(Y,Z) - S(\nabla_X Y,Z) - S(Y,\nabla_X Z)$$

putting $Z=\xi$ in above relation and using (7), (8), (10) and (15), we have

$$(n-1)A(X)\eta(Y) + B(X)\eta(Y) = (n-1)(\nabla_X \eta)(Y) - S(Y,\phi X) \quad (17)$$

Now, we note that

$$0 = (\nabla_X g)(Y,\xi) = Xg(Y,\xi) - g(\nabla_X Y,\xi) - g(Y,\nabla_X \xi)$$

$$0 = (\nabla_X \eta)(Y) - g(Y,\phi X)$$

$$(\nabla_X \eta)(Y) = g(Y, \phi X) \quad (18)$$

using (18) in (17), we get

$$[(n-1)A(X) + B(X)]\eta(Y) = (n-1)g(Y,\phi X) - S(Y,\phi X) \quad (19)$$

putting $Y=\xi$ in (19) and using (4), (8), (10) and (15), we get

$$-[(n-1)A(X) + B(X)] = (n-1)\eta(\phi X) - (n-1)\eta(\phi X)$$

$$(n-1)A(X) + B(X) = 0 \quad (20)$$

Hence, we can state the following :

Theorem (1) : In a generalised Ricci-recurrent Lorentzian Para-Sasakian manifold the associated vector field of the 1-forms A and B are in the opposite direction.

Generalised Ricci-recurrent Lorentzian Para-Sasakian manifold admitting cycle Ricci-tensor

Suppose that a generalised Ricci-Recurrent Lorentzian Para-Sasakian manifold admits a cycle Ricci-tensor, that is,

$$(\nabla_X S)(Y,Z) + (\nabla_Y S)(Z,X) + (\nabla_Z S)(X,Y) = 0 \quad (21)$$

from (1) and (21) it follows that

$$A(X)\,S(Y,Z) + B(X)\,g(Y,Z) + A(Y)\,S(Z,X) + B(Y)\,g(Z,X) + A(Z)\,S(X,Y) + B(Z)g(X,Y) = 0 \quad (22)$$

putting $Z=\xi$ in (22), in view of (7), (10) and (15), we get

$$[(n-1)A(X) + B(X)]\,\eta(Y) + [(n-1)A(Y) + B(Y)]\eta(X) + A(\xi)\,S(X,Y) + B(\xi)g(X,Y) = 0 \quad (23)$$

using (20), we get from (23)

$$A(\xi)\,S(X,Y) + B(\xi)\,g(X,Y) = 0$$

That is,

$$A(\xi)\,S(X,Y) = -B(\xi)\,g(X,Y) \quad (24)$$

Hence, we can state the following :

Theorem (2) : If a generalised Ricci-recurrent Lorentzian Para-Sasakian manifold admits a cycle Ricci-tensor then it becomes an Einstein-manifold provided that $A(\xi) \neq 0$.

References

1. De, U.C., Guha, N. & Kamilya, D. (1995) *Tensor N.S.* **56** : 312.
2. Patterson, E.M. (1952) *J. London Math. Soc.* **27** : 287.
3. Guha, N. (2000) *Bull.Cal.Math. Soc.* **92**(5) : 321.
4. Matsumoto, K. (1989) *Bull. of Yamagata Univ. Nat. Sci.* **12**(2) : 151.
5. Mihai, I. & Rosea, R. (1992) *On Lorentzian P-Sasakian Manifold, Classical Analysis,* World Scientific Pub., Singapore, p. 155.
6. Motsumoto, K. & Mihai, I. (1988) *Tensor N.S.* **47** : 189.

THE NATIONAL ACADEMY OF SCIENCES, INDIA

5, Lajpatrai Road, New Katra, Allahabad - 211002

Guidelines for the Authors/Contributors for submitting papers

Proceedings of the National Academy of Sciences, India
(Section A – Physical Sciences)

[A) WHAT TO SUBMIT

The following categories of papers are published in the Proceedings of the National Academy of Sciences, India (Section A - Physical Sciences) :

(1) **Review Articles:** This should be a critical review highlighting the present status and an overview of the past work on any relevant subject of current topical interest. It has to be written in a manner to help either in initiating the work in that particular area or in increasing the comprehension of the current challenges. If such an article is accepted by the Academy for publication, then **Rupees Two Thousand** would be given to the "corresponding author" after the publication of the paper in the Proceedings to meet the contingency expenses. Ordinarily, the Review Article should not exceed 25 printed pages.

(2) **Original Articles:** This should give new results obtained by the authors and be prepared in the format of the journal. Ordinarily such papers should not be more than 12 printed pages.

(3) **Special Issues for Conference Proceedings:** Proceedings of National and International Conferences, as a special issue of the journal, can also be brought out with organizers as Guest Editors. At least, one of the Guest Editors should be Fellow of the Academy. Guest Editors shall be responsible for proper refereeing of the papers and for ensuring their high quality.

It is presumed that the articles submitted for publication have not been submitted to any other journal by the authors. Authors shall be liable themselves for such an act.

[B) WHO CAN SUBMIT

(1) All scientists (Indian or Foreign) can directly send their article for publication. **If there are more than one author, each author should certify that he/she agrees to the submission of the review/research paper.**

(2) In addition to above, all the Fellows of the National Academy of Sciences, India are also authorized to forward quality papers in their research field for publication in the journals of the Academy. The name of the communicating Fellow would be printed in the paper as "Communicated by ....................F.N.A.Sc".

The communicating Fellow should certify that:

(i) The forwarded paper is in his/her field of specialization,

(ii) He/she has read the paper and reviewed it carefully.

However, if the Editorial Board finds it necessary, it may get the paper reviewed again.

[C] WHOM TO SUBMIT

The papers should be sent to the Managing Editor, Proceedings of the National Academy of Sciences, India (Section A – Physical Sciences); 5 Lajjpat Rai Road, New Katra, Allahabad - 211 002

[D] HOW TO SUBMIT

The authors may submit the papers directly or forwarded through a Fellow of the Academy as prescribed above. **It is mandatory to submit "An Electronic Version" as well as "three hard-copies". The text of the manuscript as per format of the journal outlined below, and preferably with scanned figures, should be supplied as a plain ASCII file (Wordstar 5.5 or 7.0 and Microsoft Word for Window 6.0 are also acceptable, but ASCII is preferred). The language of the journal is English.**

[E] FORMAT OF THE MANUSCRIPT

(i) Title of the paper should be in **bold** and running (14-font size) through the full page width.

(ii) **Author's name/Affiliations** may also run through the full page width. Names should be in 12 point font-size and **bold** while affiliations should be 8 point font size in *italics*. Please note that if any of the author is a Fellow of the Academy, then he should write F.N.A.Sc. after his name.

(iii) **Abstract** should be typed in 8 point font sizes **"bold"**.

(iv) **Keywords** (maximum 5 words/phrases, each separated by slash [/]) should follow the Abstract.

(v) **Contents of the text**

(a) This is to be typed on A4 page in double space in10 point font size.

(b) The text of the paper should be arranged into suitable headings like Introduction, Materials and Method, Theory or Model, Results, Discussion, Conclusions/Summary, Acknowledgements, References, etc.

(c) Please note that the Proceedings are published in "two column format". Therefore, the authors are required to draw the figures tables/equations in such a way that they can be easily reduced to one column width (~ 7.5 cm) at the time of publication. Figures must be original drawings or exceptionally sharp glossy prints drawn with stencil and UNO pen.

(d) All references should be indicated in the text by superscript Arabic numerals, e.g. 'Mirri[1] while working on...'. The list of references should be arranged in order of their occurrence in the text. References should be given in the following style:

1. Mirri, M.A. (1982), J. Chem. Phys. 58: 282 (for articles in journals)

White, M. J. D. (1973) Animal Cytology and Evolution, 3rd Ed., Cambridge University Press, London, p. 320 (for books)

Osgood, C.F. (1977) in Number Theory and Algebra: ed., Zasserhause, H., Academic Press, New York, p. 10 (for edited books)

Abbreviations of the names of periodicals should conform to those given in the World list of Scientific Periodicals.

[F] MISCELLANEOUS

(i) All papers will be screened by a strict refereeing procedure. However, the responsibility for the authenticity of the contents lies with the authors.

(ii) If a paper is recommended for revision, a maximum of 2 months would be given to authors for revising the manuscript after which it would be treated as a fresh communication.

(iii) Authors will receive galley proof of their paper from the Academy's Editorial Office. They should return the corrected proof within a week of its receipt. If return of the proof is delayed, the proof will be corrected by the Academy, but the responsibility will be entirely that of the author(s).

(iv) No change in the text of the paper will be made after the matter has been composed by the Press. If it is absolutely essential, a postscript may be added.

(v) Reprints: 25 free reprints will be given to the corresponding author for each paper.

[G] SUBSCRIPTION RATE OF THE JOURNALS

Annual Subscription for both Sections : Rs. 500.00; **for each Section** Rs. 250.00; **Single Copy :** Rs. 100.00, **Foreign Subscription** : (a) for one Section: US $100, (b) for both Sections US $200. **(Air Mail charges included in foreign subscription)**

Kind Attention : Fellows and Members of the National Academy of Sciences, India

(Please fill items and return to the Managing Editor – Proceedings of the National Academy of Sciences, India (Sec A – Physical Sciences; Sec B – Biological Sciences)

The Editorial Boards and Board of Editors of the Journals of the Academy viz. **Proceedings of the National Academy of Sciences, India (Sec A – Physical Sciences)**, **Proceedings of the National Academy of Sciences, India (Sec B– Biological Sciences)** and **National Academy Science Letters,** request its esteemed Fellows and Members to inform their willingness for acting as learned referees for the research papers received for publication in the above Journals. They are also requested to suggest other names of subject experts who may be requested for refereeing as per following proforma.

UPDATED DATA OF REFEREES' PANEL FOR THE JOURNALS OF THE NATIONAL ACADEMY OF SCIENCES, INDIA

(I) 1. Name, Designation, Affiliation and ....

Postal Address of the Fellow/Member ....

....

....

(a) Telephone No. (with area code) ....

(b) Fax No. (with area code).... ....

(c) E-mail Address... ....

2. State whether a Fellow or Member ....

3. Subject/Sub-disciplines of your expertise in which you are willing to act as Referee.

Sl. No.	Major Disciplines (Such as Physics etc.)	Sub-discipline alonwith super-speciality	Experimental/Theoretical or both
1.		(i) (a) (b)	
2.		(ii) (a) (b)	
3.		(iii) (a) (b)	

(II) Suggestions regarding additional referees

Sl. No.	Name(s) & Address of those whom you suggest for refereeing	His/Her Major Disciplines (such as Physics etc.)	His/Her Sub-disciplines alongwith any Super-specialities	Experimental/Theoretical or Both
1.			(i) (a) (b)	
2.			(i) (a) (b)	
3.			(i) (a) (b)	

Signature of the Fellow/Member

PROCEEDINGS OF THE NATIONAL ACADEMY OF SCIENCES, INDIA
(SECTION A - PHYSICAL SCIENCES)
EDITORIAL BOARD